

LOAN DOCUMENT

	DTIC ACCESSION NUMBER		PHOTOGRAPH THIS SHEET																					
		LEVEL		INVENTORY 0																				
AFRL-ML-TX-TR-1999-4551																								
DOCUMENT IDENTIFICATION 9 Jul 1998																								
DISTRIBUTION STATEMENT A Approved for Public Release Distribution Unlimited																								
DISTRIBUTION STATEMENT																								
<table border="1"><tr><td colspan="2">ACCESSION FOR</td></tr><tr><td>NTIS</td><td>GRAM</td></tr><tr><td>DTIC</td><td>TRAC</td></tr><tr><td>UNANNOUNCED</td><td></td></tr><tr><td>JUSTIFICATION</td><td></td></tr><tr><td colspan="2">BY</td></tr><tr><td colspan="2">DISTRIBUTION/</td></tr><tr><td colspan="2">AVAILABILITY CODES</td></tr><tr><td>DISTRIBUTION</td><td>AVAILABILITY AND/OR SPECIAL</td></tr><tr><td>A-1</td><td></td></tr></table>		ACCESSION FOR		NTIS	GRAM	DTIC	TRAC	UNANNOUNCED		JUSTIFICATION		BY		DISTRIBUTION/		AVAILABILITY CODES		DISTRIBUTION	AVAILABILITY AND/OR SPECIAL	A-1				
ACCESSION FOR																								
NTIS	GRAM																							
DTIC	TRAC																							
UNANNOUNCED																								
JUSTIFICATION																								
BY																								
DISTRIBUTION/																								
AVAILABILITY CODES																								
DISTRIBUTION	AVAILABILITY AND/OR SPECIAL																							
A-1																								
DISTRIBUTION STAMP		DATE ACCESSIONED																						
		DATE RETURNED																						
20000211 038		REGISTERED OR CERTIFIED NUMBER																						
DATE RECEIVED IN DTIC																								
PHOTOGRAPH THIS SHEET AND RETURN TO DTIC-FDAC																								

H
A
N
D
L
E

W
I
T
H

C
A
R
E

AFRL-ML-TY-TR-1999-4551



REACTOR MODEL - DATA COMPARISON FOR GAS PHASE POLLUTANT REMOVAL IN A PULSED STREAMER CORONA REACTOR

GIRIDHAR SATHIAMOORTHY

**FLORIDA STATE UNIVERSITY &
FAMU-FSU COLLEGE OF ENGINEERING
DEPARTMENT OF ENGINEERING
2525 POTTSDAMER STREET
TALLAHASSEE FL 32310-6046**

Approved for Public Release: Distribution Unlimited

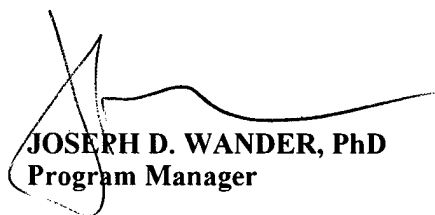
**AIR FORCE RESEARCH LABORATORY
MATERIALS & MANUFACTURING DIRECTORATE
AIRBASE & ENVIRONMENTAL TECHNOLOGY DIVISION
TYNDALL AFB FL 32403-5323**

NOTICES

USING GOVERNMENT DRAWINGS, SPECIFICATIONS, OR OTHER DATA INCLUDED IN THIS DOCUMENT FOR ANY PURPOSE OTHER THAN GOVERNMENT PROCUREMENT DOES NOT IN ANY WAY OBLIGATE THE US GOVERNMENT. THE FACT THAT THE GOVERNMENT FORMULATED OR SUPPLIED THE DRAWINGS, SPECIFICATIONS, OR OTHER DATA DOES NOT LICENSE THE HOLDER OR ANY OTHER PERSON OR CORPORATION; OR CONVEY ANY RIGHTS OR PERMISSION TO MANUFACTURE, USE, OR SELL ANY PATENTED INVENTION THAT MAY RELATE TO THEM.

THIS REPORT IS RELEASABLE TO THE NATIONAL TECHNICAL INFORMATION SERVICE (NTIS). AT NTIS, IT WILL BE AVAILABLE TO THE GENERAL PUBLIC, INCLUDING FOREIGN NATIONS.

THIS TECHNICAL REPORT HAS BEEN REVIEWED AND IS APPROVED FOR PUBLICATION.



JOSEPH D. WANDER, PhD
Program Manager



CHRISTINE WAGENER-HULME, Lt Col, USAF, BSC
Chief, Environmental Technology Development Branch



RANDY L. GROSS, Col, USAF, BSC
Chief, Airbase & Environmental Technology Division

REPORT DOCUMENTATION PAGE			Form Approved OMB No. 0704-0188	
Public reporting burden for this collection of information is estimated to average 1 hour per response, including the time for reviewing instructions, searching existing data sources, gathering and maintaining the data needed, and completing and reviewing the collection of information. Send comments regarding this burden estimate or any other aspect of this collection of information, including suggestions for reducing this burden, to Washington Headquarters Services, Directorate for Information Operations and Reports, 1215 Jefferson Davis Highway, Suite 1204, Arlington, VA 22202-4302, and to the Office of Management and Budget, Paperwork Reduction Project (0704-0188), Washington, DC 20503.				
1. AGENCY USE ONLY (Leave blank)		2. REPORT DATE 9 July 1998		3. REPORT TYPE AND DATES COVERED Master's Thesis: May 1996 - May 1998
4. TITLE AND SUBTITLE Reactor Model - Data Comparison for Gas Phase Pollutant Removal in a Pulsed Streamer Corona Reactor			5. FUNDING NUMBERS F08635-93-C-0020 PE: 6022F Project Number: 1900-A35B	
6. AUTHOR(S) Sathiamoorthy, Giridhar				
7. PERFORMING ORGANIZATION NAME(S) AND ADDRESS(ES) Department of Chemical Engineering Florida State University & FAMU-FSU College of Engineering 2525 Pottsdamer Street Tallahassee FL 32310-6046			8. PERFORMING ORGANIZATION REPORT NUMBER	
9. SPONSORING/MONITORING AGENCY NAME(S) AND ADDRESS(ES) AFRL/MLQE (Dr. Joe Wander) 139 Barnes Drive, Suite 2 Tyndall AFB, FL 32403-5323			10. SPONSORING/MONITORING AGENCY REPORT NUMBER AFRL-ML-TY-TR-1999-4551	
11. SUPPLEMENTARY NOTES POC: Joseph D. Wander, Ph.D, AFRL/MLQE, (850) 283-6240				
12a. DISTRIBUTION AVAILABILITY STATEMENT Approved for Public Release: Distribution Unlimited			12b. DISTRIBUTION CODE A	
13. ABSTRACT (Maximum 200 words) Pulsed streamer corona technology is based on the application of a high electric potential between two electrodes of inhomogeneous geometry to produce charged species in a plasma. In this study, a pulsed corona discharge produced in a wire-cylindar geometry is utilized to remove gaseous pollutants such as NO, NO2, and Halon-1211. The present study also focuses on the degradation of Halon-1211 for a range of voltages, reactor residence times, and power densities in a mixture of synthetic air. Up to 95% of 1000 ppm of Halon was obtained. A mathematical model describing the gas phase kinetics with neutral species has been developed. The present study brings out the fact that it is possible to develop a simple reactor model for describing non-thermal plasma systems.				
14. SUBJECT TERMS Pulsed streamer, corona, plasma, nitrogen oxides			15. NUMBER OF PAGES 129	
			16. PRICE CODE	
17. SECURITY CLASSIFICATION OF REPORT UNCL	18. SECURITY CLASSIFICATION OF THIS PAGE UNCL	19. SECURITY CLASSIFICATION OF ABSTRACT UNCL	20. LIMITATION OF ABSTRACT UL	

UNCLASSIFIED

SECURITY CLASSIFICATION OF THIS PAGE

CLASSIFIED BY:

DECLASSIFY ON:

Preface

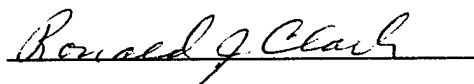
This thesis was prepared by Florida State University (FSU), Department of Chemical Engineering, under a subcontract with Applied Research Associates (contract No. F08635-93-C-0020), for the Air Force Research Laboratory (AFRL), Airbase and Environmental Technology Division, Tyndall AFB, FL 32403. The work was performed from May 1996 to May 1998. The AFRL project officer was Joseph D. Wander, Ph.D.

This thesis is submitted to the Defense Technical Information Center for publication exactly as it was submitted to Florida State University. This format does not conform to the usual style standards for AFRL reports but is acceptable.

The members of the Committee approve the thesis of Giridhar Sathiamoorthy
defended on July 9, 1998.



Bruce R. Locke
Professor Directing Thesis

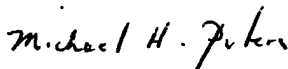


Ronald J. Clark
Committee Member



Srinivas Palanki
Committee Member

Approved:



Michael H. Peters, Chair, Department of Chemical Engineering

To
Appa, Amma, Sriram
&
Friends ..

ACKNOWLEDGEMENTS

I am highly indebted to my thesis advisor, Dr. Bruce Locke for selecting me for the corona project. I sincerely thank him for his fruitful advice and guidance throughout my research work. I am also thankful to Dr. Ronald Clark for his invaluable suggestions on chemical analysis and for serving on my thesis advisory committee. My sincere thanks to Dr. Srinivas Palanki for readily accepting to serve on my thesis advisory committee. I wish to express my gratitude to Mr. Wright Finney for his constant support in this project. His inestimable help in writing and revising this thesis is greatly appreciated.

I am also thankful to the Department of Chemical Engineering, FAMU-FSU College of Engineering, The Florida State University, and the US Air Force, for providing financial support, laboratory equipment and supplies for this project.

I wholeheartedly thank Mr. David Grymonpré for his suggestions and for helping me operate the experimental setup. My sincere thanks to Mr. Swaminathan Kalyana for assisting me with the reactor model. I also would like to thank Mr. Howell Hanson and Mr. Shawn Goldstein for their assistance with data acquisition.

Last but not the least, I am extremely grateful to my parents and my friends for their everlasting love and their emotional support.

CONTENTS

LIST OF TABLES	vii
LIST OF FIGURES	ix
ABSTRACT	xii
1 INTRODUCTION	1
1.1 Research Objectives.....	5
2 LITERATURE REVIEW	6
2.1 Electron Beam Processing.....	6
2.2 Dielectric Barrier Discharge.....	8
2.3 Corona Discharge.....	10
2.4 Reactor Model	14
3 EXPERIMENTAL APPARATUS & PROCEDURE	20
3.1 Power Supply.....	20
3.2 Reactor Specifications.....	22
3.3 Analysis.....	24
3.4 Feed Gas.....	25
3.5 Experimental Procedure.....	27
4 REACTOR MODELING	31

5	EXPERIMENTAL RESULTS & DISCUSSIONS	40
5.1	Physical Characteristics of the Discharge	40
5.2	NO Removal in Nitrogen	43
5.3	NO Removal in Dry Air	48
5.4	Ozone Formation	58
5.5	NO Removal in Dry Air in the Presence of Ethylene	60
5.6	Halon Removal in Dry Synthetic Air	76
5.7	Labeled Nitric Oxide Experiments	84
6	SUMMARY & CONCLUSIONS	88
7	FUTURE WORK & RECOMMENDATIONS	97
	APPENDICES	100
A	EXPERIMENTAL RESULTS OBTAINED IN	
	NITROGEN & DRY AIR	100
B	HALON DEGRADATION	104
	REFERENCES	105
	BIOGRAPHICAL SKETCH	113

LIST OF TABLES

Table 4.1 :	List of Chemical Reactions Considered for Modeling	38
Table 5.1 :	Peak Voltage as a Function of Dial Setting for Reactor - I and Reactor - II	42
Table 5.2 :	Energy Input as a Function of Peak Voltage for Reactor- I and Reactor- II	43
Table 5.3 :	Rate Constants for Hydrocarbon Reaction with Hydroxyl Radicals	62
Table 5.4 :	List of Additional Reactions Considered for Modeling in the Presence of Ethylene	70
Table 5.5 :	Additional Reactions Considered for Halon Breakdown	83
Table 5.6 :	Summary of N ¹⁵ O Experimental Data	86
Table A.1 :	NO and NO ₂ Data at a Peak Voltage of 40 kV in an Atmosphere of Nitrogen	100
Table A.2 :	NO and NO ₂ Data at a Peak Voltage of 44 kV in an Atmosphere of Nitrogen	100
Table A.3 :	NO and NO ₂ Data at a Peak Voltage of 49 kV in an Atmosphere of Nitrogen	101
Table A.4 :	NO and NO ₂ Data at a Peak Voltage of 40 kV in an	

	Atmosphere of Dry Air	101
Table A.5 :	NO and NO ₂ Data at a Peak Voltage of 44 kV in an Atmosphere of Dry Air	101
Table A.6 :	NO and NO ₂ Data at a Peak Voltage of 49 kV in an Atmosphere of Dry Air	102
Table A.7 :	NO and NO ₂ Data at a Peak Voltage of 40 kV in an Atmosphere of Dry Air + 500 ppm Ethylene	102
Table A.8 :	NO and NO ₂ Data at a Peak Voltage of 44 kV in an Atmosphere of Dry Air + 500 ppm Ethylene	102
Table A.9 :	NO and NO ₂ Data at a Peak Voltage of 49 kV in an Atmosphere of Dry Air + 500 ppm Ethylene	103
Table A.10 :	Ozone Formation Data in an Atmosphere of Dry Air.....	103
Table B. 1 :	Residence Times in the Reactor as a Function of Peak Voltage and Power Density for Halon Experiments.....	104
Table B. 2 :	Removal Efficiency of Halon With Changes in Power Density as a Function of Peak Voltage	104

LIST OF FIGURES

Figure 1.1 :	NO Concentration Profile in an Atmosphere of Oxygen	4
Figure 3.1 :	Schematic Representation of the Power Supply	21
Figure 3.2 :	Schematic Representation of Reactor - I	23
Figure 3.3 :	Schematic Representation of Reactor - II	23
Figure 3.4 :	Schematic Representation of the Feed System	26
Figure 5.1 :	Typical Voltage Waveform Obtained during Corona Discharge for Reactor - I	41
Figure 5.2 :	Typical Current Waveform Obtained during Corona Discharge for Reactor - I	41
Figure 5.3 :	Percentage NO Removal in an Atmosphere of Nitrogen	45
Figure 5.4 :	NO ₂ Formed in an Atmosphere of Nitrogen	45
Figure 5.5 :	NO Model Concentration Profile in an Atmosphere of Nitrogen	46
Figure 5.6 :	Model Prediction of Different Species at 40 kV in an Atmosphere of Nitrogen	47
Figure 5.7 :	Rate Constants for N ₂ Dissociation in an Atmosphere of Nitrogen	47
Figure 5.8 :	Percentage NO Removal in an Atmosphere of Dry Air	49

Figure 5.9 :	NO ₂ Formed in an Atmosphere of Dry Air	50
Figure 5.10 :	Comparison of Electron Densities	51
Figure 5.11 :	Rate Constants for Nitrogen Dissociation in an Atmosphere of Dry Air	55
Figure 5.12 :	Rate Constants for Oxygen Dissociation in an Atmosphere of Dry Air	55
Figure 5.13 :	NO Model Concentration Profile in an Atmosphere of Dry Air	56
Figure 5.14 :	NO ₂ Model Concentration Profile in an Atmosphere of Dry Air	56
Figure 5.15 :	Model Profiles of Different Species at a Peak Voltage of 40 kV in an Atmosphere of Dry Air	57
Figure 5.16 :	Ozone Concentration Profile as a Function of Residence Time	60
Figure 5.17 :	Percentage NO Removal in an Atmosphere of Dry Air + 500 ppm Ethylene	64
Figure 5.18 :	NO ₂ Formation in an Atmosphere of Dry Air + 500 ppm Ethylene.....	64
Figure 5.19 :	NO Model Concentration in an Atmosphere of Dry Air + 500 ppm Ethylene	66
Figure 5.20 :	NO ₂ Concentration Profile in an Atmosphere of Dry Air +	

500 ppm Ethylene	67
Figure 5.21 : Ethylene Breakdown at a Peak Voltage of 49 kV in Dry	
Air + 500 ppm Ethylene	68
Figure 5.22 : Model Profile of Byproducts formed at 49 kV in Dry Air +	
500 ppm Ethylene	69
Figure 5.23 : Halon Removal Efficiency at Constant Peak Voltages.....	77
Figure 5.24 : Halon Removal Efficiency for Different Power Densities	
(as a function of residence time).....	78
Figure 5.25 : Halon Removal Efficiency for Different Power Densities	
(as a function of peak voltages).....	79
Figure 5.26 : Model Comparison for Halon Degradation.....	82
Figure 5.27 : Typical Concentration Profile of Species Formed Due to	
Halon Breakdown	82
Figure 6.1 : Summary of NO Removal at a Peak Voltage of 49 kV in	
Different Atmospheres	90
Figure 6.2 : Summary of NO ₂ Formation at a Peak Voltage of 49 kV in	
Different Atmospheres	90
Figure 6.3 : Summary of NO Model Profile at a Peak Voltage of 49 kV in	
Different Atmospheres	93
Figure 6.4 : Summary of NO ₂ Model Profile at a Peak Voltage of 49 kV in	
Different Atmospheres	93

ABSTRACT

Pulsed streamer corona technology is based on the application of a high electric potential between two electrodes of inhomogeneous geometry to produce charged species in a plasma. In this study, a pulsed corona discharge produced in a wire-cylinder geometry is utilized to remove gaseous pollutants such as NO, NO₂, and Halon-1211.

Removal of 100 ppm NO in different compositions of gaseous mixture (pure nitrogen and dry air) was studied as a function of applied electric potential and residence time in the reactor. Experiments with labeled nitric oxide (N¹⁵O) were carried out to identify the pathway for NO breakdown in nitrogen.

The present study also focuses on the degradation of Halon-1211 (CClBrF₂) for a range of voltages, reactor residence times, and power densities in a mixture of synthetic air. Up to 95% removal of 1000 ppm of Halon was obtained.

A mathematical model describing the gas phase kinetics with neutral species has been developed. The unknown rate constants for electron-molecule collision reactions are determined by fitting the model data for NO removal in dry air. Model predictions of NO₂ and O₃ formation in dry air, and NO and NO₂ removal from dry air in the presence of 500 ppm ethylene are compared with the experimental data. The present study brings out the fact that it is possible to develop a simple reactor model for describing non-thermal plasma systems.

CHAPTER 1

INTRODUCTION

Acid rain, global warming, ozone depletion, and photochemical smog are preeminent environmental problems facing the world today. Toxic air pollutants such as nitrogen oxides (NO_x), sulfur dioxide (SO_2), and chlorofluorocarbons (CFC's) have been implicated as the causes of these effects. An understanding of the physical and chemical principles and subsequent development of technologies for controlling or destroying these pollutants is necessary. Among the many processes that have been studied for the destruction of these pollutants is the non-thermal plasma technique.

Plasma is a collection of positively and negatively charged particles in an otherwise neutral gas. Non-thermal plasma is a plasma in which the electron mean energies are considerably higher than those of the component of the ambient gas. Most of the input electrical energy goes into production of energetic electrons, rather than into gas heating. The electrons so produced lead to dissociation and ionization of the dominant background gas molecules resulting in the formation of reactive radicals. These radicals, in turn, initiate bulk phase reactions leading to the

decomposition of various pollutants. This is in contrast to thermal plasma processes where the whole gas is heated to break the undesired molecules. The energy selectivity and its capability to remove various pollutants makes the non-thermal plasma approach an innovative and efficient technique for the removal of very dilute concentrations of air pollutants.

Non-thermal plasmas can be produced in two different ways:

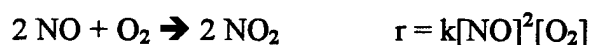
- 1) electron beam irradiation and
- 2) electrical discharges.

In the electron beam method, the direct irradiation of gases by an external source beam of highly energetic electrons causes the dissociation and ionization of the background gas. Using the results of basic studies and pilot-plant tests that have been done in Japan, Germany, Poland, and the USA, the electron beam process is considered to have an excellent potential for the simultaneous removal of NO_x and SO_2 from high sulfur, coal-fired utility boiler combustion gases.

Electrical discharge techniques can be implemented in many ways depending on the geometry of the reactor and electrical power supply. They are broadly classified as the dielectric-barrier discharge and the corona discharge. Dielectric barrier discharge (also referred to as silent discharge or partial discharge) produces plasma that is sustained between one or more dielectric surfaces backed by a conductor. A corona discharge is created by applying a high electrical potential between two electrodes of inhomogeneous geometry. Corona discharges such as

pulsed streamer corona, AC corona, and DC corona have found numerous applications (Masuda, 1988, Clements, et al., 1989). Earlier studies (Kalyana, 1996) were carried out to determine the removal of NO_x from dry air and humid air streams using a pulsed streamer corona reactor. In the present study, further experiments were carried out at lower residence times, and a reactor model was developed to characterize the reactions leading to the removal of NO in a pulsed streamer corona reactor.

NO is an odorless, toxic gas that makes up 90-95% of the NO_x emissions from fossil fuel combustion. NO oxidizes in the presence of oxygen to NO_2 according to the following reaction (Atkinson et al., 1992):



where $k = 1.2 \cdot 10^{-3} \cdot e^{530/T} \text{ m}^6 \cdot \text{mole}^{-1} \cdot \text{sec}^{-1}$ (T = temperature of the gas, °K)

The reaction rate of this oxidation reaction is dependent on the initial concentration of NO and the concentration O_2 in the gas. The concentration profile as a function of time was calculated to be

$$[\text{NO}] = \frac{1}{k^1 t + \frac{1}{[\text{NO}]_0}}$$

where $k^1 = [\text{O}_2] \cdot k$

$[\text{NO}]$ = Concentration of NO at time "t" sec

$[\text{NO}]_0$ = Concentration of NO at time $t = 0$ sec

and

$[O_2]$ = Concentration of O_2 .

As seen in Figure 1.1, the oxidation of NO is very slow and takes almost 50 minutes for 80% of 100 ppm NO to be oxidized. This can be greatly enhanced by the application of corona discharge and will be discussed in detail in Chapter 5.

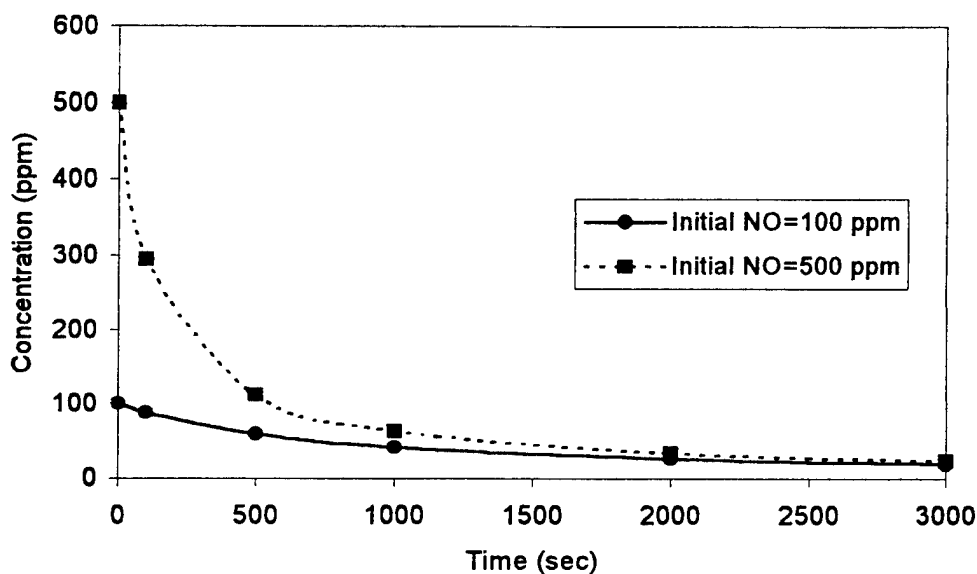


Figure 1.1 : NO Concentration Profile in an Atmosphere of Oxygen

Experiments were also carried out to study the destruction of Halon 1211. Halon 1211, otherwise known as bromochlorodifluoromethane, has been found to be an ozone depletion agent and its manufacture in the United States has been banned since 1994. A reactor model was also developed for the destruction of Halon 1211. The

present study brings out the fact that it is possible to develop a simple reactor model for describing non-thermal plasma systems.

1.1 Research Objectives

The specific goals of this research are:

- 1) To study the effect of different discharge voltages and reactor gas residence times on NO removal.
- 2) To identify the pathways for NO breakdown in an atmosphere of nitrogen using labeled nitric oxide.
- 3) To study the effect of addition of ethylene in NO removal and identify major byproducts.
- 4) To study the degradation of Halon 1211 in the pulsed corona reactor for a range of discharge voltages, residence times, and power densities.
- 5) To develop a reactor model to characterize the reactions taking place in a pulsed streamer corona reactor.

The reactor model developed in this study is a modification of the model developed by Kalyana (1996). The earlier model had two variable parameters to fit the experimental data and this led to discrepancies between model predictions and observed experimental results. In the current model, there is only one variable parameter. Detailed description of the model is given in Chapter 4.

CHAPTER 2

LITERATURE REVIEW

The aim of the present chapter is to review the various non-thermal plasma technologies utilized to date: e-beam, dielectric-barrier discharge, and pulsed corona discharge. A brief review of the fundamental aspects relevant to plasma chemistry is given towards the end of this chapter.

2.1 Electron Beam Processing

The first batch test studies on electron beam irradiation of the gases started in the early seventies (Frank et al., 1993). The success of these batch tests initiated a cooperative effort by Ebara and the Japan Atomic Energy Research Institute (JAERI) in 1972 that lead to the subsequent development of the electron beam process. In this method, the energy of the electron beam (300–800 keV) is used directly to dissociate and ionize the background gas. This results in a shower of secondary electrons, which in turn produce a cascade of ionization and dissociation events leading to the production of large volume of plasma.

E-beam processes have been used extensively for the removal of sulfur dioxide (SO_2) and nitrous oxide (NO_x) from combustion flue gases. These oxides react with the active radicals and atoms produced by the irradiation process forming their respective acids. On addition of ammonia (NH_3), these acids are converted to sulfate and nitrate salts that can be subsequently removed using a conventional particle collector. Organic compounds can also be treated using the same principle (Frank et al., 1993).

It has been reported that more than 95% SO_2 and 90% NO_x can be simultaneously removed from the flue gas under optimum operating conditions (Frank et al., 1993). NO_x removal is optimum at higher temperature whereas low temperatures favor SO_2 removal. The main reason behind this difference is that the thermal reaction of SO_2 and NH_3 is favored at lower temperature. With NO_x , however, the electron-beam initiated chemistry is primarily responsible for the removal efficiency, which are accelerated at higher temperatures. Material balances of nitrogen and sulfur components in simulated flue gas indicate that the nitrogen component of nitric oxide (NO) is converted to nitrate, molecular nitrogen, nitrogen dioxide and dinitrogen monoxide. The sulfur component of sulfur dioxide ends up in the sulfate form (Namba et al., 1990, Tokunaga et al., 1993, Matzing et al., 1994).

Several pilot plant tests are being conducted for electron beam treatment of flue gas in Japan (1) for removal of NO_x and SO_2 from flue gas from a coal-burning power plant (Namba et al., 1991, Namba et al., 1993), and (2) for removal of NO_x ,

SO₂ and HCl from flue gas of a municipal waste incinerator (Doi et al. 1993). A pilot plant is now under operation in Poland for removal of NO_x and SO₂ from flue gases of coal burning boilers (Chmielewski et al., 1992). Apart from NO_x and SO₂ removal, the electron beam process has also been studied for the removal of dilute emissions of volatile organic compounds (Paur, 1993) and chlorinated hydrocarbons (Scheytt et al., 1993).

The high capital cost of accelerators, X-ray hazards, and the necessity of ammonia addition associated with the electron-beam pollution control system have motivated studies into alternate plasma-based technologies such as those utilizing electrical discharges (Frank et al., 1993, Masuda et. al., 1993).

2.2 Dielectric Barrier Discharge

Dielectric barrier discharge, also referred to as silent discharge, is a non-equilibrium gas discharge that can be operated at elevated pressure (0.1-10 bar). Dielectric-barrier discharge processing is a very mature technology, first investigated by Siemens in 1857 (Eliasson et al., 1987) for the production of ozone. It is now routinely used to produce very large quantities of ozone for water purification and bleaching.

In dielectric barrier discharge reactors, high voltages are applied between electrodes, one or both of which are covered with a thin dielectric layer such as glass

or alumina (Penetrante et al., 1995). The presence of the dielectric leads to the formation of a large number of micro-discharges that are statistically distributed with respect to space and time. The average discharge lifetime has been estimated to range between the order of microseconds and nanoseconds with electron energies of 1-20 eV (Eliasson et al., 1990).

Apart from the well-known application as ozonizers, silent discharge plasma has also been studied for hazardous waste treatment and removal of gaseous pollutants. It has been studied for the removal of gaseous pollutants such as NO_x , SO_x , CO_x and VOC (Fujii et al., 1993, Rosocha et al., 1993).

Chang et al. (1992) reported removal efficiencies of more than 95% of 150 ppm NO in a simulated flue gas using a repetitively pulsed or AC voltage in a cylindrical dielectric barrier discharge (DBD) reactor. It was noted that the removal efficiency was sensitive to gas temperature, gas composition, and power deposition. Removal of NO decreases under dry conditions with increasing oxygen concentration at 24°C , and, at elevated temperatures, increasing water vapor concentration and decreasing CO_2 concentration result in increasing NO removal efficiencies. Similar results were also obtained by Breault et al. (1993).

At concentrations of 1000-3000 ppm hydrocarbons and 200 ppm CCl_3CF_3 in air, Rosocha et al. (1993) reported 80-90% removal for all constituents. They found COCl_2 and COF_2 as the byproducts when dry air was used but no carbonyl halide

was observed with the addition of 2% water vapor. Greater destruction was reported at higher power input.

Modified versions of the DBD such as the dielectric-pellet bed reactor (Penetrante et al., 1995) and the surface discharge reactors (Masuda, 1993) are also used in these studies.

2.3 Corona Discharge

Corona discharge is a relatively low power electrical discharge that is created by applying a high electric potential between two electrodes of inhomogeneous geometry. Examples of electrode configurations include 1) point-plane, and 2) a coaxial wire within a pipe. The word "corona" takes its name ("crown") from mariners' observations of discharges from their ships' masts during electrical storms. The corona appears as a faint filamentary discharge radiating outward from the discharge electrode (Chang et al., 1991).

Depending on the polarity of the field, electrode geometrical configuration, and the characteristic of the power supply, corona discharges can be classified as DC positive coronas, DC negative coronas and pulsed coronas of both polarities.

For a positive corona in the point-plane electrode configuration, the first ionizing events observed are weakly luminous cathode-directed or positive streamers (also referred to as onset streamers). The current pulses associated with these

streamers occur irregularly in time and are called burst pulses (Creyghton, 1994). On further increase of the voltage setting, the discharge proceeds to a streamer corona leading to a glow corona and then to a spark discharge between the electrodes.

For negative corona in the point-plane geometry, the first ionization phenomenon produces regular current pulses known as Trichel pulses. The frequency of the Trichel pulses starts at about 2 kHz near corona onset and may attain a few MHz before the current becomes continuous which results in a pulse-less corona (Creyghton, 1994). A further increase in the voltage setting results in spark discharge.

Pulsed corona is created when a non-uniform electrode geometry is energized with high voltage (HV) pulses of short rise time (ns range) and short pulse width (μ s range). In a pulsed corona discharge (also called pulsed streamer discharge), short-lived discharge plasmas are created that consist of ions and energetic electrons. These energetic electrons in turn ionize the background gas molecules, producing radicals that initiate fast chemical reactions. The typical ionization energies of these electrons are about 10-15 eV.

There are several advantages of nanosecond rise time pulsing over DC energization. The brief application of voltage that allows the production of electrons does not raise the ion temperature, which means that less energy goes into heating the gas for a given electron concentration. Because of the higher electric field at

corona onset, the electron concentration can be orders of magnitude larger than under DC conditions. This helps in dispersing the electrons more uniformly throughout the reactor volume and aids in designing reactors with larger volumes (Chang et al., 1991). Pulsed corona reactors have been shown, both in laboratory and in industrial scale, to be effective in the removal of many types of gaseous pollutants.

Clements et al. (1989) developed a pulse energized electron reactor (PEER) which utilizes pulsed streamer corona for the combined removal of SO_2 , NO_x and particles from the flue gases. The pulsed streamer corona was generated by superimposing fast rising, narrow, high voltage pulses on a DC-basis voltage applied to a non-uniform field geometry. On humid air streams, PEER performance tests provided more than 90% removal of the SO_2 in the gas stream. The initial SO_2 concentration used in the study was 1000 ppm. It was found that using fly ash with a mean diameter of 5-10 μm improved the removal efficiency.

Control of NO_x by positive and negative pulsed corona discharges was demonstrated by Masuda and Nakao (1990). Their studies showed that the speed of NO_x removal by positive pulsing is more than an order of magnitude higher than that by negative pulsing. At a peak electric field intensity of 12 kV/cm, 100% NO removal from dry air containing 180 ppm NO, 800 ppm SO_2 , and 1000 ppm NH_3 was attained with positive pulsing for a gas residence time of 10 seconds. However, with negative pulsing, 25 seconds residence time was required even at a peak field intensity of 18 kV/cm in moist air (7.2 vol %) for 100% NO removal.

Civitano (1993) investigated the effect of pulse shape and electrode geometry on NO_x removal efficiency by changing the pulse shape, the electrode geometry, and the emitting wire geometry. It was noted that when the electrode geometry is composed of an emitting wire of 3 mm diameter and the outer cylinder had an inner diameter of 200 mm, the peak voltage was around 80-90 kV. However, when the outer cylinder diameter is reduced to 100 mm, the peak voltage was in the range 40-60 kV. Removal efficiency of SO_2 was 90% with an ammonia addition of a few ppm when the energy transferred to the gas was 12 Wh/Nm^3 . For this energy input, the NO_x removal efficiency was about 60% when the NO_x inlet concentration was around 250 ppm.

Experimental studies on NO_x removal utilizing dry, semi-wet, wet, and very-low temperature plasma reactors were carried out by Shimizu (1996). Gas conditions such as temperature and composition that affected the NO_x removal energy consumption were experimentally investigated. With the dry reactor, it was shown that NO_x removal from pollutant gases can be achieved using square wave voltages. The removal was found to be better at room temperature and the study showed that the use of ethylene as an additive to the flue gas enhanced significantly the NO_x removal efficiency.

Yamamoto et al. (1992) studied the removal of volatile organic compounds in a nanosecond pulsed corona reactor. They reported complete conversion of 50 ppm toluene after a residence time of 2.5 seconds regardless of the pulse repetition rate

and pulse voltage. With methylene chloride, 95% conversion was obtained after a retention time of 7.9 seconds for both high (1000 ppm) and low (500 ppm) concentration. The maximum removal efficiency obtained for CFC-113 was reported to be 67% with 500 ppm and 7.9 seconds residence time.

Industrial-scale experiments on the use of pulsed corona for the simultaneous removal of NO_x and SO_2 from flue gas have been performed in Italy (Civitano et al., 1993). A study was sponsored by the Japanese Ministry of International Trade and Industry to perform technical and economic assessment of the pulsed corona process for coal-burning utility boilers. The study committee concluded that this method deserves development as the next generation technology for the removal of SO_2 and NO_x in utility boiler plants (Masuda, 1993). Similar conclusions were reached upon by Mizuno et al. (1993), and Puchkarev and Gundersen (1997).

2.4 Reactor Model

Modeling of plasma discharges is a necessary complement for experimental investigation not only because it would help us understand the fundamental chemistry and physics governing the discharge but also contribute to the improvement of the performance of plasma devices. It requires information on a large range of chemical and physical phenomena that occur over a wide range of time and length scales (Alekseev et al., 1993, Creyghton, 1994) to attain a detailed

analysis of such system. Efforts have been made to couple these chemical and physical phenomena.

Alekseev et al. (1993) investigated the basic gas phase chemical kinetics aspects of DeNO/DeSO₂ processes occurring in the body of a single isolated streamer. For calculating the evolution of chemical systems behind the streamer head (also called the activation front), they considered 960 elementary gas-phase reactions among 80 species. The model considered ion-neutral reactions, ionic recombination, reactions of excited species, bimolecular neutral reactions, and termolecular reactions. They concluded that the removal of NO and SO₂ was determined by the concentrations of OH, HO₂, N, O, and O₃ produced in the pulsed corona discharge.

The model developed by Mukkavilli et al. (1988) for a multiple pin-plate electrostatic corona discharge reactor considered the complex and coupled interactions between the various ionic and excited species. The reactor was divided into a number of sections assuming a space charge-free field. The model accounted for the strong variation of the electric field strength from the tip of the cathode pin to the anode plate. In a dry air system, 58 reactions involving 27 species were considered in the mathematical model. Case studies of dry and wet air systems were presented but there were no comparisons with experimental results to confirm the model.

A fluid model based on a powerful finite element method for solution of charge carrier hydrodynamic equations in a cylindrical geometry, appropriate for modeling pulsed corona discharges used in flue gas treatment, was developed by Yousfi et al. (1993). The model was used to analyze the electron transport coefficient dependence on discharge parameters (distribution of space charge electric field, charged particle densities, and current densities). To check the sensitivity of their fluid model results to the temperature of the flue gas, they coupled the fluid model to a microscopic model that was based on a direct solution of the Boltzmann equation. They concluded that there are non-negligible consequences of gas temperature variation on fluid model results (densities of charge carriers and electric field distribution).

Detailed chemical kinetics models with electron-molecule interaction, electron-ion recombination, and reactions involving neutral and excited species have been developed (McFarlane and Wren, 1991, Lowke and Morrow, 1995, Penetrante et al., 1995). They involved solving the Boltzmann equation for the electron energy distribution function (EEDF) and calculating the electron-molecule reaction rates using collision cross-section data.

Boltzmann transport equation specifies the phase-space distribution function for a given assembly of particles. Phase-space is a six dimensional coordinate system found to be adequate in describing particle position and velocity distribution.

In the plasma study, the Boltzmann equation is solved to obtain the kinetic rate coefficients of the various inelastic electron-gas collision reactions and is given as

$$\frac{\partial f}{\partial t} + v \frac{\partial f}{\partial r} + g \frac{\partial f}{\partial t} = \left(\frac{\partial f}{\partial t} \right)_c \quad (2.1)$$

with

$$g = \frac{eE}{m} \text{ in the absence of magnetic field} \quad (2.2)$$

where e is the electron charge, E is the applied electric field, and m is the mass of an electron.

The above equation relates the local variation of the electron energy distribution function $[f(\epsilon)]$ with time to the variation of the same function with electron motion or drift in physical space, change in particle velocity resulting from an applied electric field, and the changes that occur due to collisions (Nasser, 1971, Mulkavilli et al., 1988).

It is difficult to solve the Boltzmann equation exactly. Statistical methods such as the Monte Carlo technique (Yousfi et al., 1994) are time consuming and often unnecessary for a successful description. The most widely used method for glow discharges in air at atmospheric pressure is the moment method in which a spherical-harmonic (Legendre series) two term approximation of the angular dependence of the velocity is assumed (Huxley and Crompton, 1974, McFarlane and Wren, 1991, Kalyana, 1996).

The resulting electron-energy distribution can then be used to calculate the kinetic rate coefficient of electron-gas collision reaction as follows:

$$K_{eij} = \sqrt{2/m_e} \int_0^{\infty} \sqrt{e} \sigma_{ij}(e) f_0(e) de \quad (2.3)$$

where m_e is the mass of electron, e is the charge of an electron and σ_{ij} is the collision cross section (McFarlane and Wren, 1991).

The collision cross section is a fundamental physical property that measures the probability of energy transfer resulting due to collision between an electron and a gas molecule. Its value is a function of the relative velocity of particles and the energy of electrons. These calculated rate constants are used along with the species continuity equation for predicting the behavior of various species.

Thus, modeling of corona discharges has consisted of two general areas: streamer propagation analysis and bulk phase chemical reaction analysis. There are inherent difficulties associated with such modeling. They are:

- 1) Estimation or measurement of the unknown parameters of the streamer structure and propagation,
- 2) Coupling streamer propagation models or pulse characteristics to subsequent bulk phase chemical reactions,
- 3) Acquiring accurate rate constants for bulk phase chemical reactions,

and

- 4) Determining the most important reactions, of the umpteen possibilities, that are important for the analysis.

These difficulties and inaccuracy caused by unknown model input data will remain. In order to get a better understanding of the essential processes taking place during the discharge, it seems more relevant to develop a simplified model that could give qualitative comparison with experimental data. Such an attempt is made in this present study and a detailed description of the model developed for our system is explained in Chapter 4.

CHAPTER 3

EXPERIMENTAL APPARATUS AND PROCEDURES

Our study was conducted on a wire-cylinder geometry pulse corona reactor. This chapter discusses in detail the power supply, the apparatus used, and the analytical techniques (instruments) employed.

3.1 Power Supply

The pulsed power supply used in this investigation is shown in Figure 3.1. Pulsed voltage was generated using a capacitor bank and a rotating spark gap. The power supply used was similar to the configuration used by Clements et al. (1989). The modified high voltage DC T-R set (transformer-rectifier) was able to produce 0-100 kV AC at 0-28 mA. The current produced by the T-R set next passes through a 333 k Ω resistors bank, and then through an array of diodes which acts as a half wave rectifier before charging a bank of capacitors (2700 pF) during the charging cycle. The current then passes through a mechanical rotating spark gap before entering the remaining part of the electric circuit.

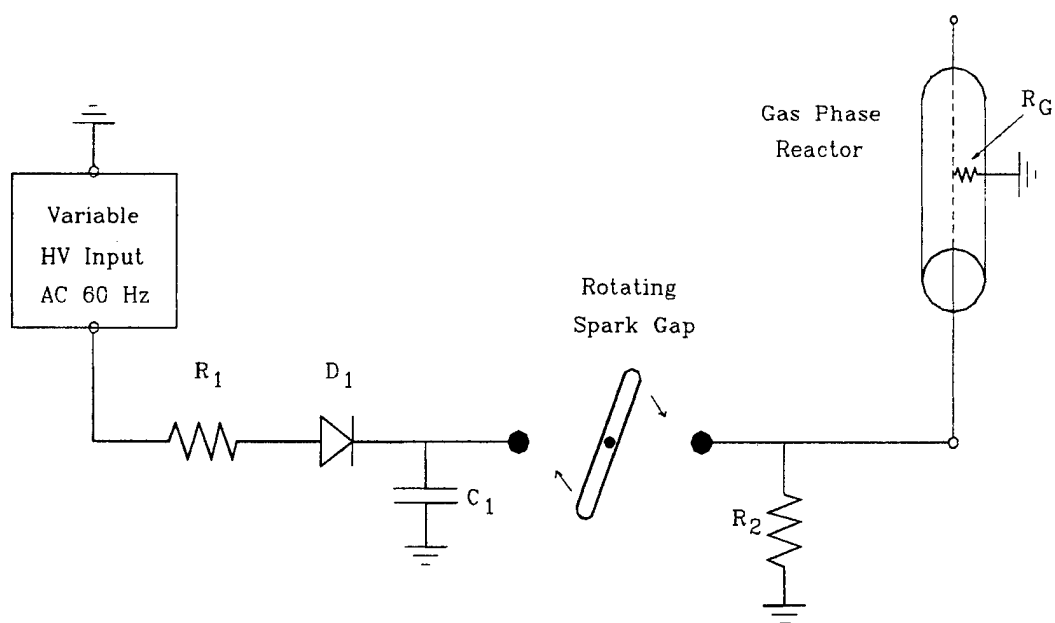


Figure 3.1 : Schematic Representation of the Power Supply

The mechanical rotating spark gap, synchronized with the AC current (60 Hz), is employed to discharge the capacitor bank twice per shaft revolution. It consisted of two spherical electrodes and a rotating rod electrode, both made of brass. The capacitors discharged whenever the rod electrode was aligned in line with the spherical electrodes. Part of the output from the spark gap passes through the central wire electrode in the reactor creating the pulsed discharge within the reactor. The other part passes through the load resistors (approx. $300\ \Omega$), which aids the gap to discharge. Two different sets of load resistors were used depending on the

diameter of the reactor used. The rotating spark gap was encased in an aluminum box for it was a source of electromagnetic interference.

3.2 Reactor Specifications

Two different sets of reactors were used in the study. One of the reactors (Reactor – I), shown in Figure 3.2, was used as a plug flow reactor, and the NO_x removal experiments were carried out in this reactor. The other reactor (Reactor – II), shown in Figure 3.3, was used as a closed batch reactor, and was used to carry out experiments with Halon 1211 and experiments with N^{15}O .

Reactor – I was a 4 inch ID and 18 inch long cylindrical stainless tube. A stainless steel wire of 0.109 inches diameter and 12 inches long was used as the high voltage electrode. The wire placed concentric to the grounded outer cylinder resulted in an electrode separation of 2 inches and an active pulsed corona treatment volume of 2.45 liters. The typical gas flow rate and residence time in the reactor ranges were from 5.1 SLM to 10.2 SLM and from 14 to 30 seconds, respectively.

Reactor – II was a stainless steel, 1 inch in diameter and 5.9 inches long, cylindrical tube. The stainless steel high voltage electrode, 0.6 inch in diameter with an effective wire length of 5 inches, was suspended concentric to the grounded outer cylinder resulting in an electrode separation of 0.42 inch. The active treatment volume was 45.4 ml and the reactor was used in a batch mode.

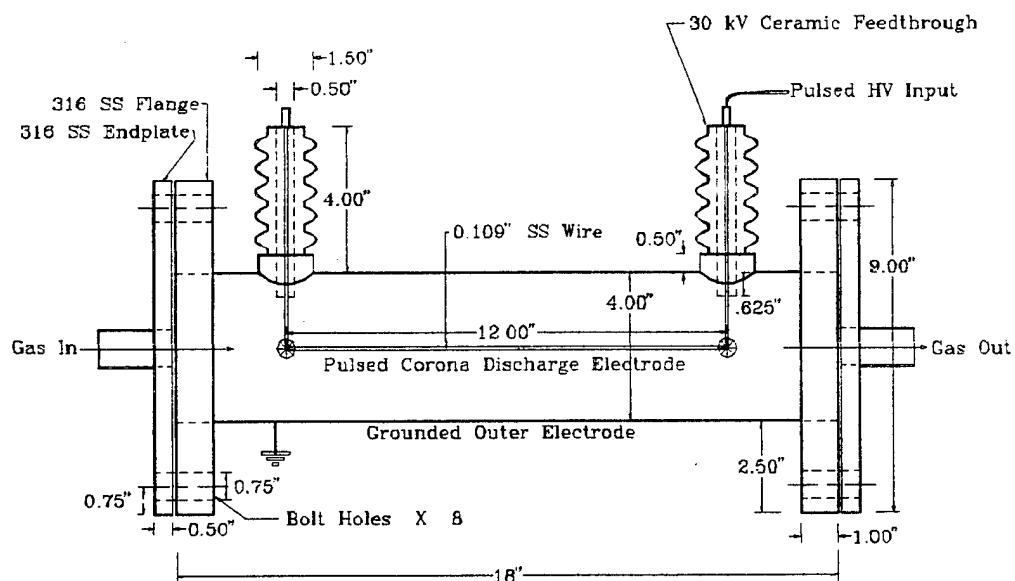


Figure 3.2 : Schematic Representation of Reactor - I.

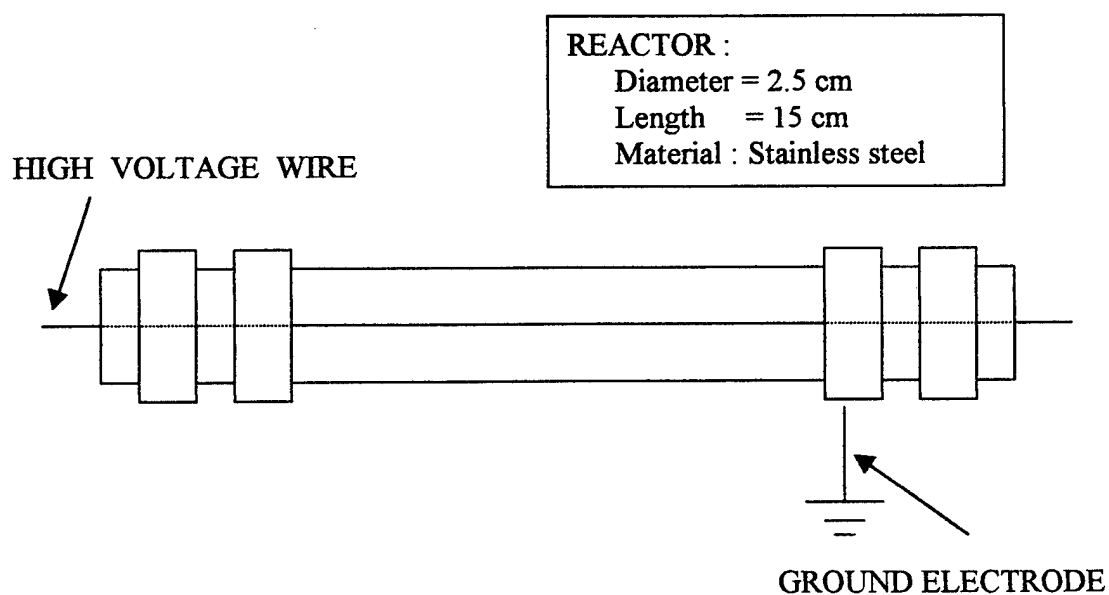


Figure 3.3 : Schematic Representation of Reactor - II.

3.3 Analysis

The outlet gas from the flow reactor was analyzed for NO, NO₂, O₃, and hydrocarbon breakdown products. Nitrogen oxides (NO and NO₂) were measured using a chemiluminescence NO-NO₂-NO_x analyzer (Thermo Environmental Instruments Inc., Model 42 H). For trace gas sample analysis, the outlet gases from the reactor were passed through a glass sampling vessel. The gases in the sampling vessel were analyzed using a GC for the concentration of ethylene, in experiments for which ethylene was present in the feed gas. Ozone concentration was determined by using the KI method. In this method, the ozone-containing gas was bubbled through a buffered solution of potassium iodide and the liberated iodine was measured by titrating with sodium thiosulphate. A Hewlett-Packard gas chromatograph/mass spectrometer (GC/MS) with a DBS methyl phenyl silicon oil column was used for the analysis of halon. This instrument is located in the Department of Chemistry at Florida State University.

When the batch reactor was employed for N¹⁵O experiments, the gas sample was analyzed on a Hewlett-Packard gas chromatograph/mass spectrometer (GC/MS) system and mass peak 28, 29, 30, and 31 molecular weights were monitored. After each analysis, a small amount of oxygen and water were added to the sample to remove the N¹⁴O and N¹⁵O from the observed 30 and 31 peak. The sample was then

reanalyzed on the GC/MS for all the above mentioned peaks. 500 ml gas bottles of $N^{15}O$ was obtained from Cambridge Isotope Laboratories, Inc., (Andover, MA).

The pulse waveform characteristics were measured using a Tektronix TDX 460 four channel digitizing oscilloscope with a P6015A 1000x high voltage probe and TCP202 AC/DC current probe. Both the probes were manufactured by Tektronix. A Cole-Parmer Trisense velocity/temperature/humidity meter was used to measure the gas temperature and humidity in the gas system.

3.4 Feed Gas System

The gas feed system along with the different analytical instrumentation and the reactor is shown in Figure 3.4. The feed gas system consisted of a set of carrier gases and a set of trace gases (added in ppm range). The carrier gases used in the study were compressed air and compressed nitrogen. Cylinders of compressed nitrogen were obtained from either Air Products or Holox (min purity 99.998%). Air supply from the engineering building was used as the source for compressed air. The air was passed through two laboratory gas drying units (calcium sulfate packed columns) and an air purifying system to remove any oil residue and moisture, before reaching the reactor. 1% NO in dry air and pure C_2H_4 in compressed gas cylinders were used as the trace gases.

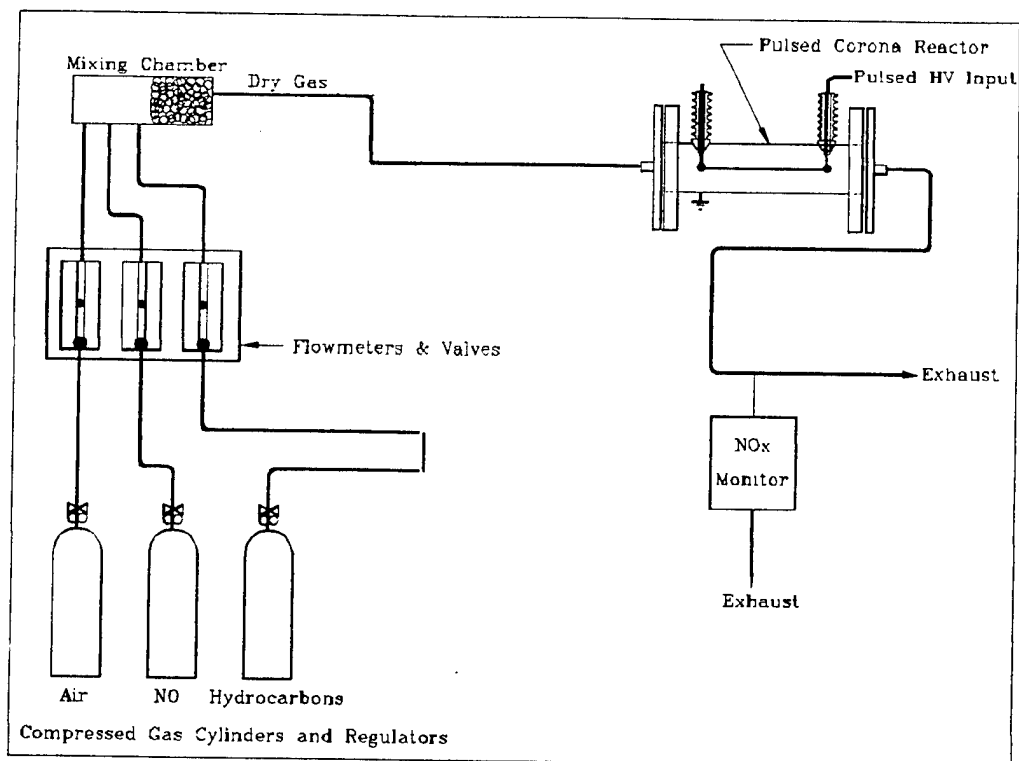


Figure 3.4 : Schematic Representation of the Feed System

The concentration of these components in the feed gas was in the ppm range (100–500 ppm). These gases and the regulators were manufactured by Air Products, Inc. (Allentown, PA).

The gas flows were monitored and controlled by flow meters and mass flow controllers. The flow meters (rotameter) were purchased from Dwyer, Inc. (Marietta, GA), and the mass flow controllers were purchased from MKS Instruments, Inc. (Andover, MA). The trace gases were controlled using a 1259C type of controller and the carrier gas was regulated using a 1559A mass flow

controller. The trace gases were mixed with the carrier gas before entering the reactor. This was accomplished by sending all the gases into a 23.5 inches long stainless steel mixing chamber that had a diameter of 2.5 inch.

3.5 Experimental Procedures

This section is divided into two sub-sections. In the first section, the experimental procedure adopted with the flow reactor is described and the second section gives a brief description of the procedure followed when the batch reactor was used.

Breakdown of NO in nitrogen and dry air was carried out in the flow system. The mass flow controllers and the NO_x analyzer were turned on at least 3 hours before the commencement of the experiments. This was required to let the instruments stabilize and to give stable and accurate readings. The NO_x analyzer was then calibrated using a sample of calibration gas. It was calibrated for NO and total NO_x concentration. Typically, 100 ppm of NO in N₂ obtained from Air Products, Inc., (Tamaqua, PA) was used as the calibration gas. The set points on the mass flow controllers were changed to the required values and the display was adjusted to zero when there was no flow of gases through them.

The feed air was delivered to the gas distribution system at 20 psig. The feed air was dried by passing it through a drying unit and was sent through a set of mass

flow controllers that controlled the flow to the reactor. In the rotating spark gap, the two spherical electrodes and the rod electrode were cleaned with sandpaper and ethanol to remove any oxidized matter on the metal. To ensure full charging of the capacitors by the power supply, the rotating rod was aligned perpendicularly to the discharge position using a strobe lamp (Digital Stroboscope Model 1965 manufactured by Ametek, Largo, FL) at a line frequency mode of 60 Hz.

The current probe and the voltage probe were connected to the reactor. The voltage probe was connected to the top of the ceramic insulator leading to the high voltage central wire electrode, and the current probe was attached across a wire connecting the outer cylinder of the reactor to the ground. The probes were connected to the oscilloscope and were used to measure different characteristics of the pulsed waveforms. The power supply was switched on once the flow rates of all the gases stabilized. The exhaust from the reactor was passed through the NO_x monitor. Readings from the NO_x monitor were taken at regular intervals until a steady concentration of NO and NO_x channel display was obtained. The characteristics of the voltage, current, and the power waveform were recorded from the oscilloscope. The voltage rise time, the peak voltage, the pulse width, the peak current, and the power input to the reactor were measured. When the ozone experiments were performed, the exhaust gas was sent to the ozone-analyzing unit and was disconnected from the NO_x analyzer.

Halon breakdown studies were carried out in a batch reactor. The reactor was filled with 1000 ppm of halon in synthetic air (<2 ppm H_2O , <1 ppm CO , and <1 ppm CO_2) at atmospheric pressure. Measured amounts of pure halon (97% Halon-1211 obtained from PCR, Inc., Gainesville, FL) was mixed with synthetic air (obtained from Air Products, Inc., Allentown, PA) in a 14 liters tank at 80 psig to get the required concentration of 1000 ppm. The tank was then connected to the reactor and the reactor was purged as a flow system for 10 min. Then, the reactor inlet and outlet were closed.

The central electrode was connected to the high voltage pulsed power supply and the outer cylinder was grounded. The voltage probe was connected to the end of the central electrode and the current probe was connected across the wire running to the ground. Experiments were carried out at different residence times (varying from 1 min to 15 min depending on the power density), peak voltages (23 kV, 25 kV and 27 kV), and power densities (0.66 kJ/l, 1.32 kJ/l and 2.65 kJ/l). A Hewlett-Packard gas chromatograph/mass spectrometer (GC/MS) with a DBS methyl phenyl silicon oil column was used for the analysis of halon.

When N^{15}O was used, the reactor was filled with N^{15}O in nitrogen. Concentrations of 5% and 10% N^{15}O were used. Samples of 5 ml or 10 ml were carefully extracted from the 500 ml gas bottles containing pure N^{15}O into a gas manifold. This was then mixed with pure nitrogen gas and the gas mixture was then expanded into the reactor. The reactor was vacuum checked for any gas leakage.

The central wire electrode was then connected to the high voltage power supply and the outer cylinder was grounded. The reactor was then subjected to the pulsed corona discharge for a time equaling the desired residence time in the reactor. Gas samples were extracted from the reactor and analyzed in a Hewlett-Packard GC/MS.

The power to the reactor was turned off once the required samples and readings were obtained. The reactor and the rotating spark gap were grounded using a grounding electrode as a precautionary measure to remove any accumulated charge.

CHAPTER 4

REACTOR MODELING

Pulsed corona discharge in a gaseous medium leads to the collision of free electrons and neutral gas molecules, resulting in the formation of new species including ions, metastable atoms, and free radicals. These products are chemically active and react with other gas molecules to form stable compounds. In this work, a simple reactor model was developed with the help of experimental data to consider the evolution of different molecular species during the pulsed corona discharge. This chapter discusses the model developed and gives a brief description of the software used.

The model solves the Boltzmann equation using KINEMA (Morgan, 1994), a commercially available software for calculating rate constants for electron-molecule collision reactions. The model then solves a set of ordinary differential equation using the software CHEMKIN (Kee et al., 1994) for predicting the concentration profile of the chemical species.

KINEMA, a plasma chemistry code, treats non-equilibrium electrons in a plasma environment by solving the Boltzmann equation on the fly as the chemistry evolves in time. The Boltzmann equation is solved by a time dependent code

(ELENDF) to give the electron energy distribution function for a given mixture of partially ionized gases. The code computes the mean electron energy, drift velocity, inelastic and super-elastic rate coefficients, and energy flow rates for the processes included in the calculation. Apart from the physical conditions of the system such as the pressure and temperature, the code requires the electron impact cross-sections of the concerned gaseous species. A detailed description of the code can be found elsewhere (Morgan and Penetrante, 1990).

In the current study, KINEMA is used to determine the field dependent rate coefficients of the electron-molecule collision reactions. Only electron-molecule collision reactions with major constituents (>1%) of the gas were considered. For example, the following reactions of electrons with nitrogen and oxygen molecules (referred to as initiation reactions) were considered in the case of an atmosphere of dry synthetic air.



Reactions (4.2) and (4.3) were not considered while modeling the reactor performance in a nitrogen atmosphere for the same reason mentioned above. The required cross-section data for molecular oxygen (O_2) was taken from the inbuilt library file and the cross-section data reported by Cosby (1993) was used for molecular nitrogen (N_2).

An earlier model developed by Kalyana (1996) coupled reactions (4.2) and (4.3), and so had only two electron-molecule collision reactions in the case of dry air. Moreover, both the rate constants were determined by fitting the model to the experimental data and KINEMA was not used to determine the field dependent rate constant. This led to discrepancies between model predictions and observed experimental results.

The electron concentration in a given reactor is not known without the solution of the detailed streamer model equation. Since each of the above reaction rates are functions of the electron concentration, the electron concentration is used as a single field dependent constant, empirically determined through fitting experimental data to the model. The output of the KINEMA program was used to determine the relative rates of reactions (4.2) and (4.3) to the rate of reaction (4.1). Therefore, only one adjustable constant, namely the effective electron concentration in the reactor, will be needed to predict the pseudo-first order rate constants $k_1[e]$, $k_2[e]$, and $k_3[e]$. These calculated rate constants were then incorporated into the input file of the software CHEMKIN.

CHEMKIN is a highly structured and modular package used for solving and interpretation of elementary gas-phase chemical kinetics problems (Kee et al., 1994). It requires the manipulation of a number of programs, subroutines, and data files. The package is composed of two blocks of FORTRAN code and two files:

- the Interpreter (code)

- the Gas-phase Subroutine Library (code)
- the Thermodynamics Database (file)
- the Linking File (file)

To solve a problem using CHEMKIN, it is necessary to write a FORTRAN code describing the set of governing equations for the system. The governing equation for a plug flow reactor model without axial dispersion or molecular diffusion is given by

$$\frac{dC_i}{dT} = \sum V_{ij} R_{ij} \quad (4.4)$$

where C_i is the concentration of species i , T is the residence time in the reactor, V_{ij} is the stoichiometric coefficient of the i th species in the j th reaction, and R_{ij} is the reaction rate.

The gas-phase subroutine library consisting of several subroutines relating to equations of state, chemical production, and thermodynamics was used for this purpose. The code used for our model was the same as that used by Kalyana (1996). However, as mentioned earlier, Kalyana (1996) had two variable parameters to fit the model to the experimental data, and in the present study, we had only one variable parameter, the average electron concentration.

A list of postulated reactions occurring in the system was prepared. The Interpreter then read these symbolic descriptions of the reaction mechanism and extracted the appropriate thermodynamic information for the species involved from

the thermodynamic database and stores the output in a binary file called the Linking file. This file contains all the required information about the elements, species, and reactions that occur in the system. Then the application code was run, calling the gas-phase subroutine libraries wherever necessary, to solve the set of governing equations.

The model solves a series of ordinary differential equations that are similar to the equation (4.4). The initial concentrations are read from an input file and then the code solves these differential equations to give the concentration profile of each species as functions of time.

Two different sets of reactions were used as input files to the CHEMKIN program. The reaction set was changed repeatedly to simulate the pulse-on and pulse-off aspects of the discharge. During the period of pulsing (pulse-on period), the average electron concentration was assumed to be fixed and the reaction set included the electron-molecule collision reactions. During the time between pulsing (pulse-off period), the electron concentration was assumed to be zero, and therefore the reaction set did not use the electron-molecule collision reactions. This was done using a shell program on a Unix operating system (Kalyana, 1996).

In the present model, the pulse width was assumed to be one microsecond and the time between two pulses was assumed to be 16.6667 milliseconds, which corresponds to a pulse frequency of 60 Hz. Hence, the reaction set with electron collision reactions was used to calculate the concentration profile for 1 microsecond

and the reaction set without electron collision reaction was used to calculate the concentration profile for the next 16.667 milliseconds. This was repeated until the final time in the reactor equaled the residence time in the reactor. This method was similar to the model used by Loiseau et al. (1994) for computing ozone production in a cylindrical oxygen-fed ozonizer, and by McFarlane and Wren (1991) for modeling electric discharges.

The set of reactions used for NO removal in nitrogen and dry air is given in Table: 4.1. The rate constants for these reactions were obtained from the literature and were crosschecked with the NIST Database (NIST Chemical Database 17, version 6.01, 1994). The criterion for choosing the reactions was to consider reactions of neutral species having rate constants greater than 1.0×10^7 . The rate constants of the initiation reactions (reactions 4.1-4.3) were obtained from experimental data.

The following assumptions were made for the model developed:

- 1) Isothermal System: Pulsed streamer corona plasma is a nonthermal plasma.

The majority of the electrical energy goes into the production of energetic electrons rather than into gas heating. Thus, it was assumed that the gas molecules in the reactor were not appreciably heated during the residence time in the reactor.

- 2) Uniform Electron Density: An equilibrium concentration of electron was assumed during the pulse-on period. Spatial variation of the electron density was not considered in this model.
- 3) Plug Flow Model: The model does not account for axial and radial dispersion in the reactor. The model was compared with experimental data collected at steady state. Hence, it is assumed that the model describes the performance of a steady state corona reactor.
- 4) Effective Field Strength: The streamer is known to have a high field region in the streamer head and a low field region in the streamer channel. However, an attempt is made to characterize the system on a macroscopic scale by calculating an "effective field strength" from the measured values of peak voltage as follows

$$\text{Field Strength} = (\text{Peak Voltage}) / (\text{Electrode Separation}).$$

- 5) Although ionization takes place during corona discharge, it was assumed in the present model that the ions do not play a major role in the chemistry of the neutral gas molecules. This assumption is valid because the corona reactor operates in the range of 25 to 48 Td and ionization generally is significant only above 50 Td (Lowke and Morrow, 1995).

Table 4.1 : List of Chemical Reactions Considered for Modeling

Chemical Reaction	Rate Constant ($\text{cm}^3 \cdot \text{mole}^{-1} \cdot \text{sec}^{-1}$)	Source	Number:
$\text{N}_2 \rightarrow 2\text{N}$	$K_1[\text{e}]$	Expt. Data	[1]
$\text{O}_2 \rightarrow \text{O} + \text{O}$	$K_2[\text{e}]$	Expt. Data	[2]
$\text{O} \rightarrow \text{O}(^1\text{D})$	$K_3[\text{e}]$	Expt. Data	[3]
$\text{N} + \text{N} \rightarrow \text{N}_2$	$6.38 \text{ E}+10$	Willis & Boyd, 1976	[4]
$\text{N} + \text{O} \rightarrow \text{NO}$	$1.45 \text{ E}+11$	Willis & Boyd, 1976	[5]
$\text{N} + \text{O}_2 \rightarrow \text{NO} + \text{O}$	$5.36 \text{ E}+07$	Atkinson et al., 1989	[6]
$\text{N} + \text{NO} \rightarrow \text{N}_2 + \text{O}$	$2.04 \text{ E}+13$	Willis & Boyd, 1976	[7]
$\text{N} + \text{NO}_2 \rightarrow 2\text{NO}$	$1.81 \text{ E}+12$	Atkinson et al., 1989	[8]
$\text{N} + \text{NO}_2 \rightarrow \text{N}_2\text{O} + \text{O}$	$1.81 \text{ E}+12$	Atkinson et al., 1989	[9]
$\text{O} + \text{O} \rightarrow \text{O}_2$	$1.02 \text{ E}+11$	Willis & Boyd, 1976	[10]
$\text{O} + \text{O}_2 \rightarrow \text{O}_3$	$1.69 \text{ E}+12$	Atkinson et al., 1989	[11]
$\text{O} + \text{O}_3 \rightarrow 2\text{O}_2$	$4.81 \text{ E}+09$	Willis & Boyd, 1976	[12]
$\text{O}(^1\text{D}) + \text{O}_3 \rightarrow 2\text{O}_2$	$1.45 \text{ E}+14$	Atkinson et al., 1992	[13]
$\text{O}(^1\text{D}) + \text{O}_3 \rightarrow 2\text{O} + \text{O}_2$	$1.45 \text{ E}+14$	Atkinson et al., 1992	[14]
$\text{O}(^1\text{D}) + \text{N}_2\text{O} \rightarrow \text{N}_2 + \text{O}_2$	$2.95 \text{ E}+13$	DeMore et al., 1987	[15]
$\text{O}(^1\text{D}) + \text{N}_2\text{O} \rightarrow 2\text{NO}$	$4.03 \text{ E}+13$	DeMore et al., 1987	[16]
$2\text{NO} + \text{O}_2 \rightarrow 2\text{NO}_2$	$7.09 \text{ E}+09$	Atkinson et al., 1992	[17]
$\text{NO} + \text{O}_3 \rightarrow \text{NO}_2 + \text{O}_2$	$1.09 \text{ E}+10$	Atkinson et al., 1992	[18]

Chemical Reaction	Rate Constant (cm ³ . mole ⁻¹ . sec ⁻¹)	Source	Number:
$\text{NO} + \text{O} \rightarrow \text{N} + \text{O}_2$	2.77 E+09	DeMore et al., 1987	[19]
$\text{NO} + \text{O} + \text{N}_2 \rightarrow \text{NO}_2 + \text{N}_2$	3.27 E+16	DeMore et al., 1987	[20]
$\text{NO} + \text{NO}_3 \rightarrow 2\text{NO}_2$	1.74 E+13	DeMore et al., 1987	[21]
$\text{NO} + \text{NO}_3 \rightarrow 2\text{NO} + \text{O}_2$	1.83 E+11	Sutherland et al., 1975	[22]
$\text{NO}_2 + \text{O}_3 \rightarrow \text{NO}_3 + \text{O}_2$	1.92 E+07	Atkinson et al., 1989	[23]
$\text{NO}_2 + \text{O} \rightarrow \text{NO} + \text{O}_2$	5.84 E+12	Atkinson et al., 1989	[24]
$\text{NO}_2 + \text{NO}_3 \rightarrow \text{NO}_2 + \text{NO}$			
+ O ₂	6.45 E+08	Baulch et al., 1983	[25]
$\text{N}_2\text{O}_4 + \text{M} \rightarrow 2\text{NO}_2 + \text{M}$	2.06 E+09	Baulch et al., 1983	[26]
$2\text{NO}_3 \rightarrow 2\text{NO}_2 + \text{O}_2$	1.92 E+08	Baulch et al., 1983	[27]
$\text{NO}_3 + \text{O} \rightarrow \text{NO}_2 + \text{O}_2$	1.02 E+13	DeMore et al., 1987	[28]
$\text{O}_3 + \text{N} \rightarrow \text{NO} + \text{O}_2$	6.02 E+07	Baulch et al., 1983	[29]
$2\text{NO}_2 + \text{M} \rightarrow \text{N}_2\text{O}_4 + \text{M}$	5.08 E+14	NIST	[30]
$\text{NO}_2 + \text{O} \rightarrow \text{NO}_3$	1.29 E+12	Atkinson et al., 1989	[31]
$\text{O}(^1\text{D}) \rightarrow \text{O}$	6.95 E+08	DeMore et al., 1987	[32]
$\text{O}(^1\text{D}) + \text{O}_3 \rightarrow \text{O} + \text{O}_3$	1.45 E+14	NIST	[33]
$\text{O}(^1\text{D}) + \text{NO}_2 \rightarrow \text{NO} + \text{O}_2$	2.95 E+13	Schofield, 1979	[34]

CHAPTER 5

EXPERIMENTAL RESULTS & DISCUSSION

5.1 Physical Characteristics of the Discharge

The most significant physical parameters of a pulsed corona discharge are obtained from the current and voltage measurements. The parameters of interest include the corona onset voltage, the peak voltage, the pulse rise time, the pulse width, the pulse current and the power input to the reactor.

The corona onset voltage is dependent upon the geometry of the reactor and the chemical composition of the gases in the reactor. In an atmosphere of dry air, the onset voltage for Reactor - I (Figure 3.2) was in between 15 and 18 kV, and it was close to 8 kV for Reactor - II (Figure 3.3). In a nitrogen atmosphere, the onset voltage dropped to about 12 kV for Reactor - I. Below the onset voltage, insignificant voltage and current readings were measured at the reactor. The current readings increased dramatically once the onset voltage was crossed. Spark over or electrical breakdown occurred above 60 kV for Reactor - I and above 25 kV for Reactor - II. The current and voltage waveforms are shown in Figures 5.1 and

Figure 5.2 respectively. For Reactor - I, the rise time of the voltage pulse varied between 25 and 35 nanoseconds, and the pulse width at half-maximum of the voltage

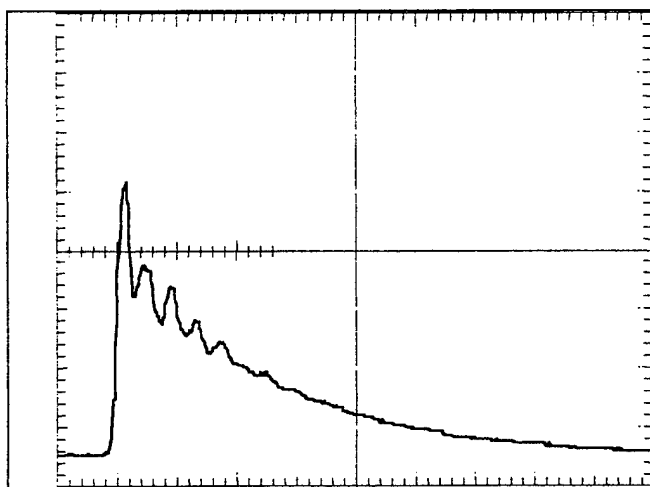


Figure 5.1 : Typical Voltage Waveform Obtained during Corona Discharge for Reactor - I.

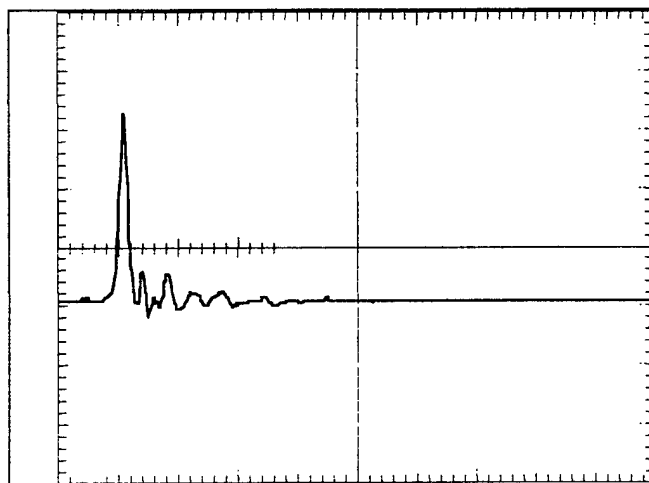


Figure 5.2 : Typical Current Waveform Obtained during Corona Discharge for Reactor - I.

pulse varied from 500 to 700 nanoseconds. On the other hand, the rise time varied from 25-30 nanoseconds and the pulse width was around 50-150 nanoseconds for Reactor - II. Table 5.1 gives the peak voltage as measured by the voltage probe for both Reactor - I and Reactor - II in dry air.

Table 5.1 : Peak Voltage as a Function of Dial Setting for Reactor- I and Reactor- II for Dry Air.

REACTOR - I		REACTOR - II	
Dial Setting (kV)	Peak Voltage (kV)	Dial Setting (kV)	Peak Voltage (kV)
30	40	16	23
35	44	18	25
40	49	20	27

Energy input to the reactor was varied by changing the voltage setting. The pulse frequency was maintained constant at 60 Hz for all the experiments. The power input to the reactor was calculated by multiplying the current and the voltage waveforms. The energy input varied from 30 mJ/pulse to 90 mJ/pulse for Reactor - I, and from 4 mJ/pulse to 17 mJ/pulse for Reactor - II as shown in Table 5.2.

Table 5.2 : Energy Input as a Function of Peak Voltage for Reactor - I and Reactor - II in Dry Air.

REACTOR - I		REACTOR - II	
Peak Voltage (kV)	Energy Per Pulse (mJ/pulse)	Peak Voltage (kV)	Energy Per Pulse (mJ/pulse)
40	31	23	4
44	54	25	12
49	87	27	17

The remaining part of this chapter will concentrate on the removal of traces (in ppm range) of NO and halon in different atmospheres.

5.2 NO Removal in Nitrogen

Experiments were conducted in an atmosphere of nitrogen at three different peak voltages (40, 44, and 49 kV) and for different residence times (14, 20, 24, and 30 seconds). All the experiments were repeated at least three times for error analysis.

Starting with an initial concentration of 100 ppm NO in N₂, it was found that the NO concentration decreased with residence time at a fixed field strength. Figure

5.3 shows the NO removal efficiency at different field strengths as a function of residence time. There was less than 5% breakdown at 40 kV. For a residence time of 30 seconds, the total NO removal was only 9 ppm. When the peak voltage was increased, there was an increase in the percentage removal of NO. The percentage removal was about 42% for a residence time of 24 seconds at 44 kV and it increased to about 60% when the peak voltage was increased to 49 kV. A slight increase in the concentration of NO₂ was noticed, but it was not substantial enough to compensate for the removal of NO by the oxidation step.

Figure 5.4 is a plot of the NO₂ concentration as a function of residence time. 5-10 ppm of NO₂ was formed from 100 ppm of NO, indicating that the remaining NO was reduced back to molecular nitrogen and molecular oxygen states. The following mechanism is proposed for NO breakdown in an atmosphere of N₂.



The atomic nitrogen required for NO removal is produced by the collision of electrons with the gas molecules and the NO is then reduced to molecular nitrogen as given by reaction (5.2).

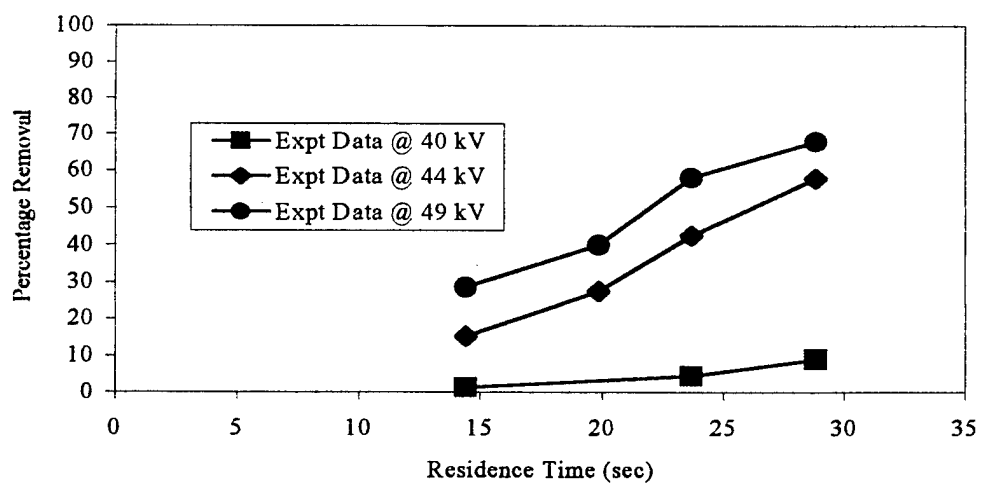


Figure 5.3 : Percentage NO Removal as a Function of Residence Time in an Atmosphere of Nitrogen

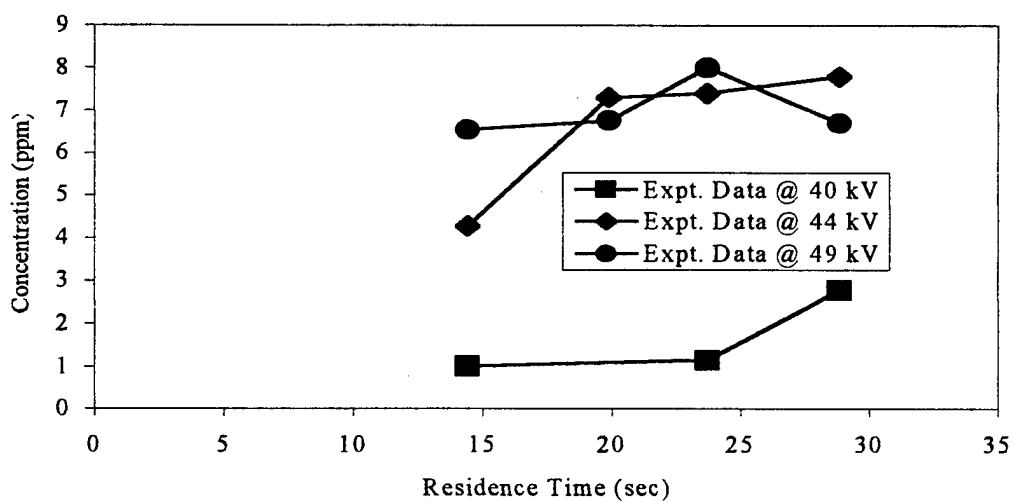


Figure 5.4 : NO₂ Formed in an Atmosphere of Nitrogen

Model comparison of NO removal in nitrogen with experimental data is shown in Figure 5.5. About 8 ppm of NO_2 is formed at 44 kV and a residence time of 30 seconds. The NO_2 concentration decreases with increases in residence time at higher field strengths. At 49 kV and a residence time of 60 seconds, the model predicts complete removal of NO_2 (Figure 5.6). The model was developed with 10 neutral species and 25 reactions. The products predicted by the model at a peak voltage of 49 kV are shown in Figure 5.6. The rate constant for reaction (5.1) was determined by fitting the model to the experimental data. As seen in Figure 5.7, the rate constant increased with increase in field strength. This was due to the increase in electron density and the rate coefficient of electron-molecule collision reactions with increase in field strength.

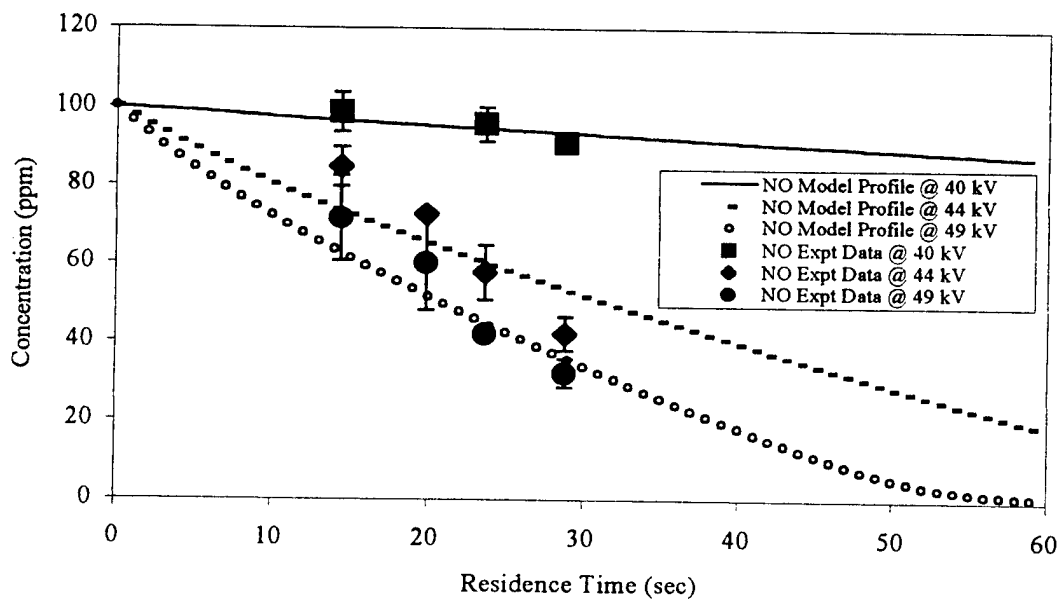


Figure 5.5 : NO Model Concentration Profile in an Atmosphere of Nitrogen

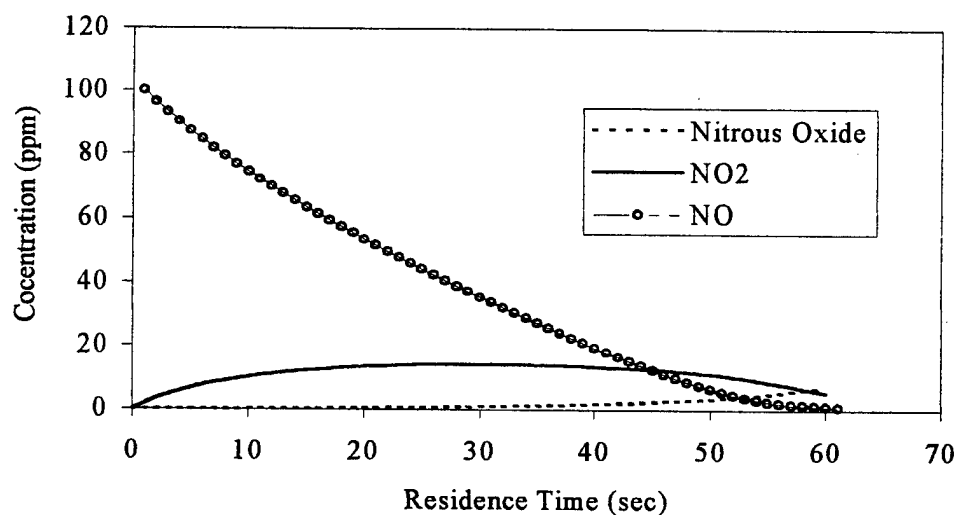


Figure 5.6 : Model Prediction of by-products at 40 kV in an Atmosphere of Nitrogen

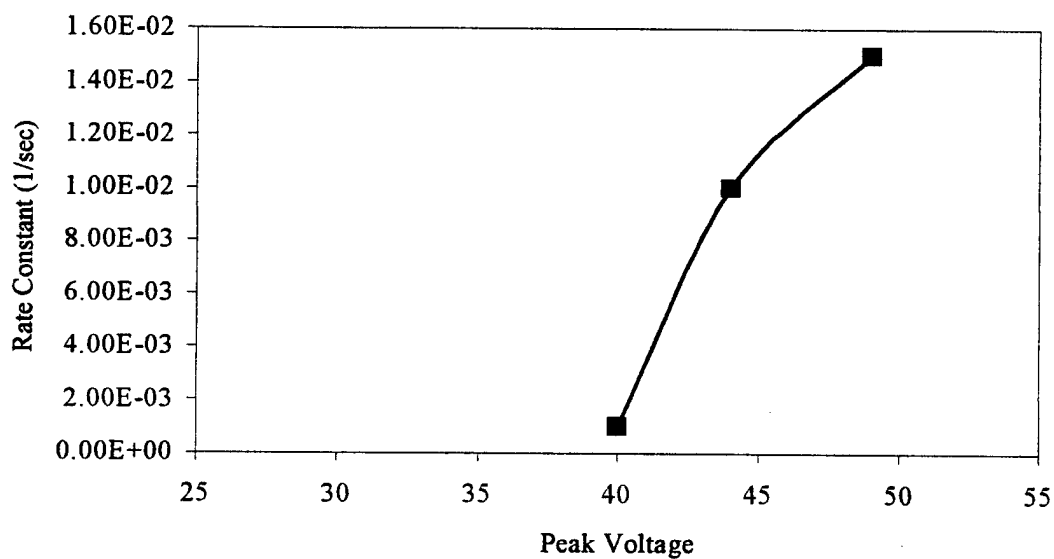


Figure 5.7 : Rate Constants for N_2 Dissociation in an Atmosphere of Nitrogen

Penetrante et al. (1995) compared different types of electrical discharge techniques for non-thermal plasma processing of NO in N₂. With a blended gas mixture of 100 ppm NO in N₂, they were able to achieve 80% breakdown for an input energy density of 80 J/l. The gas temperature was maintained at 100°C. Their model was developed with 287 reactions involving 37 species, and was found to be in good agreement with the experiment for input energy densities below 100 J/l. Model predictions indicated that the removal of NO was dominated by the reduction reaction (5.2). It was reported that in the NO-N₂ mixture, the measured energy cost for NO reduction by discharge processing is about 240 eV per NO molecule.

Theoretical analysis of NO_x removal in a pulsed operation of electrostatic precipitators was carried out by Lowke and Marrow (1995). They concluded that the main pathway for NO and NO₂ removal was the chemical reduction of these oxides to molecular nitrogen. Similar pathways were suggested by Kalyana (1996).

5.3 NO Removal in Dry Air

The effect of oxygen concentration on NO removal was studied by performing experiments in an atmosphere of dry air that typically contained 21% oxygen. NO removal experiments were carried out at four different residence times (14, 20, 24, and 30 seconds) and at peak voltages of 40, 44, and 49 kV.

Figure 5.8 shows the NO removal data as a function of residence time. At a peak voltage of 40 kV, the NO removal efficiency was less than 10% even for the longer residence time of 30 seconds. However, when the peak voltage was increased to 44 kV, there was 37% removal for a residence time of 15 seconds. For longer residence times the removal efficiency increased linearly to about 100% at 44 kV. Further increases in the peak voltage to 49 kV, increased the removal efficiency and greater than 95% removal was obtained for a residence time of 24 seconds.

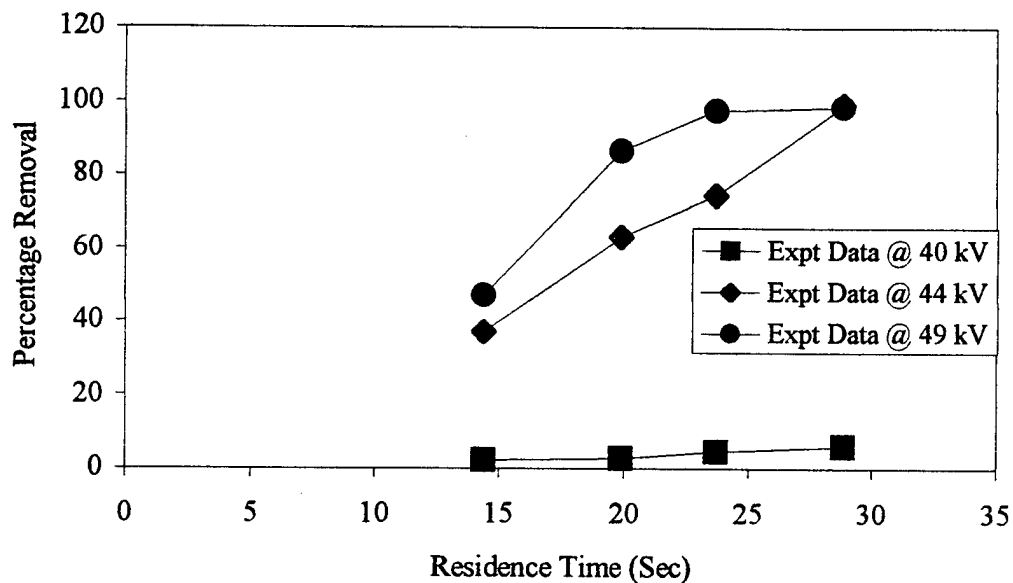


Figure 5.8 : Percentage NO Removal in an Atmosphere of Dry Air

The breakdown of NO was supplemented by the formation of NO₂. As shown in Figure 5.9, the NO₂ concentration increased monotonically for higher field strengths until it reached a maximum of 100 ppm and no breakdown of NO₂ was noticeable at 49 kV even for longer residence times. At lower field strengths, the NO₂ concentration increased with increases in reactor residence time.

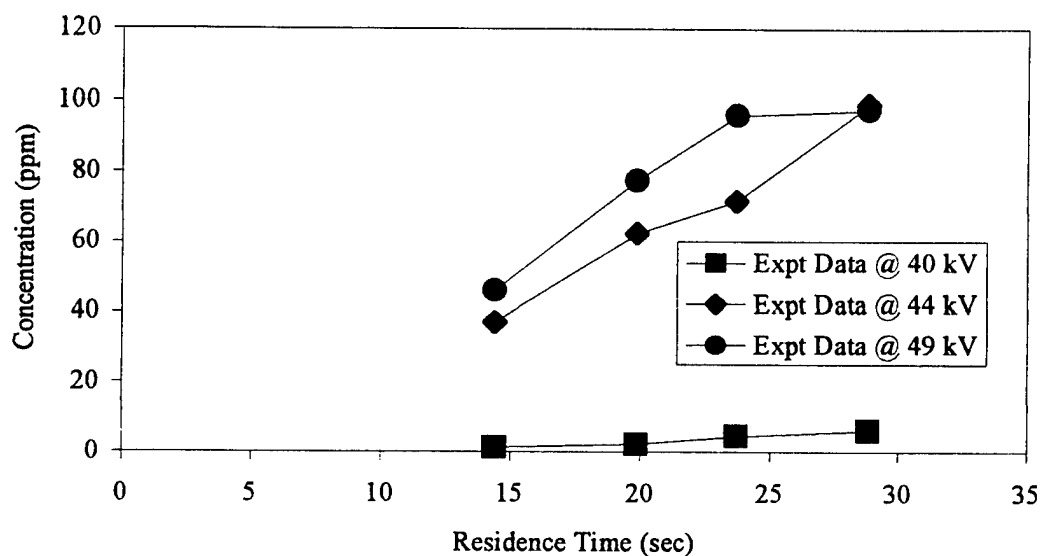
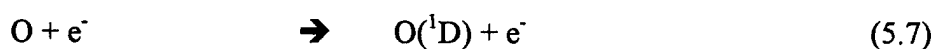
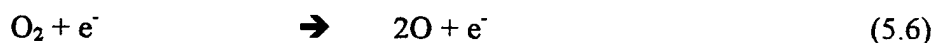
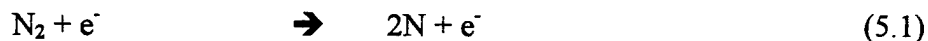


Figure 5.9 : NO₂ Formed in an Atmosphere of Dry Air

The energy consumption ranged from 95 eV per NO molecule removed at a peak voltage of 44 kV and a residence time of 29 seconds, to 172.9 eV per NO molecule removed at a peak voltage of 49 kV and a residence time of 14.8 seconds. The energy consumption was 130.71 eV/molecule at 49 kV and a residence time of

24 seconds. These corresponding values ranged from 6.5 to 11.5 gms of NO removal per kWh of power input to the reactor.

The experimental data points were used to predict the electron density in the reactor, and thence, the rate constants of the initiation reactions.



The electron density was also calculated independently from the current waveform. The current waveform was integrated for a time equaling the pulse width to estimate the total charge produced for a single pulse in the reactor and then the electron density. Figure 5.10 compares the electron densities calculated from the current waveform with the value obtained from the model.

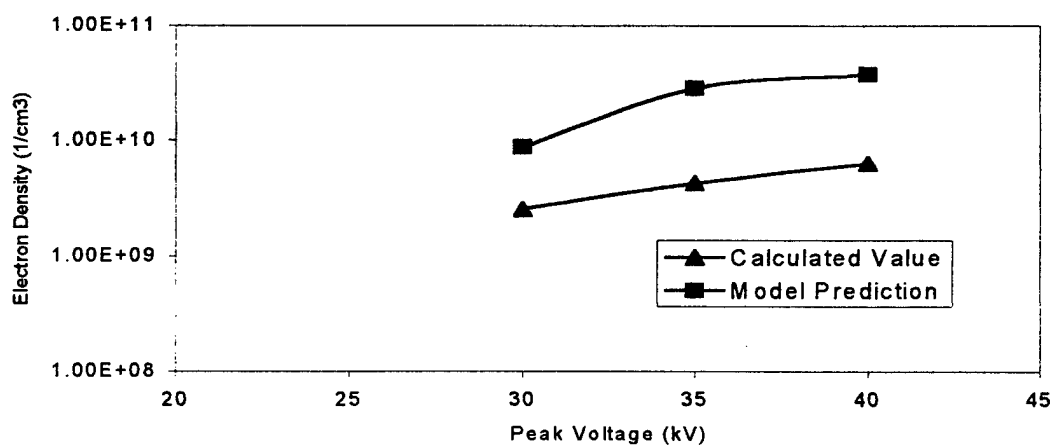


Figure 5.10 : Comparison of Electron Densities

The current waveform characterizes the current flowing through the external circuit during the pulse-on period. The differences between the calculated and predicted values of electron densities, thus suggest that the electron density (hence number of electrons) within the reactor was slightly higher than the number of electrons flowing in the external circuit. In idealistic scenario, all the electrons produced in the reactor must end up being measured by the current probe. However reactions such as the electron-attachment reaction lead to loss of electrons and would result in the formation of ions such as O^- (Chang et al., 1991, Lowke and Morrow, 1995). Such reactions were not considered in the model because ionization is significant only above 50 Td (Lowke and Morrow, 1995). The other probable reasons for the discrepancy are 1) the variability of the known rate constants of neutral gas-phase reactions and 2) the inconsistencies associated with the cross-sectional data for electron-gas collision reactions. However, it is significant to note that the calculated and the predicted values of the electron densities are of the same order of magnitude.

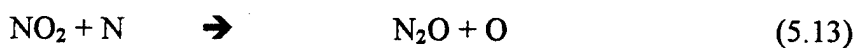
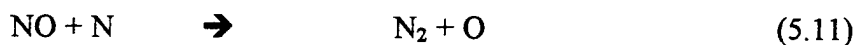
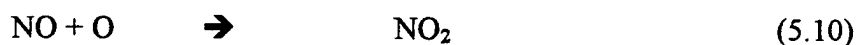
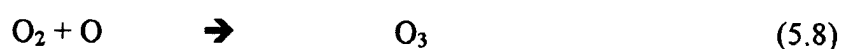
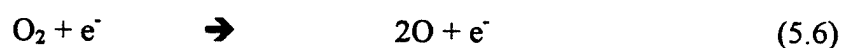
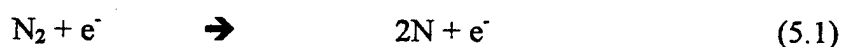
The pseudo first order rate constants (k_{1e} , k_{2e} , and k_{3e}) used in the model are plotted as functions of peak voltages in Figure 5.11 and Figure 5.12. The rate constant for nitrogen dissociation increased with increases in the peak voltages. It increased from 6×10^{-7} to 4×10^{-5} when the peak voltage was increased from 40 to 49 kV. This was due to the increase in the electron density and the rate constants of electron-molecule collision reactions (Equation 2.3) with increases in the field

strength. Oxygen dissociation rate constants were almost four orders of magnitude greater than the rate constants for nitrogen dissociation. Although the electron densities are the same, the rate constant k_3 does not increase by the same extent as k_2 , when the peak voltage is increased from 44 to 49 kV. This leads to a flattened curve for the rate constant of reaction (5.7) at higher peak voltages.

The model fit of the experimental data for NO is shown in Figure 5.13 and for NO₂ is shown in Figure 5.14. It is seen that the model fits the NO removal data closely and predicts the NO₂ concentration within experimental errors. The model concentration profile of the by-products is shown in Figure 5.15.

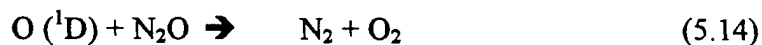
Both the model and experimental data indicate that most of the NO oxidizes to NO₂ and the model predicts less than 1 ppm of N₂O for longer residence time.

The probable mechanism could be



With an increase in the concentration of oxygen, electron collision reactions with O_2 increases leading to reaction (5.6) which was absent in an atmosphere of nitrogen. This reaction which leads to the formation of atomic oxygen has a higher rate constant than reaction (5.1). An increase in concentration of oxygen species increases the reaction rates of reactions (5.10) and (5.12) and the reaction rate of (5.11) apparently decreases because of a decrease in the concentration of NO. Thus, we have almost complete oxidation of NO to NO_2 . O_3 and N_2O predicted by the model results are due to reaction (5.8) and reaction (5.13).

The amount of N_2O predicted by the model was lower compared to the amount predicted in an atmosphere of nitrogen. This is due to the reaction of N_2O with $O(^1D)$ given by reaction (5.14) and (5.15).



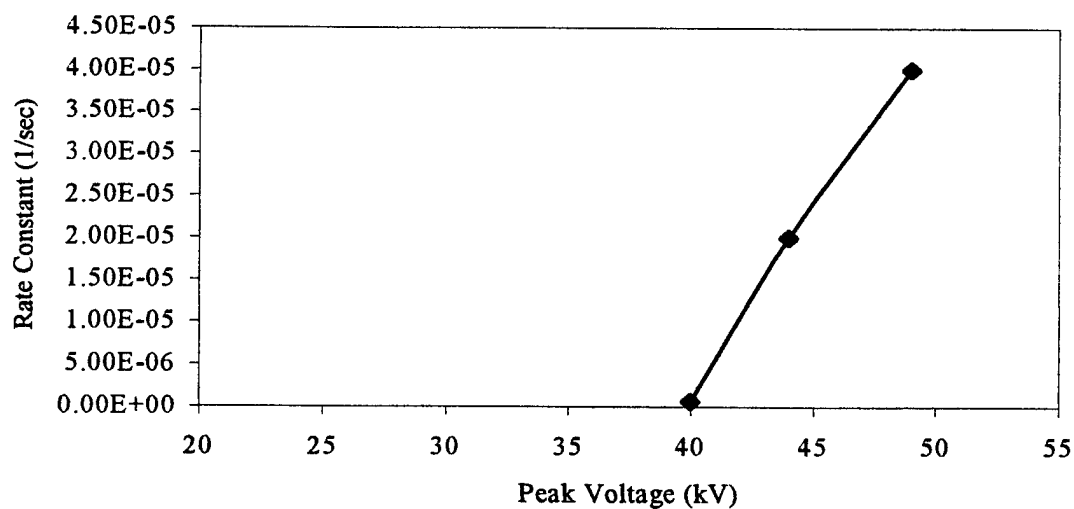


Figure 5.11 : Rate Constants for Nitrogen Dissociation in an Atmosphere of Dry Air

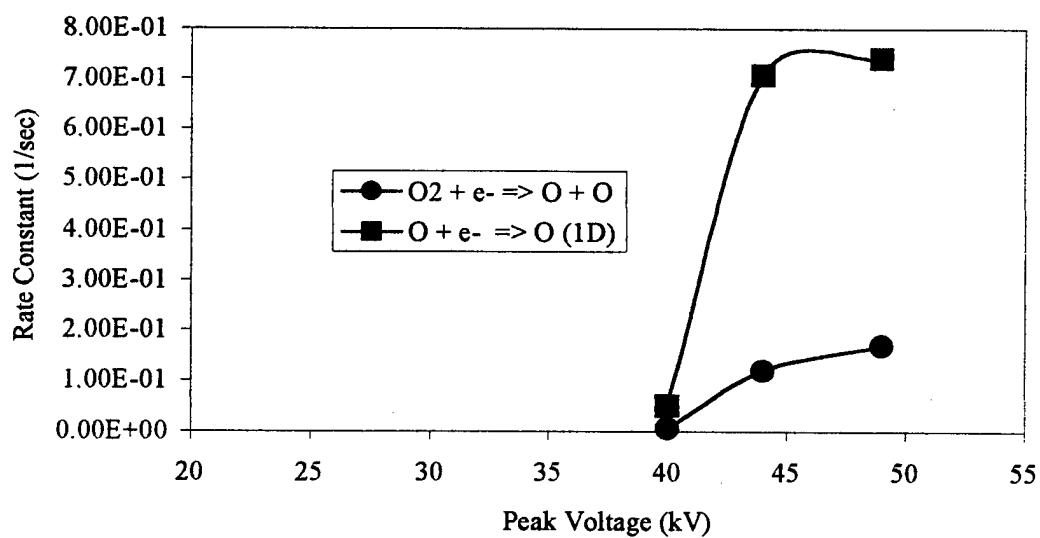


Figure 5.12 : Rate Constants for Oxygen Dissociation in an Atmosphere of Dry Air

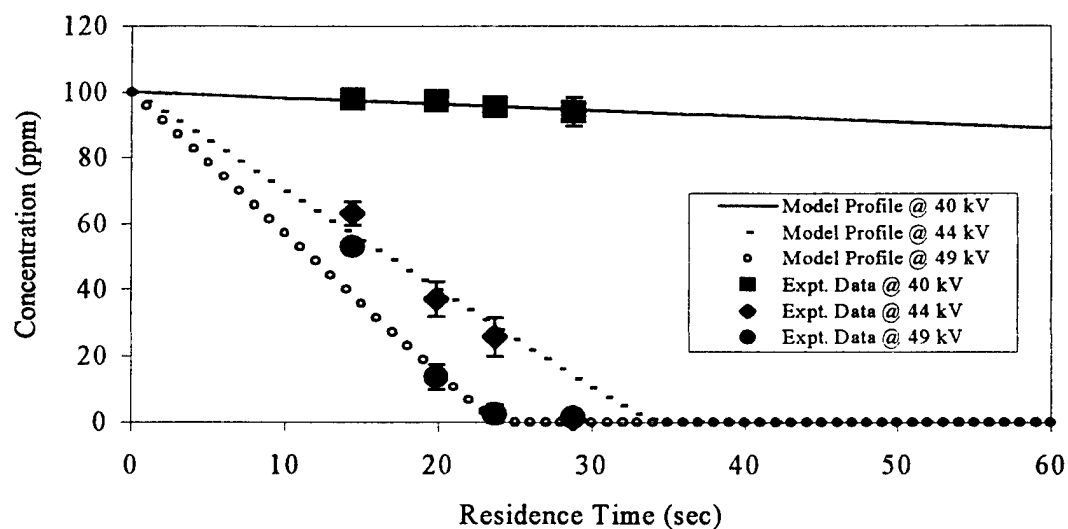


Figure 5.13 : NO Model Concentration Profile in an Atmosphere of Dry Air

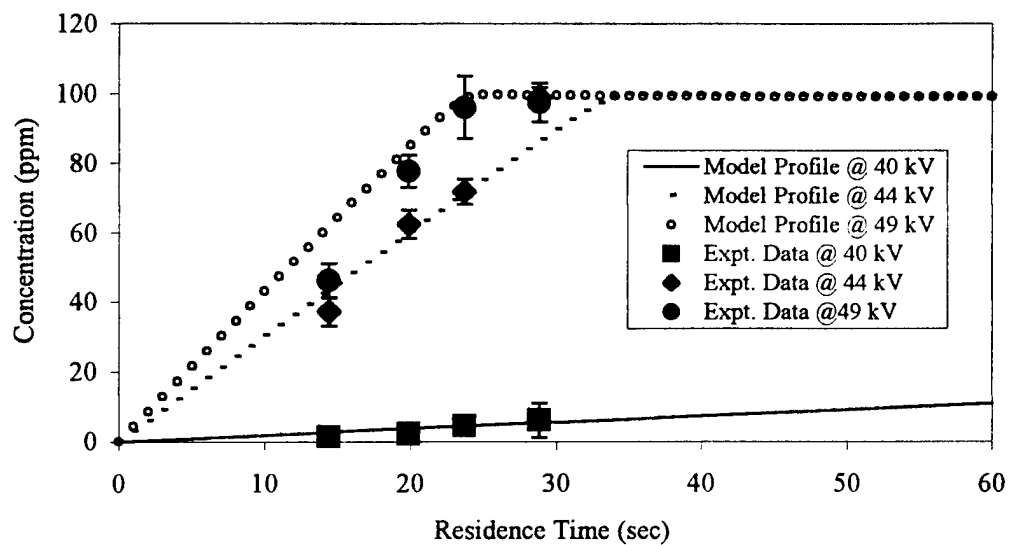


Figure 5.14 : NO₂ Model Concentration Profile in an Atmosphere of Dry Air

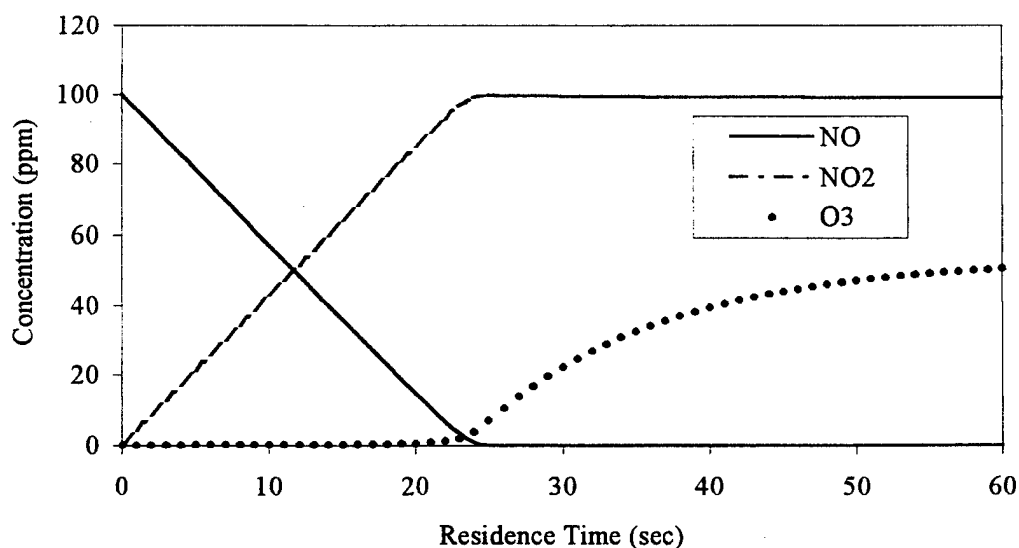


Figure 5.15 : Model Profiles of Different Species at a Peak Voltage of 49 kV in an Atmosphere of Dry Air

Masuda and Nakao (1990) reported that NO oxidized to NO₂, and that the latter was converted to other substances after the onset of pulse-induced corona in air. The total NO_x concentration remained unchanged until a critical peak field intensity was reached and beyond this, NO_x removal was noticed. With positive pulsing at $E = 12$ kV/cm in dry air containing NO (180 ppm), SO₂ (800 ppm), and NH₃ (1000 ppm), they attained 100% NO removal for a residence time of 10 seconds. They also concluded that the addition of NH₃ did not affect NO oxidation but enhanced NO₂ removal.

NO removal in a pulsed streamer corona generated by a square wave voltage was studied by Mizuno et al. (1993). Starting with 600 ppm of NO and 30 ppm of NO₂, they reported a removal rate of around 20% when the power input was 30 W at 30°C. This was obtained with a gas flow rate of 8 l/min and a residence time of 0.14 seconds in the reactor. For the same flow rate and an initial concentration of 150 ppm of NO, they attained 90% removal at a power input of 35 W.

Altogether, 34 reactions involving 11 neutral species were required to characterize our system. Earlier models developed by Penetrante (1995) required 287 reactions involving 37 species to characterize the N/O system. Mukkuvalli (1988) considered 18 electron-gas and 40 ion-molecule reactions involving N₂, O₂, and NO_x, totaling 27 species for a kinetic model in dry air. Though case studies of dry and wet air were presented by Mukkuvalli, there were no comparisons with experimental results to confirm the model. In the present model, only neutral reactions were considered and it was assumed that the effect of ionic species and their reactions could be compensated for by determining an equivalent-rate constant for the initiating reaction (5.1), (5.6), and (5.7).

5.4 Ozone Formation

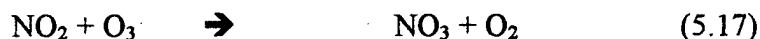
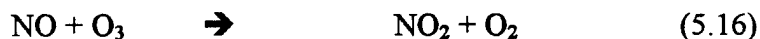
It is known that significant amounts of ozone are produced by corona discharge in dry air. To have an independent check on the reactor model developed,

experiments were carried out at 30, 40, and 50 kV (voltage settings) for three different residence times of 29, 35, and 46 seconds, and the amount of ozone produced was measured. In all these experiments, there was no NO in the feed gas.

For a given field strength the amount of ozone formed increased linearly with residence time as shown in Figure 5.16. Ozone concentration increased from 417 ppm to 682 ppm when the residence time increased from 28 seconds to 45.9 seconds at 50 kV. With an increase in the field strength larger amounts of ozone were formed. For a residence time of 46 seconds, the ozone concentration increased from 10 ppm to 682 ppm when the voltage setting was increased from 30 kV to 50 kV. The major pathway for ozone formation is given by the reaction



The singlet oxygen produced during corona discharge attaches to an oxygen molecule forming ozone. Ozone by itself reacts and oxides NO and NO₂ to their higher oxidation states resulting in an equilibrium concentration for a given field strength.



Comparison of the reactor model with the experimental data is shown in Figure 5.16.

Peyrous et al. (1989) carried out a kinetic simulation of various neutral species created by the corona effect in dry or humid oxygen. Their model simulations for recurring pulses indicate that at 300 °K, ozone concentration

increases linearly with increase in the number of pulses. The model consisted of neutral reactions, and was found to be in good agreement with their experimental results for relative hygrometry ranging from 0 to 35%.

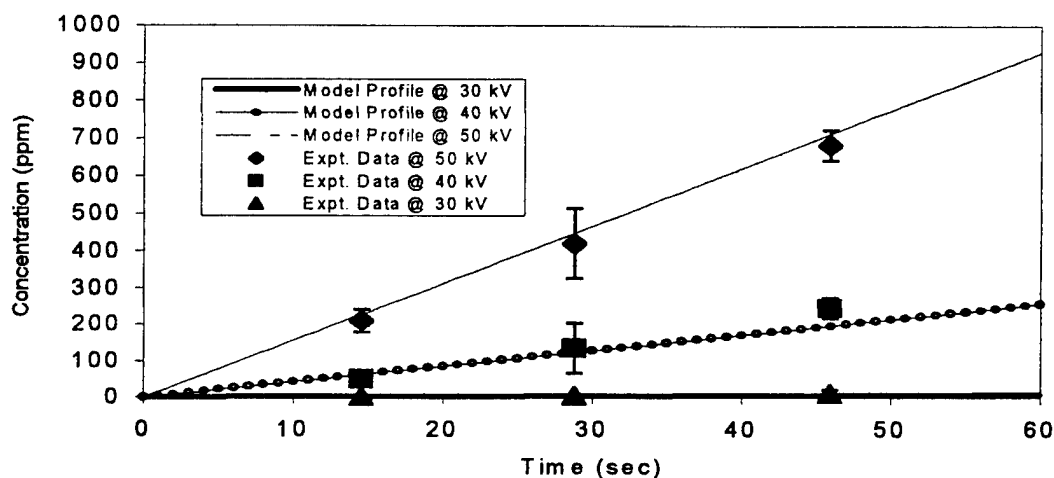


Figure 5.16 : Ozone Concentration Profile as a Function of Residence Time

5.5 NO Removal in Dry Air in the Presence of Ethylene

In Section 5.3, it was reported that complete removal of NO (100 ppm) could be achieved in an atmosphere of dry air at a peak voltage of 49 kV. However, the total NO_x concentration (NO+NO₂) was not greatly affected. To enhance the total

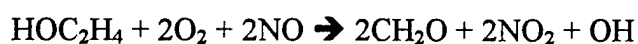
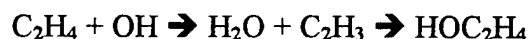
NO_x removal, a hydrocarbon was added to the gas mixture. Addition of hydrocarbons in the few ppm range has shown to be an effective way of reducing the NO_x content of flue gases.

Shimizu (1996) studied the effect of additives (C₂H₄, C₃H₈, and CH₄) on NO_x removal, and concluded that C₂H₄ was the most efficient. At a gas temperature of 30°C and a flow rate of 2 liters/min, Shimizu reported 70% NO_x removal efficiency with 500 ppm C₂H₄ additive for an initial concentration of 400 ppm NO at an input power of 20 W. For dry air, the energy consumption was about 150 J/gm to reduce 280 ppm of NO_x. He also noted that NO_x removal efficiency was not dependent on the C₂H₄ concentration, but the NO removal was proportional to C₂H₄ addition. On analysis of the by-products by FTIR, Shimizu was able to identify NO₂, O₃, CH₃COOH, and HCHO, along with some CO₂. No hazardous gas such as HCN was detected.

Mizuno et al. (1993) considered the effect of hydrocarbon on NO_x removal rate from diesel engine exhaust. They found that the removal rate was 80% at a power input of 35 W, for a gas flow rate of 2 liters/min (residence time = 0.56 seconds) and was 55% for 8 liters/min (residence time = 0.14 seconds). With the addition of 500 ppm of ethylene, the removal rate increased and even with a small input power of 20 W, the removal rate was 75% and 65% at a gas flow rate of 2 and 8 liters/min. In all their experiments, the initial concentrations of NO and NO₂ were 400 and 30 ppm respectively. They also considered the effect of other additives like

C₃H₈ and CH₄, and concluded that C₂H₄ was more effective than C₃H₈ or CH₄ as an additive for NO_x removal.

Vogtlin and Penetrante (1993) suggest that a hydrocarbon additive serves by recycling the hydroxyl radicals during the oxidation and reduction of NO. Similar reactions occurs in the atmosphere (Heicklen, 1976)



They also suggested that the efficiency of a particular hydrocarbon was limited by the reaction rate of this hydrocarbon with the hydroxyl radicals. C₂H₄ has a higher rate constant than C₃H₈ and CH₄ at room temperature (Vogtlin et al., 1993).

Table 5.3 : Rate Constants for Hydrocarbon Reaction with Hydroxyl Radicals

Species	Rate Constant @ 298 K (cm ³ .molecule ⁻¹ .sec ⁻¹)
CH ₄	8.41E-15
C ₃ H ₈	1.18E-12
C ₂ H ₄	8.53E-12

In our present study, 500 ppm of C₂H₄ was added to the simulated gas mixture (100 ppm NO in dry air). Ethylene was selected not only because of its

effectiveness in NO_x removal but also because it is one of the major combustion products in the exhaust gases.

Experimental data on NO removal in dry air with 500 ppm ethylene is plotted as a function of residence time in Figure: 5.17. The concentration profile looks similar to that obtained in the absence of ethylene (Section 5.3). The major difference is that greater NO removal is attained at shorter residence time in the presence of ethylene for a given field strength. At 44 kV, and a residence time of 20 seconds, NO concentration dropped to 37 ppm in dry air, but was down to 25 ppm when ethylene was added to dry air. For the same residence time, complete removal was attained at 49 kV with ethylene but only 86% removal was attained in dry air.

The energy consumption was also different. At a residence time of 14 seconds and a peak voltage of 49 kV, the energy consumption was 172 eV/molecule NO removed in dry air. This decreased to 82 eV/molecule with the addition of 500 ppm of ethylene.

NO_2 was formed by the oxidation of NO and the concentration profile is given in Figure: 5.18. The NO_2 concentration reached a maximum at higher field strength and diminished slowly with residence time. The maximum concentration at 49 kV was 91 ppm seen at a residence time of 24 seconds. For a similar condition, in dry air, the NO_2 concentration increased until the concentration reached 100 ppm. In other words, this implies that the total NO_x ($\text{NO} + \text{NO}_2$) was down to 90 ppm

from 100 ppm (initial) in the presence of ethylene. The NO_x concentration remained almost the same in dry air.

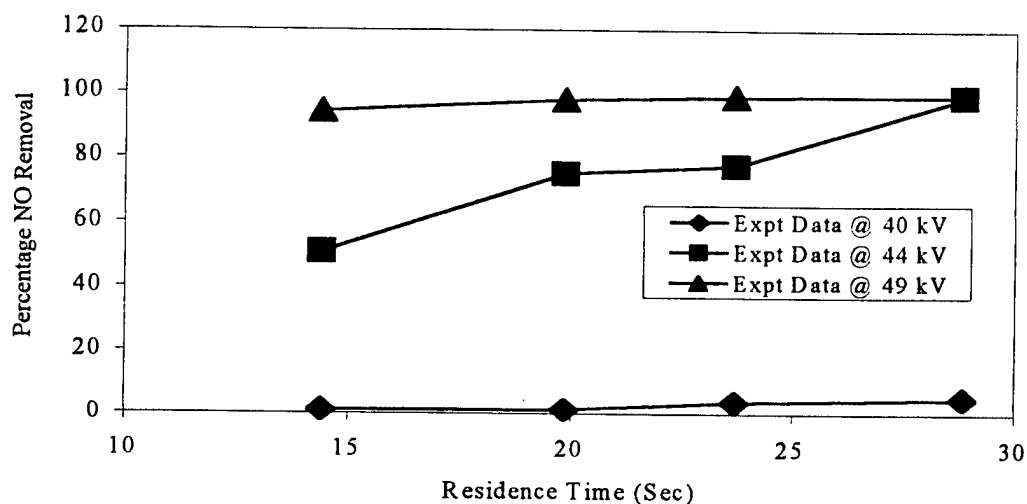


Figure 5.17 : Percentage NO Removal in an Atmosphere of Dry Air + 500 ppm Ethylene

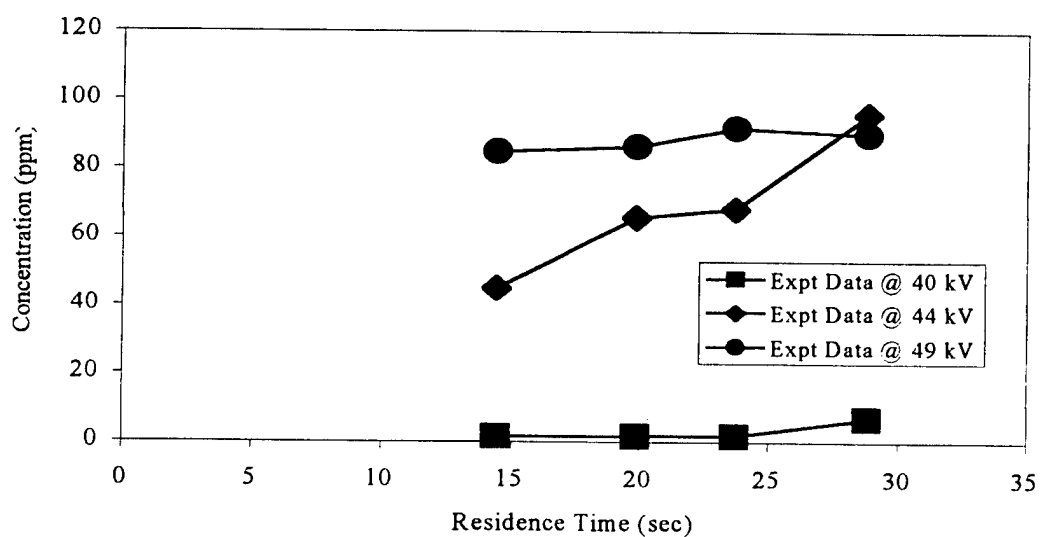
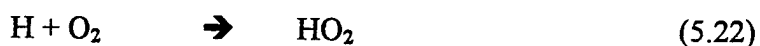
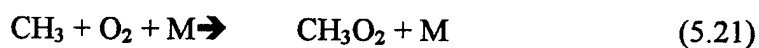
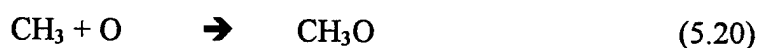
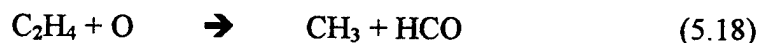
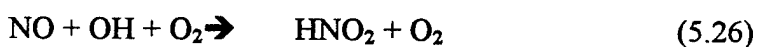
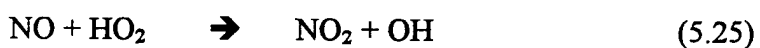
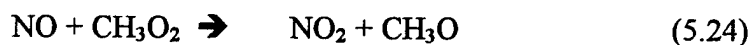


Figure 5.18 : NO_2 Formed in an Atmosphere of Dry Air + 500 ppm Ethylene

Experimental results indicate that the removal efficiency of NO increases with the addition of ethylene. This mainly results from the production of abundant radicals such as H, OH, and CH₃O, and due to the production of radicals such as CH₃O₂ and HO₂.



These radicals oxidize NO to NO₂, and other byproducts such as CH₃ONO and HNO₂.



Apart from these reactions, the radicals react with the NO₂ formed, resulting in a reduction of total NO_x content.

A reactor model with 48 neutral species totaling 123 reactions was developed to characterize the breakdown of NO in the presence of ethylene. Figure 5.19 depicts the model concentration profile of NO, and Figure 5.20 shows the NO₂ concentration profile as predicted by the model. The reactions appended to the

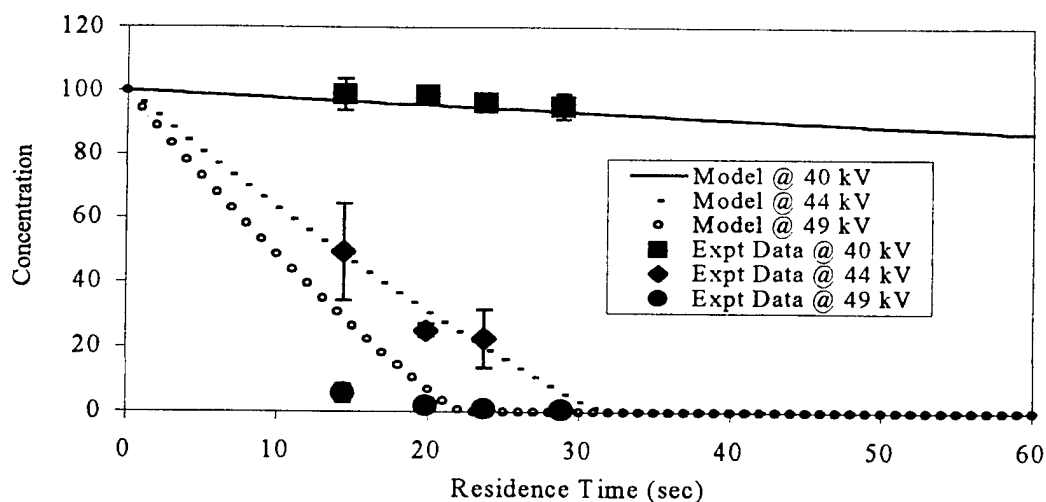


Figure 5.19 : NO Model Concentration Profile in an Atmosphere of Dry Air + 500 ppm Ethylene

original set of reactions for dry air are given in Table 5.3. It is worth noting here that the rate constants for the initiation reactions (electron-molecule collision reaction) were the same as those used to characterize the reactions in dry air. It is assumed that the electron density is not greatly affected by the addition of few ppm of C_2H_4 .

Samples were collected at the end of each experiment to monitor the C_2H_4 breakdown. Using GC analysis it was found that the concentration of ethylene remained almost the same at lower field strengths (peak voltages of 40 and 44 kV), but at a peak voltage of 49 kV and a residence time of 30 seconds, the breakdown was ranged from 75 ppm to 125 ppm of the 500 ppm ethylene present initially. Results indicate that more ethylene reacted with an increase in field strength and at longer residence times. Figure 5.21 shows the model concentration profile for ethylene breakdown at a peak voltage of 49 kV. The model indicates 55 ppm of

ethylene breakdown for a residence time of 30 seconds. For lower field strengths, the model did not predict any breakdown.

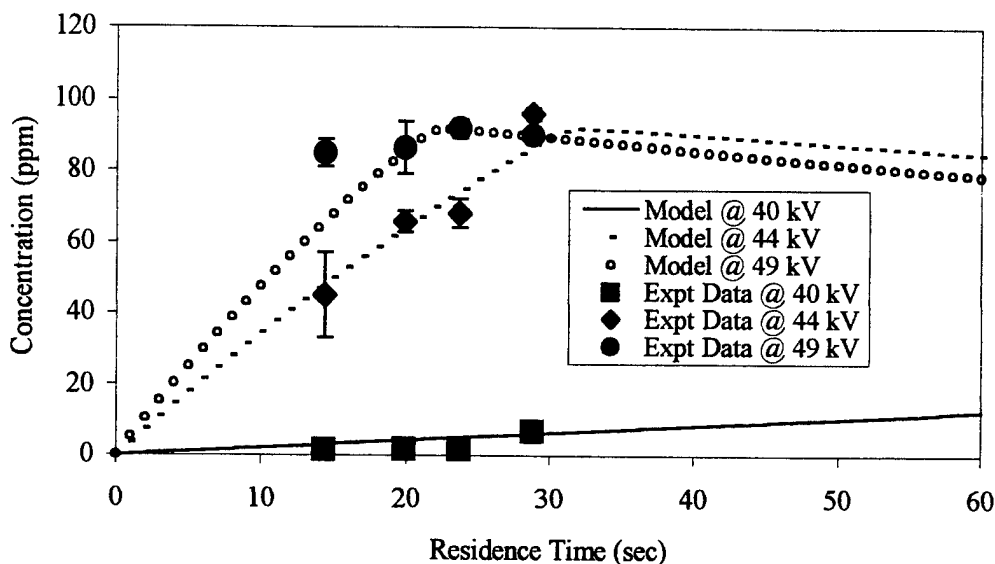


Figure 5.20 : NO₂ Concentration Profile in an Atmosphere of Dry Air + 500 ppm Ethylene

The model predicts production of up to 30 ppm each of CH₂O, CO, and O₃. The amount of ozone predicted by the model was around 15 ppm less than that in dry air. This is due to the additional reactions of O₃ with radicals such as H and OH. The model concentration profiles of major byproducts are shown in Figure 5.22. Less than 2 ppm of HNO₃ and 2 ppm of CO₂ are also expected. Similar byproducts were identified by Shimizu (1986) in a slightly different atmosphere (C₂H₄ = 500 ppm, NO = 200 ppm, O₂ = 10 % and N₂ = balance).

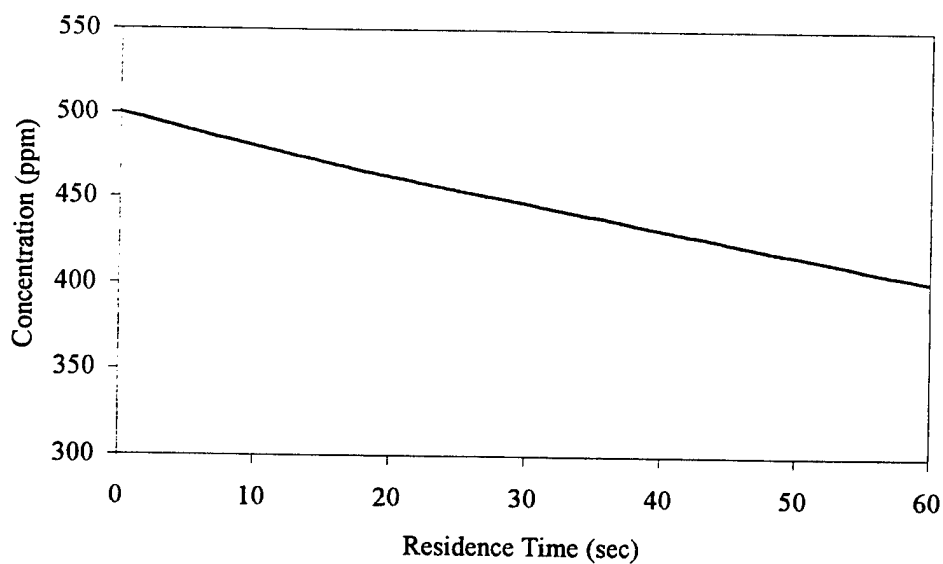
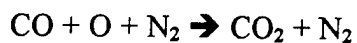
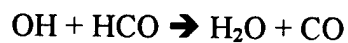


Figure 5.21 : Ethylene Breakdown at a Peak Voltage of 49 kV in an Atmosphere of Dry Air + 500 ppm Ethylene

If the plasma discharge power was high enough, it is expected that the entire hydrocarbon would be oxidized to produce CO_2 and H_2O . The probable pathway could be:



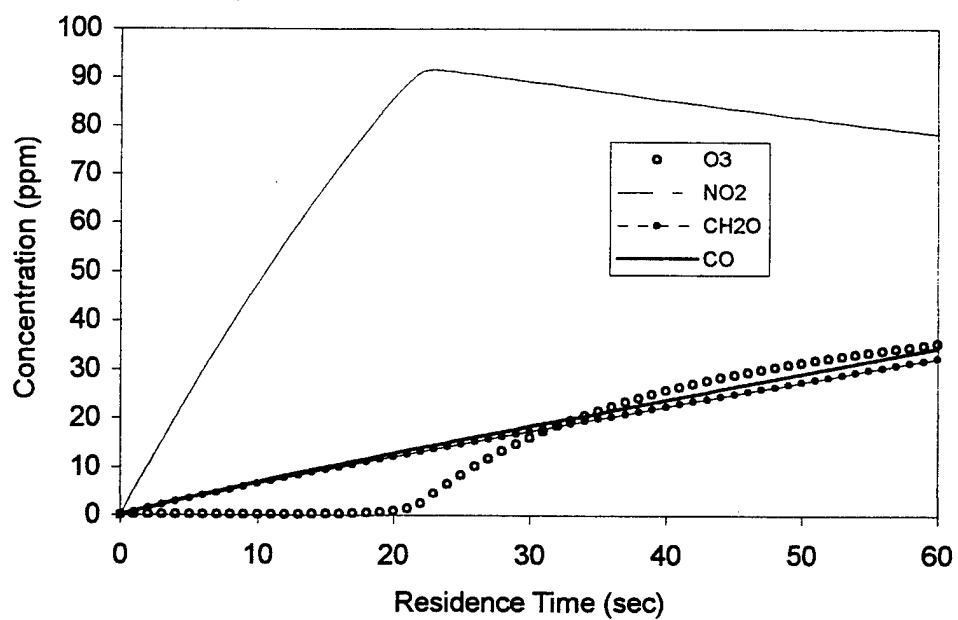


Figure 5.22 : Model Profile of Byproducts Formed at 49 kV in Dry Air + 500 ppm Ethylene

Table 5.4: List of Additional Reactions Considered for Modeling in the Presence of Ethylene.

Chemical Reaction	Rate Constant (cm ³ . mole ⁻¹ .sec ⁻¹)	Source	Number
$\text{N} + \text{OH} \rightarrow \text{NO} + \text{H}$	3.05 E+13	Atkinson et al., 1989	[35]
$\text{O}(^1\text{D}) + \text{H}_2 \rightarrow \text{H} + \text{OH}$	6.02 E+13	DeMore et al., 1990	[36]
$\text{O}(^1\text{D}) + \text{H}_2\text{O} \rightarrow 2\text{OH}$	1.32 E+14	Atkinson et al., 1992	[37]
$\text{O} + \text{H} + \text{M} \rightarrow \text{OH} + \text{M}$	1.58 E+16	Tsang & Hampson, 1986	[38]
$\text{O} + \text{HO}_2 \rightarrow \text{OH} + \text{O}_2$	3.43 E+13	Atkinson et al., 1989	[39]
$\text{O} + \text{OH} \rightarrow \text{O}_2 + \text{H}$	1.98 E+13	Atkinson et al., 1989	[40]
$\text{OH} + \text{H}_2 \rightarrow \text{H}_2\text{O} + \text{H}$	4.03 E+09	Atkinson et al., 1989	[41]
$\text{OH} + \text{OH} \rightarrow \text{H}_2\text{O} + \text{O}$	1.08 E+12	Atkinson et al., 1989	[42]
$\text{OH} + \text{OH} \rightarrow \text{H}_2\text{O}_2$	9.93 E+12	Atkinson et al., 1989	[43]
$\text{OH} + \text{HO}_2 \rightarrow \text{H}_2\text{O} + \text{O}_2$	6.62 E+13	Atkinson et al., 1989	[44]
$\text{OH} + \text{H}_2\text{O}_2 \rightarrow \text{H}_2\text{O} + \text{HO}_2$	1.02 E+12	Atkinson et al., 1989	[45]
$\text{OH} + \text{H} + \text{M} \rightarrow \text{H}_2\text{O} + \text{M}$	8.34 E+16	NIST	[46]
$\text{H} + \text{O}_2 \rightarrow \text{HO}_2$	8.49 E+11	Atkinson et al., 1989	[47]
$\text{H} + \text{O}_3 \rightarrow \text{OH} + \text{O}_2$	1.68 E+13	Atkinson et al., 1989	[48]
$\text{H} + \text{HO}_2 \rightarrow \text{H}_2 + \text{O}_2$	3.37 E+12	Atkinson et al., 1989	[49]
$\text{H} + \text{HO}_2 \rightarrow 2\text{OH}$	4.33 E+13	Atkinson et al., 1989	[50]

Table 5.4: Cont'd

Chemical Reaction	Rate Constant (cm ³ . Mole ⁻¹ .sec ⁻¹)	Source	Number:
$\text{H} + \text{HO}_2 \rightarrow \text{H}_2\text{O} + \text{O}$	1.44 E+12	Atkinson et al., 1989	[51]
$\text{H} + \text{H}_2\text{O}_2 \rightarrow \text{H}_2\text{O} + \text{OH}$	2.44 E+10	Baulch et al., 1983	[52]
$\text{HO}_2 + \text{HO}_2 \rightarrow \text{H}_2\text{O}_2 + \text{O}_2$	1.02 E+12	DeMore et al., 1987	[53]
$\text{NO} + \text{OH} + \text{O}_2 \rightarrow \text{HNO}_2 + \text{O}_2$	2.69 E+17	Atkinson et al., 1989	[54]
$\text{NO} + \text{CH}_2\text{OH} \rightarrow \text{CH}_3\text{NO}_2$	1.51 E+13	Pagsberg et al., 1989	[55]
$\text{NO} + \text{H} \rightarrow \text{HNO}$	1.47 E+14	Tsang & Herron, 1991	[56]
$\text{NO} + \text{CH}_3\text{O} \rightarrow \text{CH}_3\text{ONO}$	2.17 E+13	Atkinson et al., 1992	[57]
$\text{NO}_2 + \text{OH} + \text{M} \rightarrow \text{HNO}_3 + \text{M}$	9.44 E+17	DeMore et al., 1987	[58]
$\text{NO}_2 + \text{OH} \rightarrow \text{HO}_2 + \text{NO}$	1.39 E+13	Tsang & Herron, 1991	[59]
$\text{HNO}_2 + \text{OH} \rightarrow \text{NO}_2 + \text{H}_2\text{O}$	2.95 E+12	Atkinson et al., 1992	[60]
$\text{HNO}_3 + \text{OH} \rightarrow \text{H}_2\text{O} + \text{NO}_3$	9.03 E+10	Atkinson et al., 1989	[61]
$\text{OH} + \text{H} \rightarrow \text{H}_2 + \text{O}$	1.96 E+07	Loirat et al., 1987	[62]
$\text{H}_2\text{O}_2 + \text{H} \rightarrow \text{HO}_2 + \text{H}_2$	3.12 E+09	Warnatz et al., 1984	[63]
$\text{H}_2\text{O}_2 + \text{O} \rightarrow \text{OH} + \text{HO}_2$	1.02 E+09	Atkinson et al., 1989	[64]
$\text{O}_3 + \text{HO}_2 \rightarrow \text{OH} + 2\text{O}_2$	1.10 E+09	Levine et al., 1985	[65]
$\text{O}_3 + \text{OH} \rightarrow \text{HO}_2 + \text{O}_2$	3.36 E+10	Atkinson et al., 1989	[66]

Table 5.4: Cont'd

Chemical Reaction	Rate Constant (cm ³ . Mole ⁻¹ .sec ⁻¹)	Source	Number
$\text{HNO}_2 + \text{O} \rightarrow \text{NO}_2 + \text{OH}$	1.80 E+09	Kaiser et al., 1978	[67]
$\text{HNO}_3 + \text{HNO}_2 \rightarrow 2\text{NO}_2 + \text{H}_2\text{O}$	9.63 E+06	Kaiser et al., 1977	[68]
$\text{HNO}_3 + \text{O} \rightarrow \text{NO}_3 + \text{OH}$	1.00 E+13	NIST	[69]
$\text{HNO}_3 + \text{H} \rightarrow \text{HNO}_2 + \text{OH}$	6.02 E+10	Baulch et al., 1983	[70]
$\text{NO}_3 + \text{H} \rightarrow \text{NO}_2 + \text{OH}$	6.62 E+13	Boodaghians et al., 1988	[71]
$\text{NO}_3 + \text{OH} \rightarrow \text{NO}_2 + \text{HO}_2$	1.38 E+13	Boodaghians et al., 1988	[72]
$\text{NO}_3 + \text{HO}_2 \rightarrow \text{HNO}_3 + \text{O}_2$	7.62 E+11	Hoffmann et al., 1988	[73]
$\text{NO}_3 + \text{HO}_2 \rightarrow \text{NO}_2 + \text{OH} + \text{O}_2$	3.05 E+12	Hoffmann et al., 1988	[74]
$\text{N} + \text{HO}_2 \rightarrow \text{NO} + \text{OH}$	1.32 E+13	Brune et al., 1983	[75]
$\text{NO} + \text{HO}_2 \rightarrow \text{NO}_2 + \text{OH}$	4.99 E+12	Atkinson et al., 1989	[76]
$\text{NO} + \text{HO}_2 \rightarrow \text{HNO}_3$	8.43 E+10	Cox & Derwent, 1975	[77]
$\text{C}_2\text{H}_4 + \text{O} \rightarrow \text{CH}_3 + \text{HCO}$	4.39 E+11	Tsang & Hampson, 1986	[78]
$\text{C}_2\text{H}_4 + \text{O} \rightarrow \text{CH}_2 + \text{CH}_2\text{O}$	3.98 E+11	NIST	[79]
$\text{C}_2\text{H}_4 + \text{O} \rightarrow \text{H} + \text{CH}_2\text{CHO}$	3.76 E+11	Sridharan & Kaufman, 1983	[80]
$\text{C}_2\text{H}_4 + \text{O} \rightarrow \text{C}_2\text{H}_3 + \text{OH}$	1.46 E+09	Mahmud et al., 1987	[81]

Table 5.4: Cont'd

Chemical Reaction	Rate Constant (cm ³ . Mole ⁻¹ . sec ⁻¹)	Source	Number
$\text{C}_2\text{H}_4 + \text{N} \rightarrow \text{HCN} + \text{CH}_3$	9.93 E+10	NIST	[82]
$\text{C}_2\text{H}_4 + \text{H} + \text{M} \rightarrow \text{C}_2\text{H}_5 + \text{M}$	7.66 E+17	Lightfoot & Pilling, 1987	[83]
$\text{C}_2\text{H}_4 + \text{OH} + \text{M} \rightarrow \text{C}_2\text{H}_4\text{OH} + \text{M}$	5.45 E+19	DeMore et al., 1987	[84]
$\text{HCO} + \text{CH}_3 \rightarrow \text{CO} + \text{CH}_4$	1.21 E+14	Tsang & Hampson, 1986	[85]
$\text{HCO} + \text{O} \rightarrow \text{CO} + \text{OH}$	3.01 E+13	Tsang & Hampson, 1986	[86]
$\text{HCO} + \text{O} \rightarrow \text{H} + \text{CO}_2$	3.01 E+13	Tsang & Hampson, 1986	[87]
$\text{HCO} + \text{OH} \rightarrow \text{H}_2\text{O} + \text{CO}$	1.02 E+14	Baulch et al., 1992	[88]
$\text{HCO} + \text{O}_2 \rightarrow \text{HO}_2 + \text{CO}$	3.31 E+12	Atkinson et al., 1992	[89]
$\text{HCO} + \text{NO} \rightarrow \text{CO} + \text{HNO}$	7.23 E+12	Tsang & Herron, 1991	[90]
$\text{HCO} + \text{CH}_3 \rightarrow \text{CH}_3\text{CHO}$	1.81 E+13	Tsang & Hampson, 1986	[91]
$\text{C}_2\text{H}_4\text{OH} + \text{O}_2 \rightarrow \text{HOCH}_2\text{CH}_2\text{O}_2$	1.81 E+12	Atkinson et al., 1992	[92]
$\text{HOCH}_2\text{CH}_2\text{O}_2 + \text{HOCH}_2\text{CH}_2\text{O}_2 \rightarrow$			
$2\text{HOCH}_2\text{CH}_2\text{O} + \text{O}_2$	5.00 E+11	Atkinson et al., 1992	[93]
$2 \text{HOCH}_2\text{CH}_2\text{O}_2 \rightarrow \text{HOCH}_2\text{CH}_2\text{OH}$			
$+ \text{HOCH}_2\text{CHO} + \text{O}_2$	9.04 E+11	Atkinson et al., 1992	[94]

Table 5.4: Cont'd

Chemical Reaction	Rate Constant (cm ³ . Mole ⁻¹ .sec ⁻¹)	Source	Number
HOCH ₂ CH ₂ O ₂ + NO →			
HOCH ₂ CH ₂ O + NO ₂	5.42 E+12	Becker et al., 1991	[95]
CH ₃ + HO ₂ → CH ₃ O + OH	1.81 E+13	Baulch et al., 1992	[96]
CH ₃ + O → CH ₃ O	1.58 E+10	Dean et al., 1987	[97]
CH ₃ + O → H + CH ₂ O	8.43 E+12	Atkinson et al., 1989	[98]
CH ₃ + HO ₂ → CH ₄ + O ₂	3.61 E+12	Tsang & Hampson, 1986	[99]
CH ₃ + NO → CH ₃ NO	1.01 E+13	Kaiser, 1993	[100]
CH ₃ + NO ₂ → CH ₃ ONO	7.00 E+10	NIST	[101]
CH ₃ + NO ₂ → CH ₃ O + NO	1.39 E+13	NIST	[102]
CH ₃ + O ₂ + M → CH ₃ O ₂ + M	1.63 E+17	DeMore et al., 1987	[103]
CH ₃ O ₂ + NO → CH ₃ O + NO ₂	4.63 E+12	DeMore et al., 1987	[104]
CH ₂ O + O → OH + HCO	1.01 E+11	Herron, 1988	[105]
CH ₂ O + OH → H ₂ O + HCO	6.03 E+12	DeMore et al., 1987	[106]
CH ₂ O + OH → HCOOH + H	1.21 E+11	NIST	[107]
CH ₂ + OH → CH ₂ O + H	1.81 E+13	Tsang & Hampson, 1986	[108]
CH ₂ + HCO → CH ₃ + CO	1.81 E+13	Tsang & Hampson, 1986	[109]
CH ₂ CHO + O ₂ → CH ₂ O + CO			
+ OH	1.81 E+10	Baulch et al., 1992	[110]

Table 5.4: Cont'd

Chemical Reaction	Rate Constant (cm ³ . Mole ⁻¹ . sec ⁻¹)	Source	Number
$\text{C}_2\text{H}_5 + \text{O} \rightarrow \text{CH}_3\text{CHO} + \text{H}$	8.02 E+13	Tsang & Hampson, 1986	[111]
$\text{C}_2\text{H}_5 + \text{HCO} \rightarrow \text{C}_2\text{H}_5\text{CHO}$	1.81 E+13	Tsang & Hampson, 1986	[112]
$\text{C}_2\text{H}_5 + \text{HCO} \rightarrow \text{C}_2\text{H}_6 + \text{CO}$	1.21 E+14	Tsang & Hampson, 1986	[113]
$\text{C}_2\text{H}_3 + \text{OH} \rightarrow \text{CH}_3\text{CHO}$	3.01 E+13	Tsang & Hampson, 1986	[114]
$\text{CH}_3\text{O} + \text{HCO} \rightarrow \text{CH}_3\text{OH} + \text{CO}$	9.04 E+13	Tsang & Hampson, 1986	[115]
$\text{H} + \text{CH}_3\text{OH} \rightarrow \text{CH}_2\text{OH} + \text{H}_2$	8.39 E+12	NIST	[116]
$\text{O} + \text{CH}_3\text{OH} \rightarrow \text{OH} + \text{CH}_2\text{OH}$	4.87 E+09	NIST	[117]
$\text{OH} + \text{CH}_3\text{OH} \rightarrow \text{CH}_2\text{OH} + \text{H}_2\text{O}$	6.40 E+11	NIST	[118]
$\text{CH}_3\text{O} + \text{CH}_3\text{OH} \rightarrow$ $\text{CH}_3\text{OH} + \text{CH}_2\text{OH}$	3.10 E+08	Tsang, 1987	[119]
$\text{NO}_3 + \text{CH}_3\text{OH} \rightarrow$			
$\text{HNO}_3 + \text{CH}_2\text{OH}$	5.73 E+06	Atkinson, 1991	[120]
$\text{CH}_2\text{OH} + \text{CH}_2\text{OH} \rightarrow$ $\text{HOCH}_2\text{CH}_2\text{OH}$	9.64 E+12	Tsang, 1987	[121]
$2 \text{CH}_2\text{OH} \rightarrow \text{CH}_3\text{OH} + \text{CH}_2\text{O}$	4.82 E+12	Tsang, 1987	[122]
$\text{CO} + \text{O} + \text{N}_2 \rightarrow \text{CO}_2 + \text{N}_2$	3.88 E+12	Tsang & Hampson, 1986	[123]

5.6 Halon Removal in Dry Synthetic Air

Recent work by Yamamoto et al. (1992) demonstrated the destruction, in a bench scale gas phase pulsed streamer corona reactor, of a range of two carbon-containing chlorofluorocarbons in a range of different background carrier gases. They studied the removal of 1000 ppm CFC-113 present in 9.9% H₂ and 90% N₂ mixture in an ac-energized ferroelectric plasma reactor. With an applied voltage of 6.6 kV and a residence time of 2.0 seconds, the decomposition efficiency of CFC-113 was in the range 25.9-28.9%. The efficiency was improved to around 53% when the residence time was 4.4 seconds at an applied voltage of 6.0 kV. Longer residence times led to greater removal. It was proposed that the fluctuating electron energy was an agent for the transfer of electron energy to VOC decomposition. Further, that low voltages with longer residence time operation were superior to high voltages with short residence time plasma operation.

The present study focuses on the degradation of halon, a fire suppressant and an ozone depletion agent, and investigates the proposed theory of longer residence times and lower voltages operation being superior to high voltages and short residence times operation.

Removal of halon was studied with 1000 ppm of halon in synthetic air at atmospheric pressure. Figure 5.23 shows the decomposition of 1000 ppm of halon

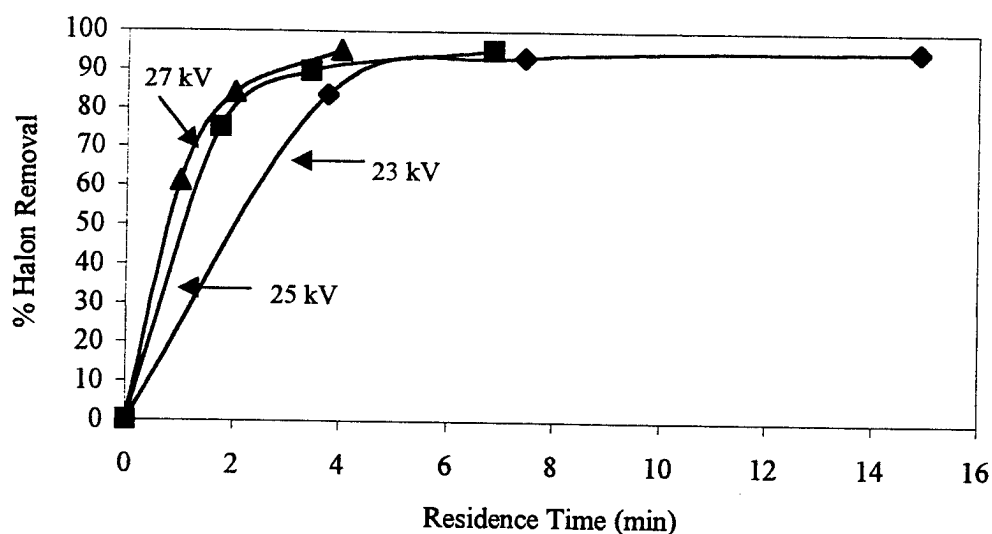


Figure 5.23 : Halon Removal Efficiency at Constant Voltage
(as a function of residence time)

as a function of reactor residence time at different peak voltages. All of the experimental data points are averages of three different trials. At a peak voltage of 23 kV, 95 (± 5) % removal efficiency was obtained for a residence time of 14 min 54 seconds. However, at 27 kV, the same efficiency was obtained for a shorter residence time (4 min). It is evident that as the residence time and peak voltages increased, the removal efficiency also increased. These results are similar to those obtained by Yamamoto et al. (1992). They reported an increase in methylene chloride conversion with increases in residence time and pulsed voltage.

The experimental results can also be compared for three different power densities. With an increase in power density, the removal efficiency increased (Figure 5.24). At a power density of 0.66 kJ/l, the removal efficiency was 83.5 (\pm 5)% for a residence time of 3 min 44 seconds, and at a power density of 1.32 kJ/l the removal efficiency increased to 89.5 (\pm 5)% for a residence time of 3 min 26 seconds. For a given power density, longer residence time leads to greater breakdown. Similar results were reported by Yamamoto et al. (1996) with CFC-113.

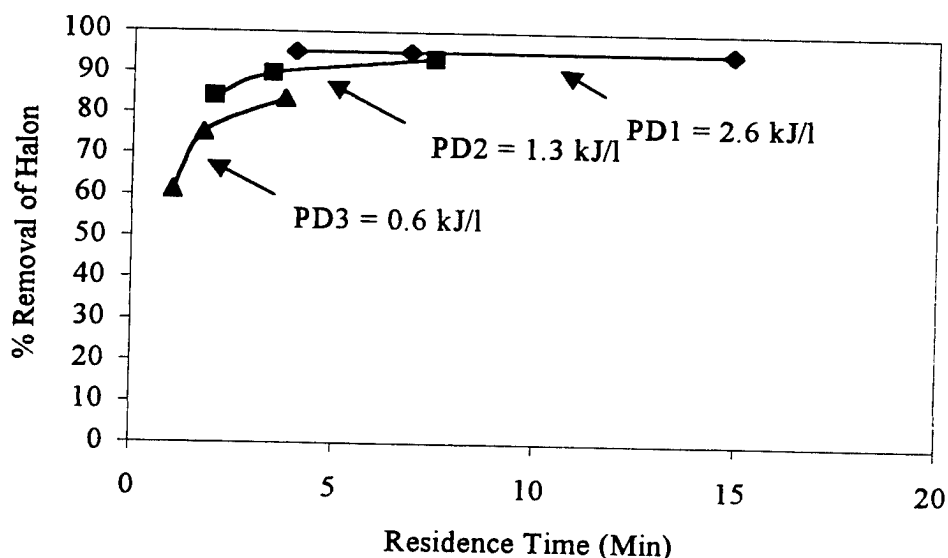


Figure 5.24 : Halon Removal Efficiency for Different Power Densities

It was also found that for the same power density, the removal efficiency decreased with increasing peak voltage (Figure 5.25). The removal efficiency

decreased from $83.5 (\pm 5)\%$ to $61.2 (\pm 5)\%$ when the peak voltage was increased from 23 kV to 27 kV at a power density of 0.66 kJ/l. This is because with an increase in the peak voltage, in order to maintain the same power density, the residence time in the reactor must decrease. This suggests that longer residence time and lower peak voltages provide better removal than higher peak voltages and shorter residence times. This also suggest that the residence time is a very important parameter in the removal of gas pollutants in a plasma reactor and that data must be reported as functions of residence times.

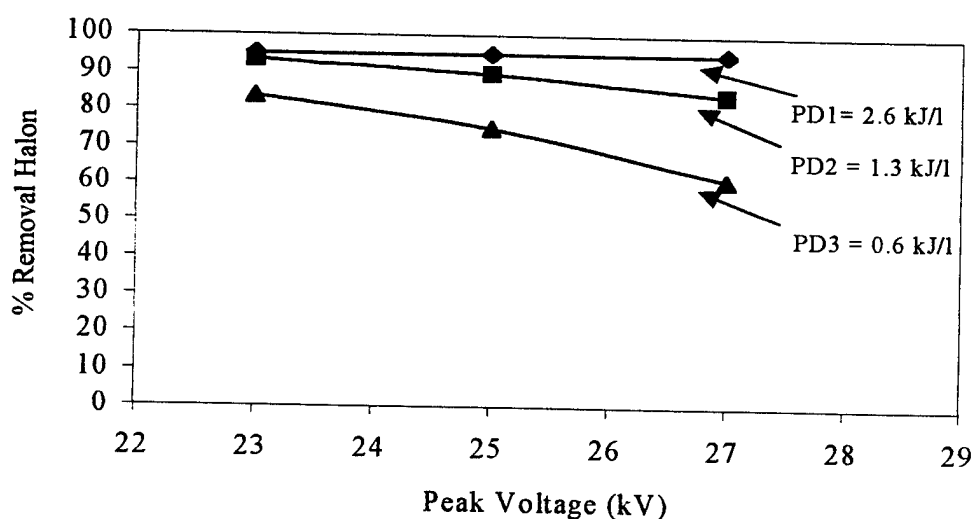
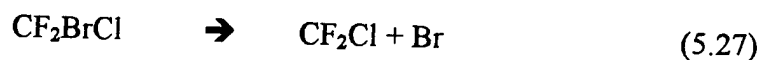


Figure 5.25 : Halon Removal Efficiency for Different Power Densities
(as a function of peak voltage)

A reactor model was developed to characterize halon removal in an atmosphere of dry synthetic air as functions of residence times. The set of reactions used for modeling is shown in Table 5.5. These reactions were used in addition to the reactions in Table 4.1. The average concentration of electron density used in this model was obtained by extrapolating the data obtained from NO removal data and ozone formation data in dry air by 75% to account for the differences in the field strengths. The model with this set of reactions could not predict the breakdown of halon with the known rate constants including the reaction of halon with $O(^1D)$. Rate constants of reactions of halon with O, N were very small at room temperature (NIST Chemical Database 17, version 6.01, 1994). It was seen that the model agrees with the experimental results when a hypothetical reaction (5.27) was appended to the original list of reactions.



This highlights the fact that there is an unknown dissociation pathway. The inclusion of this reaction was instigated after we carried out experiments with 1000 ppm of halon in an atmosphere of dry nitrogen. It was found that at a power density of 6.6 kJ/l and a peak voltage of 27 kV, 95% of the halon was destroyed. This brings out the fact that halon degradation occurs even in the absence of oxygen atoms, molecules, or ions.

This pathway could be triggered by direct electron collision (Yamamoto et al., 1996), other reactions with negative ions (O^-), by UV photons produced during

corona, by the fluctuating electric field, or by the interactions of halon with aerosol. Since the ratio of number of photons to electrons produced in the streamer is about 0.01 at atmospheric pressure, it is unlikely that UV photons will be of sufficient intensity to account for halon degradation. The calculated G-values for UV photons is about 0.007, which is about three orders of magnitude less than the G-values for oxygen atoms and two orders of magnitude less than for nitrogen atoms (Babaeva and Naidis, 1998). Further experiments must be carried out to validate other possibilities for this degradation. The rate constant for this reaction was found to be on the order of $10^2 \text{ cm}^3 \text{ mol}^{-1} \text{ sec}^{-1}$ by fitting the model to the experimental data. Figure 5.26 shows the model fit with the experimental data for the halon degradation (Sathiamoorthy et al. 1998).

The model was also used to predict the concentration of the various breakdown products. There are significant increases in the concentration of BrO , ClOO , and COF_2 . Figure 5.27 shows the typical concentration profile of these species. It was not possible to measure these short lived reaction products with our current analytical equipment and details of the reaction products formed from halon breakdown have not been reported.

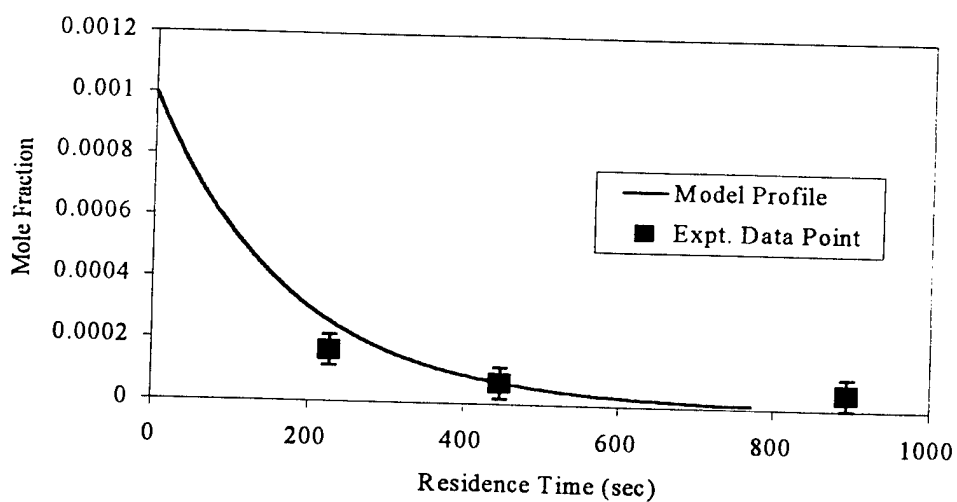


Figure 5.26 : Model Comparison for Halon Degradation

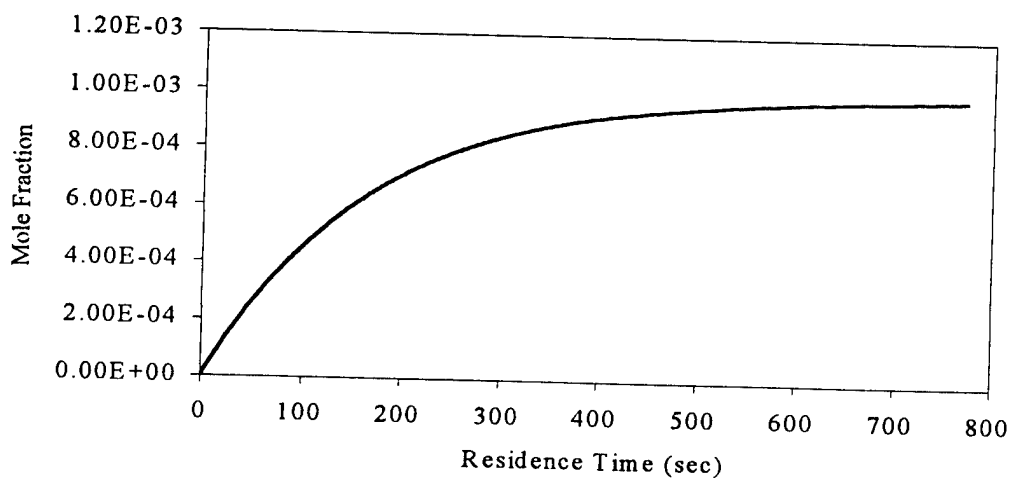


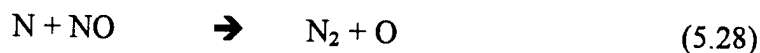
Figure 5.27 : Typical Concentration Profile of Species formed due to Halon Breakdown

Table 5.5 : Additional Reactions Considered for Halon Breakdown

Chemical Reactions	Rate Constant (cm ³ . mole ⁻¹ . sec ⁻¹)
BrO + ClO → Br + OClO	4.08 E+12
BrO + ClO → Br + ClOO	3.65 E+12
O + BrO → Br + O ₂	1.81 E+13
Br + O ₃ → BrO + O ₂	1.02 E+13
ClO + O → Cl + O ₂	1.81 E+13
CClBrF ₂ → CClF ₂ + Br	1.00 E+02
O(¹ D) + CClBrF ₂ → CClBrF ₂ + O	4.28 E+13
O(¹ D) + CClBrF ₂ → ClO + CBrF ₂	9.03 E+13
O(¹ D) + CClBrF ₂ → BrO + CClF ₂	9.03 E+13
O + CBrF ₂ → BrO + CF ₂	6.02 E+12
O + CClF ₂ → ClO + CF ₂	6.02 E+12
CF ₂ + O → COF + F	8.13 E+12
CF ₂ + O → CO + F ₂	2.71 E+12
COF + O → CO ₂ + F	5.60 E+13
CClF ₂ + O ₂ → CClF ₂ OO	5.08 E+18
CClF ₂ OO + O ₃ → COF ₂ + ClOO + O ₂	8.43 E+09
CClF ₂ + O ₃ → CF ₂ ClO + O ₂	6.03 E+09
COF ₂ + O(¹ D) → CO ₂ + F ₂	1.32 E+13
CO + O + N ₂ → CO ₂ + N ₂	3.88 E+12

5.7 Labeled Nitric Oxide Experiments

As was discussed in section 5.2, in an atmosphere of pure nitrogen, the nitrogen atom in NO was reduced back to the molecular state according to the following reaction



With a view to confirm the above pathway, experiments using labeled Nitric Oxide (N^{15}O) were carried out. The natural abundance of the stable nitrogen isotope (N-15), is reported to be as small as 0.366% (that of N-14 is 99.63%) (Tokunaga et al., 1993). Nitrogen molecule ($\text{N}^{15}\text{N}^{14}$ and $\text{N}^{15}\text{N}^{15}$) that might be formed during corona discharge thus could be distinguished from the nitrogen molecule ($\text{N}^{14}\text{N}^{14}$) of the gaseous mixture by a mass spectrometric method (Locke et al., 1997).

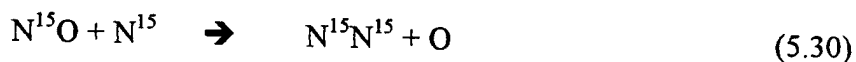
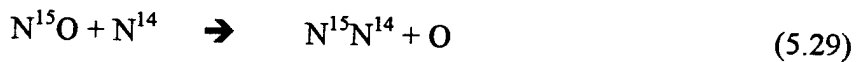
The initial concentration of N^{15}O was either 5% or 10% and three runs were conducted in an atmosphere of pure nitrogen at all reactor residence times of 4, 6, and 12 minutes. The dial voltage was maintained constant at 18 kV for all runs. Gas samples were collected in a sampling vessel after each run and analyzed on a Hewlett Packard GC/MS system. The mass peaks at 28, 29, 30, and 31 molecular weight were monitored. It was found that the 31 peak (N^{15}O) decreases monotonically with residence time for both the initial concentrations, as was

expected. The mass peak at 28 molecular weight ($N^{14}N^{14}$) did not change during the course of the run.

To check the relative abundance of $N^{15}N^{14}$ and $N^{15}N^{15}$ in the mass 29 and 30 peak, small amount of oxygen and water were introduced into the sampling vessel to react with the NO in the sample. The sample was then reanalyzed on a GC/MS. It was found that the 31 peak was completely eliminated signifying that most of the 31 peak was from $N^{15}O$. There was little change in the relative abundance of 29 and 30 peaks, indicating that the 30 peak comprised predominantly of $N^{15}N^{15}$ and not $N^{14}O$.

For either of the initial concentrations, it was noted that the relative GC/MS readings of the 29 and 30 peak increased with increase in residence time. When the initial concentration was increased from 5% to 10% the ratio of $N^{15}N^{15}$ to $N^{15}N^{14}$ increased from 0.35 to around 0.55. These indicate that at higher initial concentration and larger residence time, more N^{15} from the dissociation on $N^{15}O$ is available for recombination to form molecular nitrogen.

However, the 29 peak was always significantly higher than the 30 peak. This signifies the fact that the most favored pathway is reduction to molecular nitrogen.



Summary of the experimental results is given in Table 5.6.

Similar results were obtained by Tokunaga et al. (1993) for electron beam experiments. Gaseous mixture of simulated flue gas (1720 ppm SO_2 , 6.9% O_2 ,

92.5% N₂ (dry base), and 13% water vapor with 3840 ppm NH₃) containing 400 ppm N¹⁵O was irradiated with E-beam of dose 14 kGy at 80°C. Results indicate that 23% of 4000 ppm N¹⁵O decomposed to form nitrogen molecules. They concluded that NO_x was converted not only to NH₄NO₃ and dinitrogen monoxide, but also to nitrogen molecules by collision with nitrogen atoms

Table 5.6 : Summary of N¹⁵O Experimental Results:

	RESIDENCE TIME (MINUTES)		
	4	6	12
Mass Spec. Molecular Wt.	Relative GC/MS Mass Reading		
	10% NO in Feed		
28	1000	1000	1000
29	10.5	12.3	18.2
30	6.0	6.5	9.8
31	37.5	28.6	13.0
30/29	0.58	0.53	0.54
After Washing			
28	1000	1000	1000
29	11.1	11.9	19.1
30	5.3	5.4	9.1
31	0	0	0
30/29	0.48	0.46	0.48

Table 5.6 : Cont'd:

	RESIDENCE TIME (MINUTES)	
	6	12
	Relative GC/MS Mass Reading	
Mass Spec. Molecular Wt.	5% NO in Feed	
28	1000	1000
29	12.2	16.2
30	3.7	6.1
31	6.4	2.4
30/29	0.30	0.38
After Washing		
28	1000	1000
29	10.3	14.8
30	2.9	5.2
31	0	0
30/29	0.29	0.35

CHAPTER 6

SUMMARY AND CONCLUSION

Pulsed power supply produced with the aid of a rotating spark-gap created a corona discharge with fast rise time and narrow pulse width in a wire-cylinder geometry gas phase reactor vessels. The corona discharge so produced was effective in removing gaseous species like NO and Halon 1211 from feed gas like nitrogen and air. The effect of residence time and field strength on the removal of NO, NO₂, and Halon 1211 were studied. Experiments with N¹⁵O isotope were carried out to identify the pathway for NO breakdown in nitrogen. A reactor model was developed to characterize the reactions occurring under different conditions and the main reaction pathways for the breakdown of NO, NO₂, and halon were identified for each of the gas composition. The model predictions of NO₂ and O₃ formation in dry air, NO and NO₂ removal in dry air with 500 ppm ethylene as an additive, were compared with the experimental data. Similar comparison was also done for halon breakdown.

Two different sets of reactors were used in the study. Reactor- I was a stainless steel reactor with 4 inches ID and an effective volume of 2.45 liters. It was

used as a flow reactor. Reactor- II was a stainless steel reactor with ID of 1 inch and effective volume of 45.4 ml and was used in a batch mode. Characteristics of the power supply (pulse width, rise time, peak voltage) were measured using current and voltage probes. The energy input to the reactor was calculated by multiplying the current and voltage waveforms. These characteristics were dependent on the geometry of the reactor and the gas composition. However, in all cases, the peak voltage was significantly higher than the dial setting. The pulse width varied from 500 to 700 nanoseconds with Reactor- I and from 50 to 150 nanoseconds with Reactor- II.

Experimental results in different atmospheres indicate that maximum NO removal is attained in the presence of 500 ppm of ethylene. Figure 6.1 summarizes the NO removal at 49 kV in different atmosphere and the corresponding NO₂ concentration is shown in Figure 6.2. The greater removal in the presence of ethylene is attributed to the fact that additional reactive radicals like H, OH, and CH₃O are produced by the breakdown of ethylene. The model predicts about 55 ppm of ethylene breakdown at 40 kV for a residence time of 30 seconds and this matches the results (75-125 ppm) within experimental errors.

The smallest amount of NO₂ was formed in an atmosphere of nitrogen. At higher field strengths and longer residence times, the NO₂ was almost completely removed. This indicated the fact that most of the NO was reduced back to molecular nitrogen. The addition of O₂ to the gas mixture (i.e., experiments in dry air)

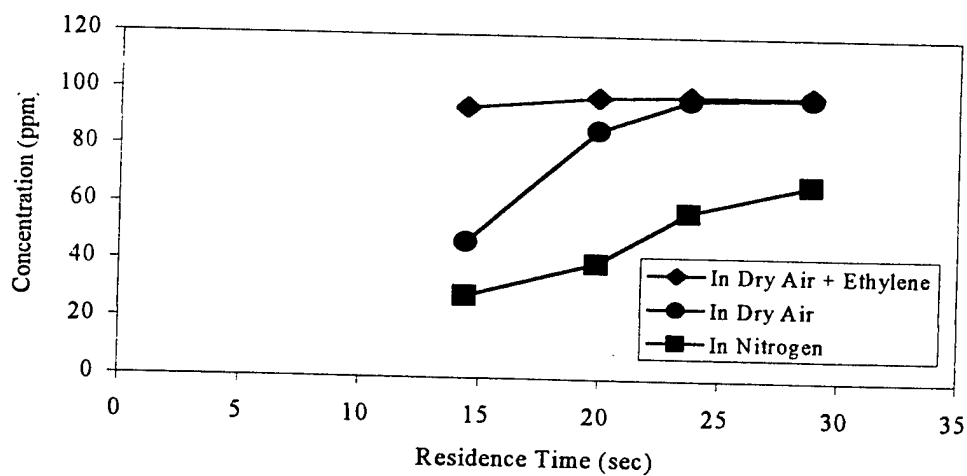


Figure 6.1: Summary of NO Removal at a Peak Voltage of 49 kV in Different Atmospheres

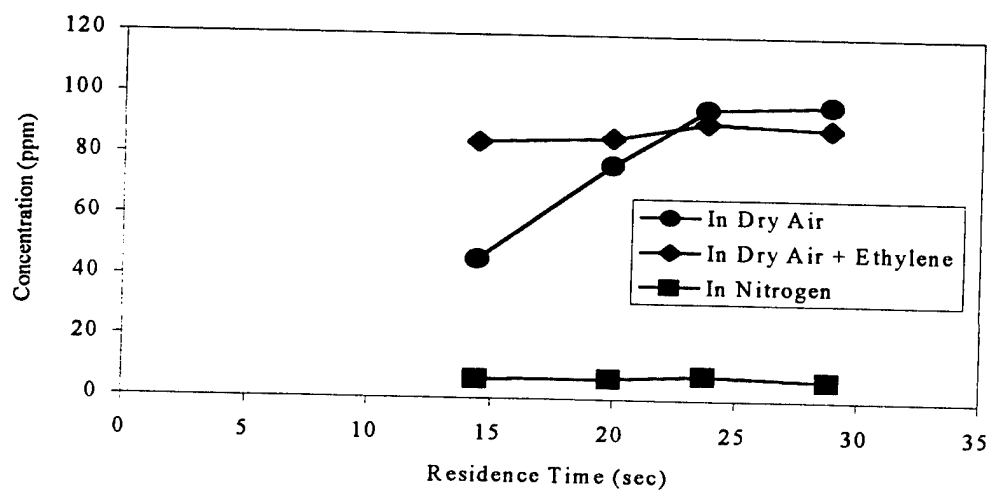


Figure 6.2: Summary of NO₂ Formation at a Peak Voltage of 49 kV in Different Atmospheres

increased the NO removal rate but most of the NO was oxidized to NO₂, thereby an insignificant change in the total NO_x concentration was achieved.

In dry air, the energy consumption ranged from around 95 eV per NO molecule removed at 44 kV and a residence time of 29 seconds to about 172 eV per NO molecule removed at 49 kV and a residence time of 14.8 seconds. This decreased significantly to about 82 eV/molecule at 49 kV and at a residence time of 14.8 seconds, in the presence of ethylene. This verifies that NO removal is energy efficient in dry air in the presence of ethylene than in dry air by itself. Penetrante et al. (1995) calculated the energy density to be about 240 eV per NO molecule removal in nitrogen atmosphere. He added that NO removal in dry air could be less energy intensive than in nitrogen. This was confirmed by our study.

Isotopically labeled nitric oxide (N¹⁵O) was used to study the reaction pathways for NO removal in nitrogen atmosphere. Results indicated that in nitrogen gas with 5% and 10% concentration of NO, the direct dissociation of NO by the discharge was highly significant. The relative importance of this dissociation decreased with decrease in NO concentration. Significant increases in the 29 and 30 mass peak on a GS/MS validated that the reduction pathway to molecular nitrogen was the main pathway for NO removal in the absence of oxygen.

A kinetic model was developed to characterize the reactions taking place in the system. NO removal in nitrogen was characterized with 25 reactions and NO removal in dry air required 34 reactions to model the system. When 500 ppm of

ethylene was added to the gaseous mixture, 89 additional reactions were required to predict NO breakdown. The model developed for NO removal in dry air was used to predict ozone formation in dry air in the absence of NO. The model was shown to be effective after comparison with the experimental data obtained earlier for ozone formation. It is worth noting here that a single value of electron-density was used in the model when the major composition of the gaseous mixture was the same. Figure 6.3 summarizes the model comparison of NO breakdown at 40 kV in different atmospheres and Figure 6.4 compares the model prediction with the experimental data for NO₂ formation.

To have a realistic model for removal of NO from exhaust gases, the model must be modified to account for the presence of all the gas molecules. The presence of molecules such as water vapor has been shown to effect the NO removal efficiency greatly (Tokunaga et al., 1984, Chang et al., 1992, Masuda, 1993). In the presence of water vapor molecules, aerosol formations are expected that lead to heterogeneous reactions (Namba et al., 1991, Yamamoto et al., 1996). Such reactions must be incorporated in future models.

Rate constants were calculated for the electron-molecule collision reactions by fitting the model to experimental data. The rate constants of all the dissociation reaction increased with increase in peak voltages, as was expected. The nitrogen dissociation rate constant increased about two orders of magnitude when the peak voltage was increased from 40 kV to 49 kV. Oxygen dissociation rate constants

were almost four orders of magnitude higher than nitrogen dissociation rate constants. The calculated rate constants for nitrogen dissociation were different for nitrogen atmosphere and dry air atmosphere. This confirms the fact that these rate constants depend on the composition of the gas.

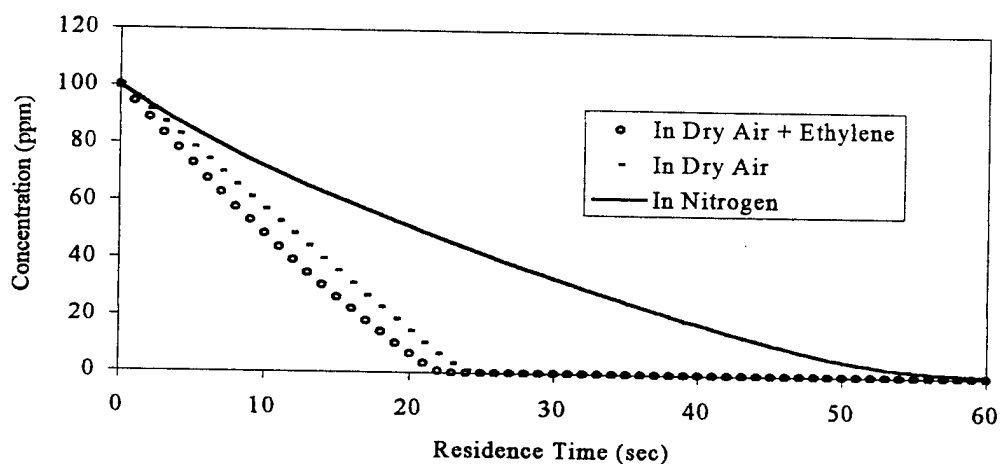


Figure 6.3 : Summary of NO Removal Model Profile at a Peak Voltage of 49 kV in Different Atmospheres

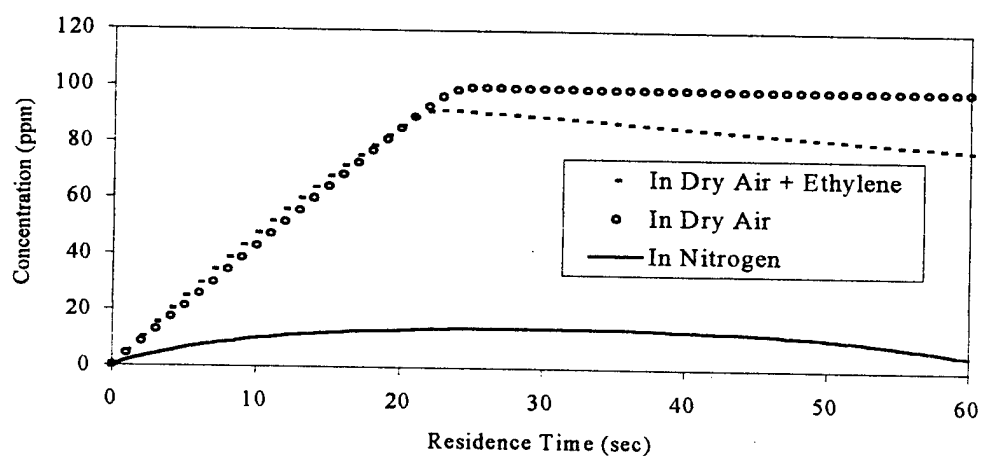


Figure 6.4: Summary of NO₂ Model Profile at a Peak Voltage of 49 kV in Different Atmospheres

The present study also shows that a pulsed streamer corona discharge could be used to destroy Halon 1211 in an atmosphere of dry synthetic air. Reactor- II was used in this study. Halon removal efficiency increased with increases in peak voltage and power density as a function of residence time. Longer residence times lead to greater removal at a fixed power density or field strength. For a given power density, it was found that the removal efficiency decreased with increase in peak voltage. This was because for the same power density, the residence time in the reactor decreases with increase in peak voltage. This indicated that the residence time was the crucial factor determining the breakdown of gas molecules than the field strength or power density.

A reactor model was developed to characterize the halon removal reactions taking place in the pulsed streamer corona reactor as a function of residence time. However, it was necessary to postulate an additional removal mechanism to account for the level of halon degradation observed in the experiments. Further study is needed to identify the breakdown products predicted by the model, and determine the mechanism for halon degradation.

Major conclusions of the present study are :

- 1) NO and NO₂ can be effectively removed in a Pulsed Streamer Corona Reactor. Addition of 500 ppm of ethylene enhanced both NO and NO₂ removal in dry air.

- 2) The energy consumption varied from 95 eV per NO molecule removed to about 172.9 eV per NO molecule removed, in dry air. The energy consumption decreased on the addition of 500 ppm of ethylene.
- 3) Experimental results with labeled nitric oxide indicate that the major pathway for NO removal in an atmosphere of nitrogen is the reduction to molecular nitrogen. Further that the direct dissociation of NO by the pulsed corona discharge was highly significant when the concentrations of NO in the mixture was in the percentage ranges (>5%).
- 4) Up to 95% removal of 1000 ppm of Halon 1211 in dry synthetic air is feasible and studies confirmed that lower voltages and longer residence times were superior to higher voltages and shorter residence times of plasma processing.
- 5) Residence time is the most important factor that determines the removal of gaseous pollutants. Therefore, it is logical to compare removal data and develop reactor models that characterize removal of pollutants as functions of residence times.
- 6) A simple reactor model with reactions involving neutral species can characterize the evolution of molecular species during corona discharge. The model predictions for NO_2 and O_3 formation in dry

air, and NO and NO₂ removal in the presence of 500 ppm C₂H₄ in dry air matched the experimental data within experimental errors.

7) The model results indicate that:

i) As few as 34 reactions (for dry air) and 123 reactions (for dry air + 500 ppm C₂H₄) are sufficiently enough to characterize the evolution of molecular species during corona discharge.

ii) The presence of additives in parts per million ranges (< 1%) does not change the major chemistry of NO removal and does not affect the electron density in the reactor.

iii) There is an unknown pathway for Halon-1211 breakdown in corona discharges that needs to be investigated.

CHAPTER 7

FUTURE WORK & RECOMMENDATIONS

The following are areas where future research work could be directed. These recommendations could make further contributions to the application of non-thermal plasma for pollution control.

- [1] Extension of the Model: Earlier work done by Kalyana (1996) indicated that NO_x removal is enhanced by the addition of water vapor. In humid air, it is expected that aerosol formation will lead to greater removal of NO_x . The model must be modified to incorporate such heterogeneous reactions to characterize NO_x removal in humid air.
- [2] Halon Breakdown: As mentioned in Section 5.6, it was necessary to postulate an additional removal mechanism to account for the level of halon degradation observed in the experiments. Further study is needed to identify the breakdown products predicted by the model, and determine the mechanism for halon degradation.

- [3] N¹⁵O Experiments: Preliminary data on the use of isotopically labeled nitric oxide to study reaction pathways for NO removal in an atmosphere of nitrogen was reported in this study. Further studies in different atmospheres including addition of oxygen and water vapor to the reactor, and more extensive variation of reactor residence time and field conditions, could be used to quantify the reaction kinetics in a pulsed corona reactor.
- [4] Sensitivity Analysis: Sensitivity analysis to choose the most important parameters of the reactor model must be carried out to estimate the effects of parameter variations, to assess uncertainties in the rate constants, and to distinguish important from unimportant model features.
- [5] Design of Reactor: Helical wire discharge electrodes have been shown to perform excellently in corona applications like ESPs and ozone generators (Shimizu, 1996). Shimizu reported that reactors with helical wire electrodes, performed better than their counterparts with conventional straight wire electrodes at lower power inputs. Catalyst coated electrodes could also be used to study the effect of surface induced reactions on the DeNO_x efficiency.
- [6] By-Product Analysis: Apart from NO and NO₂, the treated gas must also be analyzed for by-products such as N₂O, CO, and CO₂ on a regular basis. Analytical instruments such as FTIR and GC/MS could be employed to detect these species and the results must be compared with the model predictions to validate the model.

- [7] Flow System: Pressure flow meters must be installed at regular intervals along the whole length of gas distribution piping. This is necessary to prevent problems that arise due to back-pressure and this would also aid in estimating pressure drops resulting in the piping.

APPENDIX A

EXPERIMENTAL RESULTS OBTAINED IN NITROGEN AND DRY AIR

Table A.1 : NO and NO₂ Data at a Peak Voltage of 40 kV in an Atmosphere of Nitrogen

Res. Time (sec)	NO Concentration (ppm)			NO ₂ Concentration (ppm)			Mean Conc. NO	Mean Conc. NO ₂
	Run-1	Run-2	Run-3	Run-1	Run-2	Run-3		
14.41	98.8	98.9	98	0.8	0.5	1.2	98.6	0.83
23.7	90	98.1	98.9	1.9	1	0.5	95.7	1.13
28.82	88.8	94.8	87.8	3.3	1.3	3.8	90.5	2.78

Table A.2 : NO and NO₂ Data at a Peak Voltage of 44 kV in an Atmosphere of Nitrogen

Res. Time (sec)	NO Concentration (ppm)			NO ₂ Concentration (ppm)			Mean Conc. NO	Mean Conc. NO ₂
	Run-1	Run-2	Run-3	Run-1	Run-2	Run-3		
14.41	88.6	85.8	80.0	3.2	3.2	6.5	84.8	4.3
19.86	72.4	72	73.3	7.8	7.2	7.0	72.6	7.3
23.7	56.7	51.9	64.3	7.7	7.4	7.1	57.6	7.4
28.82	39.8	39.6	46.2	8.5	8.3	6.8	41.8	7.9

Table A.3 : NO and NO₂ Data at a Peak Voltage of 49 kV in an Atmosphere of Nitrogen

Res. Time (sec)	NO Concentration (ppm)			NO ₂ Concentration (ppm)			Mean Conc. NO	Mean Conc. NO ₂
	Run-1	Run-2	Run-3	Run-1	Run-2	Run-3		
14.41	80.0	74.4	60.0	4.4	6.2	9.0	71.5	6.5
19.86	67.1	69.8	45.7	6.4	6.5	7.3	69.9	6.8
23.7	42.5	41.6	41.4	7.2	8.5	8.4	41.9	8.0
28.82	33.8	28.3	33.0	7.4	6.3	6.5	31.7	6.7

Table A.4 : NO and NO₂ Data at a Peak Voltage of 40 kV in an Atmosphere of Dry Air

Res. Time (sec)	NO Concentration (ppm)			NO ₂ Concentration (ppm)			Mean Conc. NO	Mean Conc. NO ₂
	Run-1	Run-2	Run-3	Run-1	Run-2	Run-3		
14.41	99.0	98.9	95.6	1.5	0.5	1.8	97.8	1.3
19.86	97.1	97.6	97.1	1.9	2.4	2.1	97.3	2.1
23.7	97.2	95.4	94	2.4	3.9	7.0	95.5	4.4
28.82	88.9	95.9	97.2	11.5	4.2	2.3	94.0	6.0

Table A.5 : NO and NO₂ Data at a Peak Voltage of 44 kV in an Atmosphere of Dry Air

Res. Time (sec)	NO Concentration (ppm)			NO ₂ Concentration (ppm)			Mean Conc. NO	Mean Conc. NO ₂
	Run-1	Run-2	Run-3	Run-1	Run-2	Run-3		
14.41	60.3	67.5	62.7	41.2	33.2	38.5	63.5	37.6
19.86	35.7	32.5	42.6	63.7	65.5	57.8	36.9	62.3
23.7	32.2	23.5	21.2	68	71.6	75.1	25.6	71.6
28.82	0.9	1.1	1.2	96.6	100.8	101.4	101	99.6

Table A.6 : NO and NO₂ Data at a Peak Voltage of 49 kV in an Atmosphere of Dry Air

Res. Time (sec)	NO Concentration (ppm)			NO ₂ Concentration (ppm)			Mean Conc. NO	Mean Conc. NO ₂
	Run-1	Run-2	Run-3	Run-1	Run-2	Run-3		
14.41	52.9	54	52.9	51.5	42	46	53.3	46.5
19.86	9.1	16.3	15.3	82.7	74.3	75.6	13.6	77.5
23.7	5.6	1.0	0.9	88.0	93.0	107.0	2.5	96.0
28.82	1.1	2.5	0.8	91.0	101.0	100.0	1.5	97.3

Table A.7 : NO and NO₂ Data at a Peak Voltage of 40 kV in an Atmosphere of Dry Air + 500 ppm Ethylene

Res. Time (sec)	NO Concentration (ppm)			NO ₂ Concentration (ppm)			Mean Conc. NO	Mean Conc. NO ₂
	Run-1	Run-2	Run-3	Run-1	Run-2	Run-3		
14.41	98.8	98.9	98.3	1.3	1.8	1.2	98.7	1.5
19.86	98.9	98.7	98.3	1.8	1.0	1.9	98.6	1.6
23.7	96.6	95.9	96.0	1.1	2.6	4.0	96.2	2.6
28.82	96.1	94.6	89.0	6.3	6.7	11.0	93.2	8.0

Table A.8 : NO and NO₂ Data at a Peak Voltage of 44 kV in an Atmosphere of Dry Air + 500 ppm Ethylene

Res. Time (sec)	NO Concentration (ppm)			NO ₂ Concentration (ppm)			Mean Conc. NO	Mean Conc. NO ₂
	Run-1	Run-2	Run-3	Run-1	Run-2	Run-3		
14.41	52.3	66.3	29.0	46.7	30.1	58.0	49.2	44.9
19.86	26.0	27.0	22.9	67.2	66.9	62.7	25.3	65.6
23.7	13.3	25.0	28.4	71.5	67.4	64.8	22.3	67.9
28.82	0.92	0.97	0.91	96.0	97.3	94.2	0.93	95.8

Table A.9 : NO and NO₂ Data at a Peak Voltage of 49 kV in an Atmosphere of Dry Air + 500 ppm Ethylene

Res. Time (sec)	NO Concentration (ppm)			NO ₂ Concentration (ppm)			Mean Conc. NO	Mean Conc. NO ₂
	Run-1	Run-2	Run-3	Run-1	Run-2	Run-3		
14.41	3.6	8.4	5.0	85.7	51.0	87.5	5.7	84.7
19.86	4.0	1.0	0.82	82.6	82.5	93.9	1.9	86.3
23.7	0.89	0.83	0.83	91.0	94.0	89.6	0.85	91.5
28.82	0.77	0.62	0.5	89.6	92.0	88.0	0.63	89.9

Table A.10 : Ozone Formation Data in an Atmosphere of Dry Air

Res Time (sec)	Applied Voltage					
	30 kV		40 kV		50 kV	
	Mean O ₃	Std. Dev.	Mean O ₃	Std. Dev.	Mean O ₃	Std. Dev.
28.8	3.82	0.28	127.15	16.31	417.98	30.88
35.0	3.69	3.56	145.63	66.70	495.95	93.60
45.9	10.65	4.38	224.94	28.10	682.00	39.14

APPENDIX B

HALON DEGRADATION DATA

Table B.1 : Residence Times in the Reactor as a Function of Peak Voltage and Power Density for Halon Experiments

POWER DENSITY	23 KV	25 KV	27 KV
2.6 kJ/l	14 min 54 sec	6 min 51 sec	4 min
1.3 kJ/l	7 min 27 sec	3 min 26 sec	2 min
0.6 kJ/l	3 min 44 sec	1 min 43 sec	1 min

Table B.2 : Removal Efficiency of Halon with Changes in Power Density as a Function of Peak Voltage

POWER DENSITY	23 KV	25 KV	27 KV
2.6 kJ/l	95 %	95 %	95 %
1.3 kJ/l	93.3 %	89.6 %	84 %
0.6 kJ/l	83.4 %	75 %	61.2 %

REFERENCES

- [1] Alekseev, G. Y., Levchenko, A. V., and Biturin, V. A., " Flue Gas Cleaning by Pulse Corona, Part II Chemical Kinetics and Heat Transfer in NO_2/SO_2 Removal", *Research Report IVTAN-ANRA 93/2*, MOSCOW, 1993.
- [2] Atkinson, R., Baulch, D. L., Cox, R. A., Hampson, R. F., Kerr, J. A., and Troe, J., " Evaluated Kinetic and Photochemical Data for Atmospheric Chemistry", *J. Phys. Chem. Ref. Data*, **18**, 1989, 881-1097.
- [3] Atkinson, R., " Kinetics and Mechanism of the Gas-Phase Reactions of the NO_3 Radical with Organic Compounds", *J. Phys. Chem. Ref. Data*, **20**, 1991, 459-507.
- [4] Atkinson, R., Baulch, D. L., Cox, R. A., Hampson, R. F., Kerr, J. A., Troe, J., " Evaluated Kinetic and Photochemical Data for Atmospheric Chemistry", *J. Phys. Chem. Ref. Data*, **21**, 1992, 1125-1568.
- [5] Babaeva, N., and Naidis, G., Personal Communication with Bruce. R. Locke, February 1998.
- [6] Baulch, D. L., Cobos, C. J., Cox, R. A., Esser, C., Frank, P., Just, Th., Kerr, J. A., Pilling, M. J., Troe, J., Walker, R. W., and Warnatz, J., " Evaluated Kinetic Data for Combustion Modelling", *J. Phys. Chem. Ref. Data*, **21**, 1992, 411-429.
- [7] Becker, K. H., Geiger, H., and Wiesen, P., " Kinetic Study of the OH radical Chain in the Reaction System $\text{OH}+\text{C}_2\text{H}_4+\text{NO}+\text{air}$ ", *Chem. Phys. Lett.*, **184**, 1991, 256-261.
- [8] Breault, R. W., McLarnon, C., and Mathur, V. K., " Reaction Kinetics for Flue Gas Treatment of NO_x ", *Non-Thermal Plasma Techniques for Pollution Control*, Eds: Penetrante, B. M., and Schultheis, S. E., Part B, Springer-Verlag, 1993, 239-256.
- [9] Chang, J. S., Lawless, P. A., and Yamamoto, T., " Corona Discharge Processes", *IEEE Trans. on Plasma. Sci.*, **19**, 1991, 1152-1165.

- [10] Chang, M. B., Kushner, M. J., and Rood, M. J., " Gas-Phase Removal of NO from Gas Streams via Dielectric Barrier Discharges", *Environ. Sci. Technol.*, **26**, 1992, 777-781.
- [11] Chmielewski, A. G., Iller, E., Zimek, Z., Licki, J., " Investigations on Electron Beam Flue Gas Treatment Held in the Institute of Nuclear Chemistry and Technology", *The International conference on Evolution in Beam Applications*, Takasaki, JAERI, Japan, 1992, 440-448.
- [12] Civitano, L., " Industrial Application of Pulsed Corona Processing to Flue Gas", *Non-Thermal Plasma Techniques for Pollution Control*, Eds: Penetrante, B. M., and Schultheis, S. E., Part B, Springer-Verlag, 1993, 103-130.
- [13] Clements, J. S., Mizuno, A., Finney, W. C., and Davis, R. H., " Combined Removal of SO₂, NO_x, and Fly Ash from Flue Gas Using Pulsed Streamer Corona", *IEEE Trans. on Ind. Appl.*, **25**, 1989, 62-69.
- [14] Cosby, P. C., " Electron-Impact Dissociation of Nitrogen", *J. Chem. Phys.*, **98**, 1993, 9544-9553.
- [15] Cox, R. A., and Derwent, R. G., " Kinetics of the Reaction of HO₂ with the Nitric Oxide and Nitrogen Dioxide", *J. Photochem.*, **4**, 1975, 139.
- [16] Creighton, Y. L. M. "Pulsed Positive Corona Discharges, Fundamental Study and Application to Flue Gas Treatment", CIP-DATA *Kononkijke biblitheek*, Den Haag, Netherlands, 1994.
- [17] Dean, A. M., and Westmoreland, P. R., " Bimolecular QRRK Analysis of Methyl Radical Reactions", *Int. J. Chem. Kinetics.*, **19**, 1987, 207.
- [18] DeMore, W. B., Molina, M. J., Sander, S. P., Hampson, R. F., Krylon, M. J., Golden, D. M., Howard, C. J., and Ravishankara, A. R., " Chemical Kinetics and Photochemical Data for Use in Stratospheric Modeling", National Aeronautics and Space Administration, JPL Publication 87-41, 1987.
- [19] Doi, T., Osada, Y., Morishige, A., Tokunaga, O., Miyata, T., Hirota, K., Komiya, M., Nakajima, M., Miyajima, K., and Baba, S., " Pilot-plant for NO_x, SO₂, HCl Removal from Flue-Gas of Municipal Waste Incinerator by Electron-Beam Irradiation", *Radiat. Phys. Chem.* **42**, 1993, 679-682.

- [20] Eliasson, B., Hirth, M., and Kogelschatz, U., " Ozone Synthesis from Oxygen in Dielectric Barrier Discharges", *J. Phys. D: Appl. Phys.*, **20**, 1987, 1421-1437.
- [21] Eliasson, B., and Gellert, B., " Investigation of Resonance and Excimer Radiation from a Dielectric Barrier Discharge in Mixtures of Mercury and the Rare Gases", *J. Appl. Phys.*, **68**, 1990, 2026-2037.
- [22] Eliasson, B., and Kogelschatz, U., " Nonequilibrium Volume Plasma Chemical Processing", *IEEE Trans. on Plasma. Sci.*, **19**, 1991, 1063-1077.
- [23] Frank, W. N., and Hirano, S., " The History of Electron Beam Processing for Environmental Pollution Control and Work Performed in the United States", *Non-Thermal Plasma Techniques for Pollution Control*, Eds: Penetrante, B. M., and Schultheis, S. E., Part B, Springer-Verlag, 1993, 1-26.
- [24] Fujii, K., Higashi, M., and Suzuki, N., " Simultaneous Removal of NO_x, CO_x, SO_x and Soot in Diesel Engine Exhaust", *Non-Thermal Plasma Techniques for Pollution Control*, Eds: Penetrante, B. M., and Schultheis, S. E., Part B, Springer-Verlag, 1993, 257-279.
- [25] Heicklen, J., " Atmospheric Chemistry", Academic Press Inc., (London), 1976.
- [26] Herron, J. T., " Evaluated Chemical Kinetic Data for the Reactions of Atomic Oxygen O (³P) with Saturated Organic Compounds in the gas phase", *J. Phys. Chem. Ref. Data*, **17**, 1988, 967.
- [27] Huxley, L. G. H., and Crompton, R. W., " The Diffusion and Drift of Electrons in Gases", Wiley, New York, 1974, 669.
- [28] Kaiser, E. W., " Pressure Dependence of the Rate Constants for the Reactions CH₃+O₂ and CH₃+ NO from 3 to 104 torr", *J. Phys. Chem.*, **97**, 1993, 11681-11688.
- [29] Kalyana, S., " The Removal of NO_x Using a Pulsed Streamer Corona Discharge in the Presence of Ethylene", Thesis, Florida State University, 1996.

- [30] Kee, R. J., Rupley, F. M., and Miller, J. A., " Chemkin-II: A Fortran Chemical Kinetics Package for the Analysis of Gas Phase Chemical Kinetics", Sandia Report, SAND 89-8009B, 1994.
- [31] Lightfoot, P. D., and Pilling, M. J., " Temperature and Pressure Dependence of the Rate constants for the Addition of H to C₂H₄", *J. Phys. Chem.*, **91**, 1987, 3373.
- [32] Locke, B. R., Clark, R. J., Sathiamoorthy, G., and Finney, W. C., " Reactions of Isotopically Labeled Nitric Oxide (N15O) in a Gas Phase Corona Reactor", *Int. Symp. on Non-Thermal Discharge Plasma Technology for Air Pollution Control, Japan*, December 22-23, 1997.
- [33] Loiseau, J. F., Laoassie, F., Monge, C., Peyrous, R., Held, B., and Coste, C., " Numerical Simulation of Ozone Axial and Radial Distribution in a Cylindrical Oxygen-Fed Ozonizer", *J. Phys. D: Appl. Phys.*, 1994, 63.
- [34] Lowke, J. J., and Morrow, R., " Theoretical Analysis of Removal of Oxides of Sulphur and Nitrogen in Pulsed Operation of Electrostatic Precipitators", *IEEE Trans. on Plasma. Sci.*, **23**, 1995, 661-671.
- [35] Maezawa, A., and Izutsu, M., " Application of E-Beam Treatment to Flue Gas Cleanup in Japan", *Non-Thermal Plasma Techniques for Pollution Control*, Eds: Penetrante, B. M., and Schultheis, S. E., Part B, Springer-Verlag, 1993, 47-54.
- [36] Mahmud, K., Marshall, P., and Fontijn, A., " A High Temperature Photochemistry Kinetics Study of the Reaction of O(3P) Atoms with Ethylene from 290 to 1510 K", *J. Phys. Chem.*, **91**, 1987, 1568.
- [37] Masuda, S., " Pulse Corona Induced Plasma Chemical Process, A Horizon of New Plasma Chemical Technologies", *Pure Appl. Chem.*, **60**, 1988, 727-731.
- [38] Masuda, S., and Nakao, H., " Control of NO_x by Positive and Negative Pulsed Corona Discharges", *IEEE Trans. on Ind. Appl.*, **26**, 1990, 374-383.
- [39] Masuda, S., " Report on Novel Dry DeNO_x/DeSO_x Technology for Cleaning Combustion Gases from Utility Thermal Power Plant Boilers", *Non-Thermal Plasma Techniques for Pollution Control*, Eds: Penetrante, B. M., and Schultheis, S. E., Part B, Springer-Verlag, 1993, 131-137.

- [40] Masuda, S., " Destruction of Gaseous Pollutants and Air Toxics by Surface Discharge Induced Plasma Chemical Process (SPCP) and Pulse Corona Induced Plasma Chemical Process (PPCP)", *Non-Thermal Plasma Techniques for Pollution Control*, Eds: Penetrante, B. M., and Schultheis, S. E., Part B, Springer-Verlag, 1993, 199-209.
- [41] Matzing, H., Namba, H., and Tokunaga, O., " Kinetics of SO₂ Removal from Flue Gas by Electron Beam Technique", *Radiat. Phys. Chem.*, **42**, 1993, 673-677.
- [42] McFarlane, J., and Wren, J. C. "Modeling Electric Discharge Chemistry", AECL-10374 *Atomic Energy of Canada Limited*, Whiteshell Laboratories, 1991.
- [43] Mizuno, A., Chakrabarti, A., and Okazaki, K., " Application of Corona Technology in the Reduction of Greenhouse Gases and Other Gaseous Pollutants", *Non-Thermal Plasma Techniques for Pollution Control*, Eds: Penetrante, B. M., and Schultheis, S. E., Part B, Springer-Verlag, 1993, 165-185.
- [44] Morgan, W. L., and Penetrante, B. M., " ELENDIF: A Time Dependent Boltzmann Solver for Partially Ionized Plasmas", *Computer Physics Communication*, **58**, 1990, 127-152.
- [45] Morgan, W. L. "KINEMA: The Plasma Chemistry Code", Version 1.51, *Kinema Software* 1994.
- [46] Mukkavilli, S., Lee, C. K., Varghese, K., and Tavlarides, L. L., " Modeling of the Electrostatic Corona Discharge Reactor", *IEEE Trans. on Plasma. Sci.*, **16**, 1988, 652-660.
- [47] Namba, H., Tokunaga, O., Suzuki, R., and Aoki, S., " Material Balance of Nitrogen and Sulfur Components in Simulated Flue Gas treated by an Electron Beam", *Appl. Radiat. Isot.*, **41**, 1990, 569-573.
- [48] Namba, H., Tokunaga, O., and Paur, H.R., " Basic Study on Electron Beam Treatment of Coal-Fired Flue-gas Aerosol Size Distribution Measurements", *J. Aerosol. Sci.*, **22**, 1991, S475-S478.

- [49] Namba, H., Tokunaga, O., Tanaka, T., Ogura, Y., Aoki, S., and Suzuki, R., "The Study on Electron Beam Flue Gas Treatment for Coal-Fired Thermal Plant in Japan", *Radiat. Phys. Chem.*, **42**, 1993, 669-672.
- [50] Nasser, E., "Fundamentals of Gaseous Ionization and Plasma Electronics", Wiley-Interscience, 1971.
- [51] NIST Chemical Database 17, version 6.01, 1994, Eds: Mallard, W., G., Westley, F., Herron, J., T., and Hampson, R. F. *National Institute of Standards and Technology (NIST), Gaithersburg, USA.*
- [52] Pagsberg, P., Munk, J., Anastasi, C., and Simpson, V. J., "Reactions of CH₂OH with O₂, NO, and NO₂ at Room Temperature", *J. Phys. Chem.*, **93**, 1989, 5162.
- [53] Paur, H. R., "Removal of Volatile Hydrocarbons from Industrial Off-Gas", *Non-Thermal Plasma Techniques for Pollution Control*, Eds: Penetrante, B. M., and Schultheis, S. E., Part B, Springer-Verlag, 1993, 77-89.
- [54] Penetrante, B. M., Hsiao, M. C., Merritt, B. T., Vogtlin, G. E., and Wallman, P. H., "Comparison of Electrical Discharge Techniques for Nonthermal Plasma Processing of NO in N₂", *IEEE Trans. on Plasma. Sci.*, **23**, 1995, 679-687.
- [55] Peyrous, R., Pignolet, P., and Held, B., "Kinetic Simulation of Gaseous Species Created by an Electrical Discharge in Dry or Humid Oxygen", *J. Phys. D: Appl. Phys.*, **22**, 1989, 1658-1667.
- [56] Puchkarev, V., and Gundersen, M., "Energy Efficient Plasma Processing of Gaseous Emission Using a Short Pulse Discharge", *Appl. Phys. Lett.*, **71** (23), 1997, 3364-3366.
- [57] Rosocha, L. A., Anderson, G. K., Bechtold, L. A., Coogan, J. J., Heck, H. G., Kang, M., McCulla, W. H., Tennant, R. A., and Wantuck, P. J., "Treatment of Hazardous Organic Wastes Using Silent Discharge Plasmas", *Non-Thermal Plasma Techniques for Pollution Control*, Eds: Penetrante, B. M., and Schultheis, S. E., Part B, Springer-Verlag, 1993, 281-308.
- [58] Sathiamoorthy, G., Locke, B. R., Finney, W. C., Clark, R. J., and Yamamoto, T., "Halon Destruction in a Gas Phase Pulsed Streamer Corona Reactor", (submitted to *J. of Advanced Oxidation Technologies*)

- [59] Scheytt, H., Esrom, H., Prager, L., Mehnert, R., and von Sonntag, C., "Ultraviolet Light and Electron Beam Induced Degradation of Trichloroethylene", *Non-Thermal Plasma Techniques for Pollution Control*, Eds: Penetrante, B. M., and Schultheis, S. E., Part B, Springer-Verlag, 1993, 91-101.
- [60] Shimizu, K., "Gas Treatment Utilizing Pulsed Discharge Plasma", Thesis, Toyohashi Univ. of Technology, 1996.
- [61] Sridharan, U. C., Kaufman, F., "Primary Products of the $O+C_2H_4$ Reactions", *Chem. Phys. Lett.*, **102**, 1983, 45.
- [62] Thompson, J. E., and Ravishankara, A. R., "Kinetics of $O(^1D)$ Reactions with Bromocarbons", *Int. J. Chem. Kinetics.*, **25**, 1993, 479-487.
- [63] Tokunga, O., and Suzuki, N., "Radiation Chemical Reactions in NO_x and SO_2 Removal from Flue Gas", *Radiat. Phys. Chem.*, **24**, 1984, 145-165.
- [64] Tokunaga, O., Namba, H., and Hirota, K., "Experiments on Chemical Reactions in Electron-Beam Induced NO_x/SO_2 Removal", *Non-Thermal Plasma Techniques for Pollution Control*, Eds: Penetrante, B. M., and Schultheis, S. E., Part B, Springer-Verlag, 1993, 55-62.
- [65] Tsang, W., and Hampson, R. F., "Chemical Kinetic Data Base for Combustion Chemistry. Part-I Methane and Related Compounds", *J. Phys. Chem. Ref. Data.*, **15**, 1986, 1087.
- [66] Tsang, W., "Chemical Kinetic Data Base for Combustion Chemistry. Part-2 Methanol", *J. Phys. Chem. Ref. Data.*, **16**, 1987, 471.
- [67] Tsang, W., and Herron, J. T., "Chemical Kinetic Data Base for Propellant Combustion-I. Reactions Involving NO , NO_2 , HNO , HNO_2 , HCN , and N_2O ", *J. Phys. Chem. Ref. Data.*, **20**, 1991, 609-663.
- [68] Vogtlin, G. E., and Penetrante, B.M., "Pulsed Corona Discharge for Removal of NO_x from Flue Gas", *Non-Thermal Plasma Techniques for Pollution Control*, Eds: Penetrante, B. M., and Schultheis, S. E., Part B, Springer-Verlag, 1993, 187-198.

- [69] Yamamoto, T., Ramanathan, K., Lawless, P. A., Ensor, D. S., Newsome, J. R., Plaks N, and Ramsey, G. H., " Control of Volatile Organic Compounds by an ac Energized Ferroelectric Pellet Reactor and a Pulsed Corona Reactor", *IEEE Trans. on Ind. Appl.*, **28**, 1992, 528-534.
- [70] Yamamoto, T., Lawless, P. A., Owen, M. K., Ensor, D. S., and Boss, C., " Decomposition of Volatile Organic Compounds by a Packed-bed Reactor and a Pulsed-Corona Plasma Reactor", *Non-Thermal Plasma Techniques for Pollution Control*, Eds: Penetrante, B. M., and Schultheis, S. E., Part B, Springer-Verlag, 1993, 223-237.
- [71] Yamamoto, T., Futamura, S., and Zhang, A. " Integrated Nonthermal Plasma Technology for Controlling Hazardous Air Pollutants", *Proceedings of NEDO Symposium, University of Tokyo, Japan*, Nov 1 1996, 15-32.
- [72] Yamamoto, T., " VOC Decomposition by Nonthermal Plasma Processing - A New Approach", *Proc. Of IEJ-ESA 1996, Symp. on Electrostatics, Japan*, 1996, 1-16.
- [73] Yamamoto, T., Chang, J. S., Berezin, A. A., Kohno, H., Honda, S., and Shibya, A., " Decomposition of Toluene, o-Xylene, Trichloroethylene, and their Mixture Using a BaTiO₃ Packed-Bed Plasma Reactor", *J. Advanced Oxidation Technologies*, **1**, 1996, 67-78.
- [74] Yousfi, M., Poinsignoss, A., and Hamani, A., " Electron Database Needed for Discharge Modeling in Flue-gas Treatment", *Non-Thermal Plasma Techniques for Pollution Control*, Eds: Penetrante, B. M., and Schultheis, S. E., Part A, Springer-Verlag, 1993, 229-329.
- [75] Yousfi, M., Hennad, A., and Alkaa, A., " Monte Carlo Simulation of Electron Swarms at Low Electric Fields", *Phys. Rev. E.*, **49**, 1994, 3264-3273.
- [76] Willis, C., and Boyd, A. W., " Excitation in the Radiation Chemistry of Inorganic Bases", *Int. J. Rad. Phys. Chem.*, **8**, 1976, 71-111.

BIOGRAPHICAL SKETCH

Giridhar Sathiamoorthy, a Tau Bate, was born on February 13, 1975 at Jamshedpur, Bihar, India. He enrolled in the undergraduate program at Andhra University, Visakhapatnam, India in the fall of 1992. He received his Bachelor of Technology Degree in Chemical Engineering (with Distinction) in the spring of 1996.

In the fall of 1996, he became a Seminole, when he registered at Florida State University. He enrolled in the Chemical Engineering graduate program at FAMU-FSU College of Engineering to pursue his Master of Science degree. During this time, he worked with the corona group as a research assistant and focussed on gas-phase reaction kinetics. He was also a teaching assistant for one semester with the Department of Chemical Engineering. His professional interests are in the areas of process and environmental engineering.